DEVELOPMENT AND USE OF A HIGH SENSITIVITY, FAST RESPONSE NITRIC OXIDE DETECTOR FOR AIR QUALITY MONITORING AND EDDY CORRELATION FLUX MEASUREMENTS

by

Kevin Lawrence Civerolo

Dissertation submitted to the Faculty of the Graduate School of the
University of Maryland at College Park in partial fulfillment
of the requirements for the degree of
Doctor of Philosophy
1996

Advisory Committee:

Professor Russell R. Dickerson, Chair/Advisor
Assistant Research Scientist Bruce G. Doddridge
Special Professor Bruce B. Hicks, NOAA/ARL
Professor Robert D. Hudson
Professor Thomas C. O'Haver

ABSTRACT

Title of Dissertation: DEVELOPMENT AND USE OF A HIGH SENSITIVITY, FAST RESPONSE NITRIC OXIDE DETECTOR FOR AIR QUALITY MONITORING AND EDDY CORRELATION FLUX MEASUREMENTS

Kevin Lawrence Civerolo, Doctor of Philosophy, 1996

Dissertation directed by: Professor Russell R. Dickerson
Department of Meteorology

Reactive nitrogen, released principally as nitric oxide (NO), is very important to the chemistry of the atmosphere. Reactive nitrogen compounds contribute to the problems of acid deposition and over-nutrification in sensitive estuaries such as the Chesapeake Bay. Furthermore, nitric oxide and nitrogen dioxide are key components of the photochemical production of ozone, contributing to poor air quality during the summer months. Few reliable NO measurements exist outside of urban areas, however, making it difficult to predict episodes of elevated ozone. The development and characterization of a high sensitivity NO detector based on chemiluminescent reaction with ozone is described.

Measurements of ozone, NO, and other chemical species made at a site on Maryland's Eastern Shore are presented here for the development of a chemical climatology. This site is under urban, agricultural, and rural influences. These chemical measurements are combined with knowledge of air parcel history through back trajectory analysis, to help explain observed pollution levels. Comparison with other ozone measurements throughout the Chesapeake Bay area are used to assess the quality of summertime air over the Washington-Baltimore region.

To estimate the rate at which NO is emitted from this agricultural site, eddy correlation flux measurements are also presented. Eddy correlation is the direct micrometeorological technique for measuring turbulent fluxes, which can occur on time scales of 1 s or less, thus requiring fast response instrumentation to capture most of the flux. Fluxes measured at this site compare favorably with the few and widely scattered values reported in the literature. Finally, there is an indication that by not tilling agricultural soil, NO fluxes may be reduced by a significant amount. While soil emissions of NO are small compared to anthropogenic emissions in urban areas, they contribute about 8.4 Gg N yr^{-1} to the Chesapeake Bay watershed. Any reductions during the summer months can help to reduce ozone levels and improve air quality.

DEDICATION

I dedicate this work to the following people: my parents Edwin and Mary, my siblings Eric and Kelly, and my good friend Stacey.

ACKNOWLEDGEMENTS

I want to first thank my advisor Russell Dickerson for all his time, patience, and support. Thanks for convincing me to see this through until the end, Russ. I appreciate the efforts of the other members of my committee: Bruce Doddridge, Robert Hudson, Bruce Hicks, and Thomas O'Haver. Thanks for all your comments and ideas, especially Bruce D. Thanks go out to Richard Valigura, without whose tireless help I would not have been able to make the flux measurements. To Edward Cole - thanks for all your help in the machine shop, and thanks for listening to my sob stories. You always had time for my "emergencies." Thanks go to Ken Staver and Russ Brinsfield at the Wye Research and Education Center for their support.

I never could have done this without the support and help of the other members of the Air Chemistry Group. Past members include Olga Poulida, Leslie Moy, Jae-Hwan Kim, Charles Piety, Paul Kelley, and Melody Owens. Thanks for all the help with HY-SPLIT, Leslie. Present members include Kevin Rhoads, Raymond Morales, Shobha Kondragunta, Kristen Hallock, Willnetta Ball, Ana Prados, and Fernando Rodriguez. Kev - thanks for the help processing data and at the Wye, but more importantly thanks for all those weird discussions at 3 in the morning about everything and nothing. To Adam Schlosser (an honorary Air Chem member), Chris Frye, Matt Barlow, Dave Dewitt, Dan

Schaefer, and everyone I've forgotten by name - cheers. Thanks Adam, PK, and Jodi for dragging me kicking and screaming to the gym.

Thanks go out to the University Motor Pool. Sorry about returning all those cars covered in mud and corn stalks. Thank you Gary, Joe, Keith, Duane, Exree, and Johnny for making the spring of 1995 so memorable and heartbreaking for me at the same time. Thanks to Eric, Rob, David, Bob, and Joe for making Thursday nights fun and certainly interesting. Thanks to Harry, Shirley, Katie, Ric, Margit, and everyone else in the front office for being so patient with me.

Finally, I would like to thank the people most important to me. Mom and Dad, it looks like I made it. Thanks for ALWAYS being there for me, unconditionally. To Eric - hope those Hokies make us proud. To Kelly - good luck with little William. Last, but certainly not least, I want to thank you, Stacey, for pushing me, for supporting me, for making me laugh, for sharing adventures with me, and for everything else. Let me know when I can return the favor.

TABLE OF CONTENTS

LIST OF TABLES

LIST OF FIGURES

Chapter 1

Introduction and Chapter Overview

1.1 Reactive Nitrogen Chemistry in the Atmosphere

Reactive nitrogen compounds play critical roles in the chemistry of the atmosphere. Reactive nitrogen is principally released as nitric oxide (NO) from a variety of known sources. Natural sources include lightning discharges [e.g. Borucki and Chameides, 1984; Lawrence et al., 1994], injection from the stratosphere [Levy et al., 1980], and microbial activity in soil [e.g. Galbally and Roy, 1978; Lipschultz et al., 1981], although soil emissions are greatly affected by application of nitrogen-based fertilizers. Anthropogenic sources of NO into the atmosphere include high-temperature fossil fuel combustion [e.g. Logan, 1983] and biomass burning (which may also be a natural source) [Crutzen et al., 1979]. While natural and anthropogenic sources contribute roughly equally to the emission of NO on a global scale, man-made input may exceed natural sources in urban areas by an order of magnitude or more [Logan, 1983].

Soils emit 8-10 Tg of NO as nitrogen per year (Tg N yr^{-1}) to the atmosphere, with an uncertainty of about a factor of two [e.g. Logan, 1983; Stedman and Shetter, 1983]. This is equal to about half the amount that fossil fuel burning contributes to the total global budget of 40-50 Tg N yr^{-1}. In the U.S., soil emissions of NO may be about 14% as large as anthropogenic emissions

during the summer [Williams et al., 1992]. Williams et al. [1992] also showed that while only 4% of the area in the U.S. is used to grow corn, these agricultural lands account for over 40% of the total soil emission. Nitric oxide is formed in soils as an intermediate step in the processes of nitrification and denitrification [e.g. Johansson and Galbally, 1984; Firestone and Davidson, 1989]. Different varieties of bacteria are responsible for either (1) oxidation of ammonium to nitrite, and then nitrite to nitrate (nitrification), or (2) conversion of nitrate to molecular nitrogen (denitrification).

Once in the troposphere, NO quickly reacts with ambient ozone (O_3), forming nitrogen dioxide (NO_2):

$$NO + O_3 \rightarrow NO_2 + O_2 \qquad \text{(R1.1)}$$

Nitrogen dioxide can then be photolyzed, allowing for the regeneration of O_3:

$$NO_2 + h\nu \rightarrow NO + O \quad (300 < \lambda < 400 \text{ nm}) \qquad \text{(R1.2)}$$

$$O + O_2 + M \rightarrow O_3 + M \qquad \text{(R1.3)}$$

where M denotes a third body, usually nitrogen (N_2) or oxygen (O_2). Nitric oxide may also be converted to NO_2 by reaction with the hydroperoxy radical (HO_2) or with various organic peroxy radicals (RO_2, where R denotes an organic

compound) [e.g. Crutzen, 1973]:

$$HO_2 + NO \rightarrow NO_2 + OH \qquad (R1.4)$$

$$RO_2 + NO \rightarrow NO_2 + RO \qquad (R1.5)$$

where OH is the hydroxy radical. Subsequent photolysis of NO_2 can lead to further O_3 production via reactions R1.2 and R1.3 in the troposphere. The OH radical is important because of its oxidizing capacity in the atmosphere; it is the most important photochemical sink for many compounds including methane (CH_4), sulfur dioxide (SO_2), hydrochlorofluorocarbons (HCFC's), and carbon monoxide (CO).

In environments where there is no appreciable amount of peroxy radicals, reactions R1.1-R1.3 comprise a steady state set. That is, there is no net production of any of the three molecules NO, NO_2, and O_3. The sum of NO and NO_2 is referred to as NO_x. The most important sink for NO_x is generally through the formation of nitric acid (HNO_3):

$$OH + NO_2 + M \rightarrow HNO_3 + M \qquad (R1.6)$$

followed by wet or dry deposition of HNO_3, a highly reactive and water soluble gas. The lifetime of NO_x with respect to the above reaction ranges from a few

hours to a few days [e.g. Logan, 1983]. Other loss pathways include dry deposition of NO_2, and the formation of dinitrogen pentoxide (N_2O_5) during the nighttime or in winter:

$$NO_2 + O_3 \rightarrow NO_3 + O_2 \qquad \text{(R1.7)}$$

$$NO_2 + NO_3 + M \rightleftharpoons N_2O_5 + M \qquad \text{(R1.8)}$$

Nitric oxide and NO_2 may be converted to other higher oxides of nitrogen. The family of total reactive nitrogen is referred to as NO_y [Logan, 1983; Fehsenfeld et al., 1987] and includes (but is not restricted to) the following compounds: NO, NO_2, HNO_3, peroxyacetyl nitrate ($CH_3C(O)OONO_2$, or PAN), nitrogen trioxide (NO_3), N_2O_5, nitrous acid (HONO), peroxynitric acid (HO_2NO_2), particulate nitrate ($p\text{-}NO_3^-$), and various organic nitrates. At a fairly rural site in central Pennsylvania, Buhr et al. [1990] determined that summertime NO_y was principally made up of HNO_3 and PAN, the sum of which constitutes about 50-70% of total reactive nitrogen. About 20% of the total was NO_x. Doddridge et al. [1992] state that wet and dry deposition are the major removal mechanisms of nitrate from the atmosphere. The authors estimated the amount of nitrate which the Chesapeake Bay watershed takes in (due to dry deposition) to be about 6-30 Gg N yr^{-1}.

One reason why PAN is so important is that it is a reservoir for both NO_x

and peroxy radicals [Singh and Hanst, 1981]. It is formed according to the following reaction scheme:

$$CH_3CO + O_2 + M \rightarrow CH_3C(O)OO + M \qquad (R1.9)$$

$$CH_3C(O)OO + NO_2 + M \rightleftharpoons CH_3C(O)OONO_2 + M \qquad (R1.10)$$

where CH_3CO is the acetyl radical, formed by oxidation of ethane, acetaldehyde or isoprene, or by photolysis of various organic compounds; and $CH_3C(O)OO$ is the peroxyacetyl radical. PAN is thermally unstable, and according to the rate constant for decomposition [Atkinson et al., 1989], its lifetime is only about 22 min at 30°C. If PAN can be transported to the middle or upper troposphere, it is much longer-lived. For example, at -20°C PAN has a lifetime of 105 days. Thus, if PAN can accumulate along transport paths and later decompose, it can be a source of NO_x to normally unpolluted regions.

1.2 The Importance of Reactive Nitrogen

Oxides of nitrogen are very important to the chemistry of the troposphere. In the natural atmosphere [e.g. Chameides and Walker, 1973; Crutzen, 1973; Crutzen, 1974; Fishman and Crutzen, 1978], CO and methane are oxidized by OH, leading to the production of HO_2 and methyl peroxy radicals (CH_3O_2), respectively. Peroxy radicals in turn react with NO to form O_3 (Reactions R1.4

and R1.5) in the unpolluted troposphere.

In the presence of large amounts of nitrogen oxides, hydrocarbons, and sunlight typical of urban areas in the summer, photochemical smog [Haagen-Smit, 1952] consisting of O_3 and other pollutants is increasingly becoming a problem. Ozone and other pollutants like PAN are eye irritants [e.g. Finlayson-Pitts and Pitts, 1986], reduce human respiratory function [e.g. Folinsbee et al., 1988], deteriorate many man-made materials such as rubber [e.g. Finlayson-Pitts and Pitts, 1986], and reduce plant growth and crop yield [e.g. Heck et al., 1982]. High ozone is not a local phenomenon. If ozone and its precursors can be transported to the middle and upper troposphere, their lifetimes increase because of the colder temperatures. Dickerson et al. [1987], Pickering et al. [1990], and Poulida [1993] showed that deep cumulus convection is an effective way of transporting pollutants away from the surface, turning a local problem into a regional and even hemispheric problem.

In recent years, deposition of nitrate to delicate environments such as the Chesapeake Bay watershed has been receiving increased attention. Sources of nitrate may include anthropogenic emission of NO_x, runoff of fertilizers and animal wastes, and discharges from municipal and industrial sources [Fisher et al., 1988; Fisher and Oppenheimer, 1991]. There are a variety of consequences which result from excessive nitrate loading, including the acidification of streams and lakes [Galloway and Likens, 1981]. A recent report by the Chesapeake Bay

Research and Monitoring (CBRM) Division of the Maryland Department of Natural Resources [CBRM, 1995] states that nitrate, after being released into the atmosphere as NO_x, reaches the Bay and surrounding watershed via wet or dry deposition. Acidic waters cause damage to many varieties of freshwater fish, especially during their sensitive developmental stages. Acidic deposition can also alter soil chemistry, threatening plant life.

Another related problem is over-nutrification. Increased nitrate loading to watersheds promotes the growth of phytoplankton, which in turn increases the demand for dissolved oxygen. Anoxia, the condition of near-zero levels of available oxygen, occurs as organic material from previous years settles and collects along the bottoms of bays [Taft et al., 1980; Officer et al., 1984]. For the Chesapeake Bay, this has deleterious economic and ecological implications for oysters, clams, and other bottom-dwelling organisms.

Nitrate levels above 10 mg/L in drinking water can cause health problems in humans, too [e.g. Fisher et al., 1988]. Bacteria can reduce any nitrate not absorbed in the human gastrointestinal tract to nitrite. The pH in the digestive tract of infants can be greater than 4; thus, some of the nitrate may be reduced to nitrite before the nitrate is absorbed completely. Nitrite can oxidize the iron in hemoglobin, rendering it ineffective as an oxygen carrier [Fisher et al., 1988]. The resulting asphyxiation which can occur may lead to the condition called infantile methemoglobinemia. Nitrite can also combine with amines in the body

to form potentially carcinogenic compounds.

1.3 The Purposes of This Study

For the aforementioned reasons, it is very important to understand nitrogen oxides in the troposphere. The concentrations of these compounds range over several orders of magnitude. For example, [NO] can be as low as 1-2 parts per trillion by volume (pptv) in the marine boundary layer [e.g. McFarland et al., 1979; Torres and Thompson, 1993; Rhoads et al., 1996], as high as 2 parts per million by volume (ppmv) in heavily polluted air, with continental background levels on the order of a few hundred pptv to 1 part per billion by volume (ppbv) or less [Doddridge et al., 1991; Doddridge et al., 1992; Parrish et al., 1993; Poulida, 1993; Carroll and Thompson, 1994; Poulida et al., 1994]. Data over non-urban areas are sparse, where ambient levels are lowest and most difficult to measure. The focus of this dissertation is to describe the development and implementation of a high sensitivity, fast response detector capable of making low ambient concentration and eddy correlation flux measurements of NO. In the next section, various techniques for measuring NO are discussed.

1.4 Techniques for Detection of Nitric Oxide

There are currently several well-established methods for measuring NO concentrations. They include tunable diode laser spectroscopy [Reid et al., 1982;

Schiff et al., 1983; Fried et al., 1991], two-photon laser-induced fluorescence [Bradshaw et al., 1985; Davis et al., 1987; Hoell et al., 1987], and chemiluminescent reaction with O_3 [Clough and Thrush, 1967; Fontijn et al., 1970]. These methods will be briefly discussed in this section.

1.4.1 Tunable Diode Laser Spectroscopy (TDLS)

Measuring NO using tunable diode laser spectroscopy (TDLS) is a technique based on Beer's Law absorption of infrared (IR) radiation at the 1853.737-1853.748 cm^{-1} doublet. The TDL consists of two small lead/salt semiconductors which form a p-n junction. Application of an electrical current causes lasing to occur in the 500-3500 cm^{-1} wavenumber region (depending on the semiconductors chosen), and slight adjustments of the current allow for tuning over a band of a few hundred wavenumbers. The TDL linewidth typically ranges from about 2×10^{-5} to 1.7×10^{-2} cm^{-1} [Reid et al., 1982], considerably smaller than pressure-broadened linewidths on the order of 0.05 cm^{-1}, making the TDL highly sensitive to a specific IR wavelength region.

Unfortunately, the detection limit of the TDL is about 0.5 ppbv [Schiff et al., 1983], too high for measurements in the marine boundary layer or even in rural continental air. This is due to absorption in the IR being several orders of magnitude weaker than in the ultraviolet or visible range, as vibrational and rotational transitions in the IR involve small changes in energy. A practical

consideration involves carefully monitoring the operating conditions; for example, the TDL must be kept at 77 K. For these reasons, TDLS is not a widely used technique for measuring NO.

1.4.2 Two-Photon Laser-Induced Fluorescence (TP-LIF)

The technique of two-photon laser-induced fluorescence (TP-LIF) involves the sequential excitation of NO molecules, using first an ultraviolet (UV) wavelength of 226 nm, and then an IR wavelength (1.06-1.15 μm). The resulting fluorescence around 187-220 nm is blue-shifted with respect to both excitation wavelengths, and therefore can be isolated from most system noise and interfering species using longwave cut-off filters and solar-blind photomultiplier tubes. The desired wavelengths are generated by sequentially pumping tunable diode lasers with two neodymium:yttrium/aluminum/garnet (Nd:YAG) lasers, with a 2 ns separation of pumping. This system has a detection limit of 5 pptv or less for an averaging time of 30 s [Davis et al., 1987]. However, the expense, complexity, and skill required to operate and maintain the TP-LIF system prevent this detector from being widely used.

1.4.3 NO/O_3 Chemiluminescence

The most commonly used technique for measuring NO is via chemiluminescent reaction with ozone. This method of detection will be discussed in

greater detail in Chapter 2, and will only be introduced in this section.

The mechanism is as follows. When NO and O_3 are allowed to react with each other, some excited state NO_2 can form. It can deactivate to the ground state by emitting a photon in the 590-3000 nm wavelength range. An IR-sensitive photomultiplier tube detects this photon signal proportional to the ambient NO concentration.

The chemiluminescent detector has many advantages for widespread use. It does not require the constant monitoring and maintenance that sophisticated laser systems need, making it the ideal method for long-term, unattended air quality measurements [e.g. Doddridge et al., 1991; Doddridge et al., 1992]. The most sensitive chemiluminescent systems have detection limits on the order of a few pptv [Kley and McFarland, 1980; Carroll et al., 1985; Torres, 1985; Ridley and Grahek, 1990], making them suitable in even the most pristine environments. Hoell et al. [1987] demonstrated that airborne chemiluminescent and TP-LIF instruments exhibited good agreement in the 5-20 pptv range. Finally, such detectors can be configured to have very fast response [e.g. Delany et al., 1986] so that they can be used to measure NO fluxes using eddy correlation. The issues of time response and fluxes will be discussed in the following section.

1.5 Flux Measurements of Reactive Nitrogen

As previously stated, reactive nitrogen is generally released into the at-

mosphere as NO, undergoes conversion to NO_2 or other species, and is removed from the atmosphere as nitrate or HNO_3. Thus, the study of reactive nitrogen must take into consideration the directional nature of these sources and sinks. Fluxes are measures of the rate of emission or deposition per unit area per unit time of a given chemical species (or any scalar quantity for that matter, such as temperature). Emission fluxes of NO measure the rate of input into the troposphere, from which nitrogen budgets can be constructed. A discussion of flux measurement techniques for NO and other species follows in this section.

1.5.1 Chamber Techniques

The first technique for measuring NO fluxes is the box or chamber technique [Galbally and Roy, 1978; Johansson and Granat, 1984; Slemr and Seiler, 1984; Parrish et al., 1987; Williams et al., 1988; Williams and Fehsenfeld, 1991]. This method involves placing a container over a patch of soil and monitoring the change in concentration of NO in time. Chambers are glass or lined internally with a non-reactive material such as Teflon. Chambers may be either "static," in which NO emission is measured as the increase in NO concentration shortly after the box is placed over a patch of soil; or "dynamic," in which compressed air containing no reactive nitrogen compounds is passed through the box and the NO is allowed to reach a steady-state level. A variation of the dynamic chamber technique involves passing ambient air through the chamber and mea-

suring the change in [NO]. While this technique is relatively simple to employ, there is concern that the chambers (1) may perturb the soil/microbial environment, and (2) are not able to capture the spatial variability and, thus, may not be representative of a larger area [Parrish et al., 1987]. Also, this is a technique suitable for making only emission, not deposition, measurements.

1.5.2 Gradient Techniques

A method of measuring fluxes more representative of a wider area is the gradient technique. Parrish et al. [1987] used this technique to measure NO fluxes, while various groups have measured fluxes of nitrates [e.g. Huebert et al., 1988] or HNO_3 [e.g. Huebert and Robert, 1985] with this method. This technique is logical to use because a species emitted from or deposited to the surface exhibits a gradient in concentration in the vertical direction. For example, NO can be emitted at the surface, and as it transports upwards it is quickly diluted or removed by reacting with O_3 (R1.1). It is assumed that NO transport is purely due to vertical turbulent mixing. The flux is given by:

$$F_{NO} = K \times \frac{d[c]}{dz} \qquad (1.1)$$

where d[c] is estimated from the difference in concentration of NO at two mea-

surement heights separated by dz, and K is the eddy diffusion coefficient (units are $m^2\ s^{-1}$), a proportionality parameter which in general is a function of altitude and atmospheric stability.

Parrish et al. [1987] demonstrated good agreement between simultaneous chamber and gradient technique flux values at a grassland site. Bakwin et al. [1990] used a similar gradient technique at night to examine the NO flux from a rain forest canopy, using vertical measurements of NO and O_3, in which the authors assumed that titration by O_3 was the dominant loss mechanism for NO. Bakwin et al. [1990] estimated the nighttime flux of NO from the soil to be:

$$F_{NO} = \frac{\partial}{\partial t}\left(\int [NO]dz\right) + \int k[NO][O_3]dz \qquad (1.2)$$

where k is the rate of reaction between NO and O_3. Their estimate of the NO flux was based on vertical measurements at 8 levels between 0.02 and 41 m. They assumed that there was no production of NO by photolysis of NO_2 at night, and that there were no sources of NO in the forest canopy above 41 m. While this method for measuring fluxes does not require fast response sensors, it does require the added complication of measurement of NO at more than one height, and is only a parameterization of the flux. Finally, this technique is only useful when there is a strong vertical gradient. If the atmosphere is convective,

the air is well-mixed and gradients vanish.

1.5.3 Eddy Accumulation Technique

Another technique for measuring fluxes which does not rely on fast response chemical instrumentation is the eddy accumulation technique [e.g. Dabberdt et al., 1993]. The technique involves segregating sample air into two reservoirs, one for vertical wind speed $w > 0$, and the other for $w < 0$. Knowledge of the difference in concentration and the volume rate of collection gives the average flux. A simplification of this technique, known as relaxed eddy accumulation [e.g. Oncley et al., 1993], states that the flux of a scalar is given by the product of the standard deviation of w, a scaling parameter b (which depends on the distribution of w), and the concentration difference. While in theory eddy accumulation could be used to measure NO fluxes, no such measurements have been published to date.

1.5.4 Eddy Correlation Technique

The eddy correlation method is the most direct method for measuring NO fluxes [Wesely et al., 1982; Delany et al., 1986; Hicks et al., 1986; Wesely et al., 1989], and currently there are few measurements of nitric oxide fluxes using this technique. The first eddy correlation measurements of reactive chemical species involved ozone flux measurements, either with instruments based on

O_3/NO chemiluminescence [Eastman and Stedman, 1974] or on O_3/ethylene chemiluminescence [Wesely et al., 1978]. The eddy correlation technique is employed in the present study, and will be discussed in greater detail in Chapter 4. The theory [Priestley, 1959] is as follows. Given any scalar χ (such as NO mixing ratio) and turbulent eddy of density ρ and vertical velocity w, the instantaneous vertical flux is given by:

$$F = w\rho\chi \tag{1.3}$$

where $\rho\chi$ is the concentration of the scalar (in grams per unit volume for a chemical species). The scalar quantities w and χ can be expressed as a sum of a mean part ($<w>$ and $<\chi>$, the time average or Reynolds average) and departures from the mean w' and χ'. Neglecting advective effects, density fluctuations, and sources and sinks away from the surface, and assuming horizontal surface homogeneity, the average flux can be expressed as:

$$<F> = <(\rho\chi')w'> \tag{1.4}$$

Vertical eddies can occur on time scales of 0.01 s or less [e.g. Hicks, 1970], and eddy correlation sensors should have response times on the order of at least 0.1 -1 s. A rule of thumb estimate of the frequency response of a sensor

is that it should have at least 2u/z Hz response, where u is the mean wind speed and z is the height of measurement above the zero plane [e.g. McMillen, 1987].

It is clear, then, that having fast response in addition to high sensitivity is desirable of any sensors using the eddy correlation method. Such a sensor for making NO eddy correlation flux measurements and other air quality measurements is fully described in this study.

1.6 Emissions of NO From Soils Using the Eddy Correlation Technique

The most common technique for measuring NO soil emissions is the chamber technique, and only a few eddy correlation flux measurements exist. Wesely et al. [1982] measured the flux of NO_x at 6 m over a soybean field, and found that NO was only about 10% of NO_x, meaning that the NO_x flux was dominated by deposition of NO_2. Delany et al. [1986] measured NO_x fluxes over grassland, finding NO flux values ranging between -20 and 30 ng N m^{-2} s^{-1}. Wesely et al. [1989] also measured NO fluxes over grass using the eddy correlation technique, finding values of fluxes ranging from 1.4 to 4.2 ng N m^{-2} s^{-1}. The authors also stated that rapid in-air reactions involving NO and O_3 could reduce the apparent NO emission flux. The effect of rapid in-air reactions was modeled by Gao et al. [1991], who state that when the ratio of NO_2/NO is greater than the photostationary state (PSS) value, the photolysis of NO_2 dominates and causes the NO flux to increase with height; when it is less than the PSS

value, the reaction NO + O_3 dominates and the NO flux decreases in height.

There is a need for more eddy correlation NO flux measurements, as there have been few reported in the literature. This dissertation will include such measurements made over a fertilized corn canopy in the summertime at a site on Maryland's Eastern Shore.

1.7 Objectives and Chapter Overview

Chapter 1 has presented a brief introduction to NO_x chemistry in the troposphere. Included has been background information on measurement techniques, eddy fluxes, and a justification for the research presented in this dissertation.

Chapter 2 of this dissertation will contain a discussion on the development, calibration, and careful characterization of this fast response, high sensitivity NO detector in the laboratory. Included is a discussion on the theoretical basis of the NO/O_3 chemiluminescent reaction utilized by the detector.

Once fully developed, the instrument must be shown to be robust and tested in the field. A location on Maryland's Eastern Shore is chosen as a field measurement site. It is a site with urban, rural, and agricultural influences, and is often downwind from the Baltimore-Washington urban centers. Nitric oxide measurements in conjunction with complementary chemical measurements and air parcel back trajectory analysis will be described in Chapter 3, in order to

characterize the chemistry of the site (adding to the sparse existing data set of such measurements) and to make statements on regional air quality with respect to high ozone levels.

Chapter 4 describes eddy correlation flux measurements made at this site. As stated earlier, nitrogen loading to the Chesapeake Bay and its surrounding watershed is increasingly becoming an issue. Estimates on emission and deposition of NO_x are critical to understanding the nitrogen budget. Emission of NO from the fertilized Wye research site will be examined.

Chapter 5 is a summary of the findings. It suggests potential future research for improving the NO detector and extending the scope of the various measurements.

Chapter 2

Instrument Design and Characteristics

This chapter offers a detailed description of the nitric oxide detector. The development, characterization, and calibration techniques are discussed. Included is a description of the laboratory data acquisition system, which allows for the fast (10 s^{-1}) recording critical for determining the time response of the instrument.

2.1 Theoretical Background

The technique employed by the instrument involves the chemiluminescent reaction between NO and ozone [Clough and Thrush, 1967; Fontijn et al., 1970]. In the presence of a large excess of O_3, NO is quickly converted to NO_2:

$$NO + O_3 \rightarrow NO_2 + O_2 \qquad \text{(R1.1)}$$

$$NO + O_3 \rightarrow NO_2^* + O_2 \qquad \text{(R2.1)}$$

where about 10% of the NO_2 formed is in an electronically-excited state [Fontijn et al., 1970], denoted by the superscript "*." Some of the excited state NO_2 is quenched by colliding with a third body (usually N_2 or O_2, denoted as M):

$$NO_2^* + M \rightarrow NO_2 + M^* \qquad \text{(R2.2)}$$

At pressures of about 10 torr, an appreciable fraction of the NO_2^* will relax to the ground state by emitting a photon in the wavelength range $590 < \lambda < 3000$ nm, with a peak at 1200 nm:

$$NO_2^* \rightarrow NO_2 + h\nu \quad (590 < \lambda < 3000 \text{ nm}) \qquad \text{(R2.3)}$$

The quantity $h\nu$ is the chemiluminescent photon energy. At pressures greater than 1 torr, Kley and McFarland [1980] showed that the photon energy is approximately given by:

$$I \propto \frac{k_{R2.1}}{k_{R1.1}} \times \frac{k_{R2.3}}{k_{R2.2}} \times [NO] \times \frac{F}{p/p_0} \qquad (2.1)$$

where: the k's are the respective rates of the reactions denoted in the subscript, so that $k_{R2.1}/k_{R1.1}$ is the fraction of excited-state NO_2 formed, and $k_{R2.3}/k_{R2.2}$ is approximately the fraction of NO_2^* which emits a photon; [NO] is the mixing ratio; $F/(p/p_0)$ is the pumping speed (L/min) of the pump which maintains low pressure (~10 torr) for the reaction, chosen to allow the residence time in the system to be 2-3 times as long as the lifetime of NO with respect to chemilumi-

nescence; F is the sample flow rate; and p/p_0 is the pressure of the reaction relative to ambient.

Steffenson and Stedman [1974] showed that in order to optimize the performance of a given NO detector, several parameters must be considered. The reaction chamber design must be chosen to provide efficient mixing close to the photomultiplier tube which detects the chemiluminescent signal, a tube which must be chosen to have sensitivity in the infrared region and low dark noise. These two parameters are described in Section 2.2.2. Maximizing the pumping speed is also necessary for peak detector performance. The effect of flow rate on detector sensitivity will be examined in Section 2.4. Finally, the lifetime of NO with respect to reaction with ozone must be short compared to the time spent in the reaction chamber itself. For a given reaction chamber and flow rate, the ratio of these two lifetimes is proportional to the amount of ozone generated. Section 2.2.1 addresses ozone generation for this detector.

2.2 Instrument Description

Figure 2.1 shows a schematic of the NO detector as typically configured. In this section, the components of the instrument will be discussed.

2.2.1 Ozone Generation

To produce a large amount of ozone, the following O_3 generator was used

(see Figure 2.2). The ozonizer was developed by Gary Hampton at the National Center for Atmospheric Research (NCAR). The ozonizer consists of 4 stainless steel plates embedded in a block of Teflon, which are offset from each other to allow for gas flow through the block. Oxygen is introduced into the ozonizer, and a large excitation voltage of ~6500-7000 VAC is applied between the plates and the grounded stainless steel case. The potential difference is sufficient to create atomic oxygen, allowing for the formation of O_3 by the following three-body reaction:

$$O + O_2 + M \rightarrow O_3 + M \qquad \text{(R1.3)}$$

The geometry of the ozonizer plates is such that the maximum electric field density occurs along the top edges of the plates, the activation sites for ozone generation. Having the plates offset from each other ensures that the gas flow is tortuous and allows for successively encountering each activation site. Finally, thin ceramic plates, with dimensions of 11.4 cm × 11.4 cm × 0.063 cm, made of high purity (99.5%) conductor grade alumina (Model 501699, Coors, Colorado), sandwich the stainless steel plates, preventing ionization and the formation of free electrons, which "short circuit" the ozone reaction.

This ozonizer is capable of converting about 2% of the oxygen flow to O_3. The reaction between ozone and atomic oxygen prevents unlimited genera-

tion of O_3. The optimum operating settings are an oxygen flow of 250 cc/min delivered at pressures slightly above ambient, with an excitation high voltage of 6650 VAC. Appendix A describes how these settings were determined.

2.2.2 The Chemiluminescent Detector

The chamber in which the chemiluminescent reaction takes place was designed by Ridley and Grahek [1990]. It is an aluminum, cylindrical, 230 cc vessel plated with gold. Gold is chemically inert and helps reflect the infrared photons [Dickerson et al., 1984]. The low pressure of 10 torr is maintained with a vacuum pump (Model 1012A, Alcatel, Massachusetts), with a nominal pumping speed of 310 L/min at standard temperature and pressure (STP; 0°C, 1 atm.). In practice, this pump is capable of pulling 800-1000 cc/min (STP) over extended amounts of time at 10 torr, corresponding to pumping speeds of about 61-76 L/min. Because the pump is pulling very high amounts of O_3, an ozone killer heated to thermally dissociate O_3 is installed upstream of the pump. The pump is also outfitted to run on Fomblin oil (Leybold, Pennsylvania), a synthetic fluorocarbon-based oil suitable for highly oxidizing environments.

At ambient NO concentrations of even 100 pptv, potential interferences to this chemiluminescent technique, such as O_3/hydrocarbon reactions [Delany et al., 1982; Drummond et al., 1985], can be comparable to the NO signal itself. Therefore, there is a zero or background signal which must be subtracted. To

correct for this zero signal, the sample air must be periodically mixed in a pre-reaction vessel upstream of the reaction chamber. In this mode of operation, NO is removed by reacting with ozone, and any subsequent signal detected after the prereactor is due to interfering reactions. The volume of the prereactor is three times that of the reaction chamber, ensuring a near complete removal of the ambient NO. Solenoid valves are used to automatically switch between measurement and background modes.

The chemiluminescent photons produced first pass through a red longpass filter (transmittance τ=0.5 at cut-on wavelength 610 nm; Model RG610, Schott, Pennsylvania) to remove unwanted wavelengths. They are subsequently detected with an infrared-sensitive photomultiplier tube (PMT; Model R1333, Hamamatsu, New Jersey), which has sensitivity to photons with wavelengths as long as 900 nm. Because the PMT is sensitive to infrared photons, the thermionic emission of the PMT dynode chain itself must be minimized. This is accomplished by placing the PMT in a cooled housing (Model TE-206RF, Products for Research, Massachusetts), which lowers the temperature around the PMT to -50°C. The temperature was checked with a thermocouple.

Finally, the chemiluminescent signal is processed using a photon counting system. Photons are discrete quanta by nature, hence the signal should not be averaged in time as a current in order to maintain maximum sensitivity. The photon counter (Model A-101, Amptek, Massachusetts) consists of a pulse-height

discriminator set to cut out PMT noise, a charge-sensitive preamplifier, and TTL wave-shaping electronics. Figure 2.3 shows a circuit diagram of the A-101, which plugs into an Amptek PC-11 printed circuit board. The photon counter amplifies the pulse from the PMT anode and converts it into a 5 V, 220 ns square wave pulse. The circuit board is mounted to the inside of the PMT socket assembly to minimize the noise in the anode signal wire. These square wave pulses are then recorded with a frequency counter, which will be described in the next section. The output of the instrument is stored in units of counts s^{-1}.

2.3 Data Acquisition

As previously mentioned, this NO detector must have fast response. Acquisition of data at a rate of at least 10 measurements s^{-1} is desired. All laboratory data are stored on a Dell 486 computer using a Lab-PC+ data acquisition board (National Instruments, Texas). The data acquisition board and associated software are capable of recording 4 differential (or 8 single-ended) analog voltage signals (12-bit), 24 TTL-compatible digital I/O lines, and 3 independent 16-bit counter/timer channels. One of the counter/timer channels is used to record the NO signal.

2.4 Instrument Calibration

Once the instrument is constructed, linearity and calibration tests must be

performed. Typical ambient concentrations away from pollution sources tend to be low. For example, at a rural site in North Carolina during the summer of 1991, Poulida et al. [1994] found daytime hourly average NO mixing ratios ranging from 10's of pptv to greater than 1 ppbv. Linearity over a wide range of concentrations must therefore be demonstrated.

A technique for calibrating the detector in the laboratory involves generating a dynamic dilution of a known NO standard in zero air, purified air which contains no reactive compounds. Various NO calibration gas flows can be mixed with a constant zero air flow, resulting in different dilutions (and, therefore, concentrations).

The sensitivity (S) of the detector is defined as the slope of the calibration curve:

$$S = \frac{M}{[NO]_{cal}} \tag{2.2}$$

where M is the measured number of counts per second (minus the background signal and any signal due to the zero air) and $[NO]_{cal}$ is the known NO concentration in pptv. Figure 2.4 shows a calibration curve ranging from 0.21 ppbv to 10.64 ppbv. The sensitivity of this calibration is about 2.1 counts s^{-1}/pptv.

The calibration curve was generated in a carefully controlled environment. In a field environment, ambient humidity lowers the sensitivity by quen-

ching the chemiluminescent reaction and reducing the number of photons. Competing O_3 chemiluminescent reactions, such as reactions with hydrocarbons [Delany et al., 1982], tend to increase the background signal. Hence, in practice, the sensitivity of the instrument tends to be lower. Typically, the sensitivity is about 1 count s^{-1}/pptv. Higher instrument inlet flows and higher amounts of O_3 generated would drive the sensitivity up.

To demonstrate the effect of flow rate into the NO detector on the sensitivity of the instrument, the sample inlet flow was varied (Figure 2.5). Although the sensitivity of the NO detector during this determination was less than 1 count s^{-1}/pptv, it is clear that sensitivity increases with increasing inlet flow. Long-term sampling is difficult on the vacuum pump in such a corrosive ozone-rich environment, and thus the flow rate cannot be increased indefinitely. The sample flow rate for long periods of time is never chosen above 1000 cc/min.

In field operation, the NO detector is typically calibrated with the method of standard additions. In this technique, a known flow of calibration gas is added directly to the sample flow. Assuming the sample flow signal is relatively flat, the signal due to the added calibration gas alone can be subtracted from the signal due to calibration gas and ambient flow together. This technique is more representative of real field operation, and does not involve the artificial generation of a dry dynamic dilution.

2.5 Detection Limit

Because hourly averaged [NO] values can be of the order of 10's of pptv [e.g., Poulida et al., 1994] or even on the order of 1-2 pptv [e.g. Torres and Thompson, 1993], it is necessary to have an NO detector with a minimum detectable limit several orders of magnitude lower than is available on commercial instruments. Photon counting involves the measurement of a number of counts in a given period of time, and therefore follows Poisson statistics. The convention used to define the detection limit (D.L.) is:

$$D.L. = 2 \times \frac{\sqrt{BG}}{S} \tag{2.3}$$

where BG is the signal of the instrument when in background mode and S is the sensitivity in counts s^{-1}/pptv [Ridley and Grahek, 1990].

The detection limit determination is as follows. In this case, the instrument is operated with a zero air flow of about 800 cc/min in background mode for 30 minutes and the background signal in "counts" was recorded once per second. The recording of background signals was actually done before the sensitivity determination from Section 2.4, rather than exposing the instrument to high levels of calibration gas. I determined an average background signal of 400 counts s^{-1}. With a sensitivity of 2.1 counts s^{-1}/pptv, the detection limit from Equation 2.3 is ~20 pptv for a 1 s accumulation period. This is a typical case;

in field operation, various factors such as poorer temperature control cause the background to be higher, usually closer to 700-800 counts s^{-1}. It is critical to keep the PMT as cool as possible to keep the dark signal to a minimum. For similar detection limit determinations, I have observed an average background signal as low as about 300 counts s^{-1}, corresponding to a theoretical detection limit of 16 pptv for a 1 second accumulation period, assuming a sensitivity of 2.1 counts s^{-1}/pptv.

2.6 Time Response

Fast response chemical instrumentation is critical for making eddy correlation measurements. This section shows the time response of the NO detector to two different varying inputs: a series of step changes in concentration, and a sinusoidally varying concentration.

2.6.1 Response to a Step Change in Concentration

One test of an instrument's response time is to see how it responds to a square wave or "step" input. This section discusses the theory and results behind such a test.

Doebelin [1990] defines the normalized response of a system to a step change:

$$x'(t') = 1 - \exp(-t') \qquad (2.4)$$

where x′ is the ratio of the output to input signals, t′ is the normalized time (t/τ), t is the elapsed time, and τ is the response time. One "e-folding" response is defined as the time required for the detector to increase an amount $1\text{-}e^{-1}$ (~63%) of the input signal.

Figure 2.6 is a schematic of the apparatus for the response time determination [Civerolo and Dickerson, 1991]. Using three-way solenoid values, the gas flow introduced into the detector was sequentially alternated between compressed air alone ([NO]~0 ppbv) and compressed air with calibration gas added ([NO]~5 ppbv). The flow controller and multiple vents ensured nearly constant pressure and flow into the detector.

Figure 2.7 shows the results of this time response test. The output concentration in counts s^{-1} is plotted as a function of time in 0.2 s increments. At the time, 5 measurements s^{-1} was the fastest rate of acquisition I could achieve. Upon examination of this figure, the e-folding response of the detector is less than 0.2 s. A finite residence time of about 0.1 s in the internal tubing limits the response of the instrument. Hence, the response time is estimated to be between 0.1-0.2 s.

2.6.2 Generation of a Sinusoidal Input Signal

A more realistic test of the instrument's response is to see how it responds to an input which varies sinusoidally, since scalar fluctuations in the

atmosphere can be thought of as a superposition of sine waves [e.g. Kaimal and Finnigan, 1994]. This section reviews the theoretical basis and experimental realization of such a test.

Given a sinusoidal input to a system, the ratio of the output to input signals, x′, the normalized output, is given by:

$$x' = \frac{1}{\sqrt{1 + (2\pi f_i/f_b)^2}} \tag{2.5}$$

where $2\pi f_i$ is the input frequency in radians s^{-1}, and f_b is the breakpoint frequency (s^{-1}), defined as the reciprocal of the response time of the detector [Doebelin, 1990]. Thus the e-folding response time can be determined from the normalized output and the input frequency.

Figure 2.8 shows the experimental test apparatus. An aluminum disk (15 cm diameter) is attached to a DC motor with a variable voltage power supply. Appendix B describes the calibration of the motor, the rate of revolution of the wheel as a function of input voltage. The wheel has a semicircular notch cut into it, and serves as an interface between a sample line containing a calibration gas mixture and a line leading to the NO detector. The notch, when the wheel is moving, allows for a 50% duty cycle; the NO detector only "sees" the gas mixture half of the time. The apparatus is kept under a fume hood, and a small fan prevents excess gas from building up around the wheel. The fan is adjusted

such that the input signal is maximized; if the fan is too weak gas can accumulate around the wheel, and if it is too strong it will carry the NO gas up the fume hood instead of allowing it to pass through the notch. The notch in the wheel is the only pathway between the two gas lines.

This apparatus actually represents a 50% duty cycle square wave input. A normalized square wave function is of the form:

$$x_{sq}(t) = 1,\ 0 < \omega t < \pi \qquad (2.6)$$
$$= 0,\ \pi < \omega t < 2\pi$$

while a normalized sinusoidal input over the same period is:

$$x_{sine}(t) = 0.5 + \sin(\omega t) \qquad (2.7)$$

Over a period of 2π radians (one revolution), the integrals of the two functions in Equations 2.6 and 2.7 are equivalent:

$$\frac{1}{2\pi}\int x_{sq}\,dt = \frac{1}{2\pi}\int x_{sine}\,dt = \frac{1}{2} \qquad (2.8)$$

That is, the number of NO molecules reaching the detector is equivalent for a 50% duty cycle step input and a sinusoidally varying input, over one revolution.

2.6.3 Response to a Sinusoidal Input

The wheel is first kept stationary, allowing a measurement of the input signal by passing the calibration gas mixture through the notch. In this experiment the undisturbed signal due to calibration gas alone averaged 308,634 counts s^{-1}. The signal due to room air accounts for less than 1% of this total signal, so it is ignored. Next, the wheel is allowed to rotate at various speeds: 0.5, 1.0, 1.5, 2.0, 3.0, 5.0, and 10 revolutions s^{-1}. Figures 2.9 (a) and (b) show the instrument output for wheel speeds of 1.0 and 1.5 revolutions s^{-1}, respectively. Averaging the response signal for nine consecutive cycles, the output amplitude is found to be 157,117 counts s^{-1} for the wheel speed of 1.0 revolutions s^{-1}, and for a wheel speed of 1.5 revolutions s^{-1} the output was 106,741 counts s^{-1}. The ratio of output to input amplitudes, therefore, are 0.509 (for 1.0 revolutions s^{-1}) and 0.346 (for 1.5 revolutions s^{-1}), corresponding to response times of 0.27 and 0.29 s, respectively. Again, the residence time in the internal tubing is about 0.1 s. If I assume that the errors in the input frequency and normalized output amplitude are as high as 10%, then the error in response time determination is estimated to be 17%. Thus the response time of the NO detector to a sinusoidal input is estimated to be 0.28±0.05 s.

The response times from the two determinations, therefore, are similar. While it appears that the detector can respond to a step change in concentration in 0.2 s or less, the second test is more representative of variations in the atmosphere.

To demonstrate that this system can discern input frequencies of up to 5 revolutions s^{-1}, the response of the instrument for wheel speeds of 2 and 5 revolutions s^{-1} are shown in Figures 2.10 (a) and (b), respectively. Even at 5 revolutions s^{-1}, the NO detector can follow the changes in input concentration rather well. The output of the detector at 10 revolutions s^{-1} was not distinguishable from random noise.

2.7 Summary

Table 2.1 lists the optimum operating conditions for the detector as determined by the results from this Chapter and in Appendix A. Also listed are the resulting characteristics achieved under these optimum settings. The detection limit is about 20 pptv for a 1 s accumulation time. Its response time is about 0.1-0.2 s to a step change input, and about 0.28±0.05 s to a sinusoidal input. In the next chapter the utilization of the instrument in the field setting will be discussed.

Chapter 3

Observations and Chemical Characterization of the Research Site

During various periods in 1993-1995 chemical measurements were made at a site on the Eastern Shore of Maryland. The site is in a field at an agricultural research station, east of Baltimore and Washington by about 100 km. While the Eastern Shore is more rural than the area west of the Chesapeake Bay, westerly flow advects pollution and ozone precursors to the site. Observations made during the spring and summer months are used to develop a "climatology" of air quality at the site. These measurements will contribute to the small existing data set in this region, outside of urban areas.

Elevated ozone levels throughout the southeastern U.S. during the summer months lead to poor air quality, so it is important that O_3 and its precursors (in particular nitrogen oxides) are carefully monitored. Knowledge of the history of air parcels provides insight into the sources of ozone and its precursors at the research site. Back trajectory analysis is used to qualitatively determine pollutant origin.

Chemical measurements and air parcel trajectory analysis provide important information about ozone formation at one particular site. However, elevated ozone concentrations are a regional problem. It is necessary to compare

observations at the Wye site with other measurements in the mid-Atlantic region to examine the role that urban areas play in the photochemical production of ozone. These issues will be addressed in this chapter.

3.1 Research Site Description

The history of this site (38°55′ N, 76°09′ W) has been well documented previously [e.g. Staver and Brinsfield, 1990; Brinsfield and Staver, 1991]. Measurements were made in the middle of a 16 ha plot of land at the Wye Research and Education Center in Queen Anne's County, Maryland, a center belonging to The University of Maryland system. Corn (maize), used for poultry feed, is grown on this field. I chose the site (see Figure 3.1) because of its collocation with an air sampling tower established by the National Oceanic and Atmospheric Administration's Air Resources Laboratory (NOAA/ARL). Standard meteorological parameters (sampled every 15 min) and nitric acid (sampled weekly) are measured from the NOAA/ARL tower, providing the necessary complementary data needed to characterize the site.

The soil in about half of the field is tilled before planting in mid-May, while the other half of the field is not tilled. Measurements were made along this dividing line. The site is generally flat (<3% grade) and is about 5 m above sea level. Surface runoff flows directly into the nearby Wye River, a tributary of the Chesapeake Bay. The center is a well-established agricultural research

station, so local pollution sources (e.g. tractors, cars) and livestock can occasionally affect the site. The Baltimore-Washington urban corridor is < 100 km west of the site, and the prevailing southwesterly flow in the summer can bring fresh pollution to the site.

At the time of planting (mid-May) the field is fertilized with "liquid nitrogen," a mixture that is 30% nitrogen by weight. This fertilizer mixture, by weight, consists of the following: 42.2% ammonium nitrate (NH_4NO_3), 32.8% urea, 25% water, and 0.1% ammonium hydroxide (NH_4OH, to adjust the pH). A second fertilizer application occurs in mid-June. In 1995, 34 kg N ha^{-1} of fertilizer were injected 5 cm into the soil on May 16, and then 125 kg N ha^{-1} were applied to the soil surface on June 15-16. Additionally, phosphorates and herbicides are applied at various times after planting. The timetable for fertilizer application is nearly identical from year to year. The soil is generally slightly acidic but variable in the field (pH ~ 6-7). The corn grows rather quickly, and by late August is nearly 3 m tall. The corn is allowed to dry out, and is harvested in mid-September. Rye cover grass is planted before the corn seed is laid down in both fields. It is removed by tilling the one field, and by using additional herbicide (Paraquat) on the untilled field.

3.2 Experimental Procedures

Measurements at the Wye site were made during the past three years. In

1993, NO, NO_x, NO_y, O_3, CO, and solar UV flux were measured from September 2-28. In 1994, the same suite of chemical species except for total reactive nitrogen was monitored from August 27 to October 10. In an attempt to compile long-term data at the site, measurements in 1995 were made over a much longer period: O_3 and CO, January 6 through September 21; NO, March 18 through August 3; NO_x, June 10 through August 3; NO_y, August 3 through September 21; and UV flux from March 18 to September 21. These sampling dates are summarized in Table 3.1.

Before 7/5/95, all instruments were housed in a mobile laboratory parked along the field dividing line, with the UV radiometer mounted on the roof. All inlet sample lines were set at 8 m on a collapsible tower attached directly to the laboratory. In order to make flux measurements (Chapter 4), the instrument housing had to be much smaller so as not to perturb the wind fields. Therefore, all instruments were moved into two 1 m × 2 m × 1 m air conditioned sheds in anticipation of making the flux measurements. After 7/5/95, sampling lines were mounted at about 6 m on the NOAA/ARL tower, mentioned before.

All sampling lines were made of inert black Teflon. The O_3 and CO instruments share a 0.62 cm OD line. By introducing 220 ppbv of ozone at the sample line inlet and then directly to the instrument intake, I showed that there is a 3.5% loss of ozone along the sampling line, and indicated concentrations were adjusted accordingly. Both reactive nitrogen systems (described in a later

section) have independent 0.31 cm OD sampling lines.

3.3 Instrumentation

This section describes the techniques of the various instruments used. All techniques are well-established, and all instruments have been used previously in similar air monitoring experiments by the Air Chemistry Group at the University of Maryland [e.g. Doddridge et al., 1992; Poulida et al., 1994].

3.3.1 Reactive Nitrogen Compounds

Nitric oxide was measured with two chemiluminescent detectors, the instrument described in this dissertation, and a similar slower response instrument. The other instrument was a commercial instrument modified for increased sensitivity [Delany et al., 1982; Dickerson et al., 1984] having a detection limit of 16 pptv (as configured, signal-to-noise ratio (S:N) of 1:1 at the $\pm 2\sigma$ noise level with a 20 s integration time). Both instruments were periodically calibrated with a standard addition of NO calibration gas.

Nitrogen dioxide was measured with a broadband UV ($300 \text{ nm} < \lambda < 400 \text{ nm}$) photolytic converter in conjunction with an NO detector downstream [Kley and McFarland, 1980; Poulida, 1993; Poulida et al., 1994]. The converter consists of a xenon arc lamp and a pyrex cell in which the energy from the lamp is sufficient to dissociate some of the NO_2 to NO. The signal when the air stream

passes through the converter is the sum of the ambient NO plus a fraction of the NO_2 converted to NO, and the signal when the air stream bypasses the converter is due to NO only. The difference between the two signals is proportional to the amount of NO_2 photolyzed to NO. The efficiency of conversion of NO_2 to NO is typically about 50-70%, and this was checked once a week using a gas phase titration [Poulida, 1993; Poulida et al., 1994]. During the 1993 and 1994 late summer campaigns, this photolytic converter was used in conjunction with the fast response detector, and in 1995 it was used with the slow response detector in June and July.

Total reactive nitrogen was measured by passing the sample air over a molybdenum converter heated to 370°C, and then detecting the resultant NO with a downstream chemiluminescent detector [Fehsenfeld et al., 1987; Nunnermacker, 1990]. At this temperature, molybdenum oxides react with NO_y to form NO and other products, nearly quantitatively. Again, this conversion efficiency was checked, using NO_2 in a gas phase titration. At the Wye site during 1993, this converter was used with the slow response NO detector.

3.3.2 Ozone

Ozone was measured with a commercial instrument which relies on UV absorption at 254 nm. The detector has two cells, with a UV source at one end and vacuum phototubes at the other end. In one cell, the sample air stream

goes through a catalytic converter removing O_3. The lamp intensity is not attenuated in this cell, and this is the reference signal. The other stream bypasses the catalytic converter, and the lamp intensity is attenuated by the ambient O_3. This is the measure signal. The true O_3 signal is a function of the ratio of the "measure" to "reference" lamp intensities. The two cells switch back and forth between "reference" and "measure" signal. The instrument has a detection limit of 1-2 ppbv (S:N=1:1, $\pm 2\sigma$ noise level, 10 s averaging time).

3.3.3 Carbon Monoxide

Carbon monoxide was measured with a commercial nondispersive gas filter correlation analyzer modified for increased sensitivity [Dickerson and Delany, 1988]. The detector relies on IR absorption by CO at 4.7 μm. It has a detection limit of 24 ppbv (S:N=2:1, $\pm 1\sigma$, 60 s averaging time) and an uncertainty of about 5 ppbv for hourly averages. To account for instrumental drift and to establish a background level, a heated palladium/alumina catalyst, which converts ambient CO to CO_2, is installed internally, and a timer switch re-routes the sample stream through the catalyst for 5 min every half hour [e.g. Doddridge et al., 1994].

3.3.4 Solar Ultraviolet Flux

Total solar UV flux was measured with an Eppley (Rhode Island) UV

solar radiometer, consisting of a diffuser plate, an interference filter, and photodiode. The signal from a solar radiometer is a proxy for the photolysis rate of NO_2 [e.g. Dickerson et al., 1982; Madronich, 1987]. Water vapor and high temperatures reduce the sensitivity of the radiometer, which was factory calibrated on April 28, 1993 (calibration factor was 0.398 mW cm^{-2} per mV), and January 6, 1995 (calibration factor was 0.474 mW cm^{-2} per mV). The reason for the discrepancy in calibration factors was due to changing the load resistor from 600 Ω to 1400 Ω just before the 1995 calibration. Temperatures above 35°C were only observed during the month of July, 1995. Water did leak into the radiometer in September, 1995; thus, I did not use UV flux as a proxy for the photolysis rate of NO_2 during this month.

3.4 Observations

The basic statistics of observed hourly averaged concentrations of daytime NO, NO_2, NO_y, O_3, and CO from 1993-95 at the Wye research site are summarized in Tables 3.2-3.4. The statistics shown are mean, median, minimum, maximum, central 67% (16.5%-83.5%), and central 95% (2.5%-97.5%). The central 67% and 95% are analogous to ±1 and ±2 standard deviations, respectively, if mixing ratio was a normally distributed variable. For 1995, the data are broken down by month.

Nitric oxide is photochemically active, so that only daytime (solar UV

flux > 1 W/m^2) values are considered in the following analysis. Nitric oxide may be emitted by the soil at night, though. As photochemistry becomes more active in the summer months, NO tends to be titrated by reacting with increased levels of O_3 and HO_2, and NO_2 is converted to other forms of NO_y, leading to the lowest observed concentrations during the summer months [e.g. Doddridge et al., 1992].

Once NO is formed it is quickly converted to NO_2, and on average there is about 2-4 ppbv more NO_2 than NO at the site. High levels of NO_2 and NO_x to NO_y ratios imply fresh emissions and air which has not undergone much photochemical aging, that is, conversion to NO_y. This assumes that species such as HNO_3 have not been lost through deposition along the transport path.

Ozone is highest when photochemistry is most active. During the summer of 1995, observed hourly averaged O_3 levels reached above 120 ppbv fifteen times in July, and three times in August. The National Ambient Air Quality Standard is based on exposure to 120 ppbv for an hour, and on July 15 [O_3] was greater than 130 ppbv for four consecutive hours. This particular period of high ozone will be examined later.

Carbon monoxide is relatively inert, and its main loss mechanism is oxidation by the OH radical [Levy, 1971]. The OH radical is primarily formed by photolysis of O_3 ($\lambda < 318$ nm), followed by $O(^1D)$ reacting with water vapor. Photolysis of formaldehyde can also lead to the formation of HO_2, which in turn

leads to OH production via reaction R1.4 [Lee at al., 1995]. Thus, OH is tied to the level of photochemistry, meaning that the highest levels occur in the summer. This in turn leads to the highest concentrations of CO in the winter and lowest levels in the summer. Oxidation of CO by OH is a significant source of tropospheric O_3 [Crutzen, 1974].

3.5 Diurnal Variations

Sunlight is critical to the chemistry of reactive nitrogen and O_3. It is, therefore, interesting to examine the average daily evolution of these species.

Reactive nitrogen diurnal variations are shown in Figures 3.2-3.4 for the three years. Nitric oxide (Figures 3.2 and 3.3) tends to be lowest at night, but sometimes nonzero due probably to soil emissions. Soil emissions will be highest after application of nitrogen-based fertilizer. As the sun comes up, the tight boundary layer begins to break up, and air arriving at the site mixes downward. As photochemistry becomes stronger, NO is converted to NO_2 and the NO levels tail off to sub-ppbv levels once again. Nitrogen dioxide (Figures 3.2 and 3.4) levels tend to decrease during daylight hours as the boundary layer grows deeper and NO_2 is converted to HNO_3 or PAN (leading to the highest NO_y levels), or is deposited to the surface. The NO_2 mixing ratios increase into the evening as photochemistry stops and the shallow nocturnal boundary layer is formed. Deposition of HNO_3 in the shallow nighttime boundary layer causes NO_y levels to

be lowest at night (Figure 3.2).

Ozone (Figures 3.5 and 3.6) levels are lowest at night and then increase during daylight hours. By late afternoon, O_3 levels reach their daily maximum. Deposition to the surface and lack of photochemical activity decrease ozone levels at night.

Carbon monoxide (Figures 3.5 and 3.7) is relatively long-lived, and there is little discernible variation in CO concentrations over the period of a day. Its lifetime with respect to OH oxidation is a few months [e.g. Spivakovsky et al., 1990]. Thus the variation in atmospheric CO is most apparent on monthly or seasonal time scales, rather than on a daily scale.

3.6 The $[NO_x]/[NO_y]$ Ratio

The most active fraction of NO_y, and therefore the most important for ozone production, is in the form of NO_x. The ratio of NO_x/NO_y in a given parcel of air can be indicative of the degree of photochemical processing that has taken place, neglecting deposition of NO_y along the parcel trajectory path. A low ratio implies that most of the NO_2 has been converted to HNO_3 or PAN, while a ratio approaching unity implies fresh NO_x emissions. Concurrent NO_x and NO_y measurements during 1993 allowed for the analysis of this ratio at the Wye site.

Figure 3.8 shows the diurnal variation of the NO_x/NO_y ratio, reaching a

maximum early in the day before photochemistry becomes important, a minimum during sunlight hours, and a nighttime increase due to continued NO emissions and deposition of HNO_3 to the surface. The mean and median ratios for the project were 0.646 and 0.652, respectively. On more than one occasion the ratio was about equal to one, and the minimum hourly average ratio was 0.260, emphasizing the urban influence of nearby Baltimore and Washington. Winds during this time were predominantly from the west.

The U. S. Environmental Protection Agency designates the molybdenum converter as the reference method for NO_2 in urban areas to verify compliance with NO_2 air quality standards. In the polluted troposphere, the NO_x/NO_y ratio approaches unity. However, only about two-thirds of the NO_y at the Wye site is NO_x. Thus, measurements using the molybdenum converter technique reported as NO_2 could result in errors of 30-40%, and can potentially be as high as a factor of 4. This demonstrates the need for a highly specific technique for measurement of NO_2, such as the photolysis technique.

As a comparison, the ratio at two relatively rural sites, with occasional urban influence - Bondville, IL and Scotia, PA - had median ratios of 0.32 and 0.31, respectively [Parrish et al., 1993]. A rural site in central North Carolina had a median ratio of 0.26, and never reached higher than 0.57 [Poulida et al., 1994]. Dickerson et al. [1995], based upon measurements in Bermuda, determined that the NO_x/NO_y ratio was 0.12 for clean marine air not affected by local

sources or the North American continent.

3.7 The Relationship Between CO and NO_y

Carbon monoxide and reactive nitrogen compounds tend to have common sources, such as biomass burning [e.g. Crutzen et al., 1979] and fossil fuel combustion in mobile sources (cars) [e.g. Logan, 1983]. It is therefore interesting to see how the two are related.

Figure 3.9 plots the ratio $[CO]/[NO_y]$ as a function of $[NO_y]$ from the 1993 project, using hourly averaged concentrations. The average ratio for this project was 39. This compares favorably to typical ratios found by Parrish et al. [1991] at a site in Pennsylvania which is generally rural, but does "see" some urban influence. At a more rural site at 1100 m in central Virginia, Doddridge et al. [1992] found the average ratio to be 51, with mean $[NO_y]$ about 5.23 ppbv (in the fall), compared to 7.67 ppbv at the Wye site.

High $[NO_y]$ values imply relatively fresh anthropogenic emissions [e.g. Doddridge et al., 1992], generally in the form of NO_x. Therefore, at $[NO_y] > 10$ ppbv, the ratio $[CO]/[NO_y]$ provides a lower bound to the emissions ratio of CO to NO_x. The National Acid Precipitation Assessment Program (NAPAP) emissions inventory for 1985 estimates the yearly emission of CO and NO_x to be 5533 kTons and 2173 kTons, respectively, for the region including Maryland, Virginia, West Virginia, Delaware, Pennsylvania, and the District of Columbia

[NADP, 1990]. The molar (or ppbv) emissions ratio is, then, 4.18. A recent update [EPA, 1995] estimates the emissions ratio to be 6.40, based on extrapolations from 1990.

Employing the approach of Parrish et al. [1991] and Doddridge et al. [1992], the ratio of CO to NO_y at the site can be written:

$$[CO] = [CO^*] + p \times [NO_y] \tag{3.1}$$

where $[CO^*]$ is a background level of CO, and p is the molar emissions ratio of CO to NO_x. Choosing $[CO^*]$ to be 134 ppbv, the intercept from a simple linear regression plot of CO versus NO_y, results in a CO/NO_y molar ratio p = 7.73. That is, 7.73 is a lower bound on the CO/NO_x emissions ratio. This compares favorably to molar emissions ratios in the Denver metropolitan area of 7.2 in the summer and 8.2 in the winter [Parrish et al., 1991]. For comparison, the expected curves for p = 5, 10, and 20 are also shown in Figure 3.9. This choice of CO^* is similar to the Parrish et al. [1991] value of 127 ppbv, as both sites (outside of Boulder, CO, and the Wye) are relatively non-urban with occasional urban influences.

A closer look at the molar emissions ratio reveals information about the possible sources of the pollution. Considering only electric utilities output, the molar ratio is about 0.07 nationally [EPA, 1995]. If only moving vehicle emis-

sions are considered, the ratio is 10.32 nationally, and 7.56 for the five-state region considered previously. Assuming that all the NO_x is eventually converted to NO_y, and that mobile pollution sources dominate over point sources in this region, there is good agreement between the emissions inventory estimates and the analysis presented here. To corroborate this assertion, one would need to develop a flow climatology of the region to see whether or not air parcels in general are significantly affected by local point sources. This is beyond the scope of this current thesis.

To examine the value of this ratio for high levels of O_3, I have considered only the top 2.5 percentile of ozone mixing ratios ($[O_3]>66$ ppbv). The corresponding average CO/NO_y is 48 (±3), ranging from 33 to 59. The average $[NO_y]$ during high $[O_3]$ periods was 4.87 ppbv, only slightly lower than the median of 5.24 ppbv. Values for NO_x/NO_y during these times were only about 0.30-0.35, indicating only a modest degree of photochemical processing, not unexpected considering that these measurements were made during late summer/early fall in 1993. The highest ozone concentrations were observed during July 1995. Unfortunately, there were no concurrent NO_y measurements. For $[O_3]>110$ ppbv in 1995, the average CO/NO_x ratio was about 123, compared to a ratio of 92 during September 1993.

It should be noted that point sources of anthropogenic emissions such as coal-burning power plants tend to produce high amounts of NO_x and sulfur diox-

ide (SO_2) and relatively low amounts of CO, while fossil fuel combustion (e.g. mobile sources) tends to produce relatively high amounts of NO_x and CO. Therefore, a more complete analysis should include measurements of SO_2 for quantitative source attribution.

3.8 Back Trajectory Analysis

In order to characterize regional air quality, the origin of pollutants and precursors must be known. Knowledge of mesoscale and synoptic scale air motions is necessary to help explain observed levels of these pollutants at a given site. Surface winds are affected by local vegetation and man-made structures, and are thus not adequate for the following analysis.

Back trajectory analysis becomes a useful tool for examining large-scale air motions. I used the Hybrid Single-Particle Lagrangian Integrated Trajectories (HY-SPLIT) Model [Draxler, 1992] to determine pollutant origin. The HY-SPLIT model incorporates rawinsonde and high resolution Nested Grid Model (NGM) wind fields, based on analyses every hour on a 90 km grid, to represent the trajectory flow field. The model is user-friendly and runs on a personal computer. Draxler [1992] showed that absolute error in trajectory calculations, compared to aircraft observations of tracers, are of the order of 15-30% of the total travel distance, with transport times of four days. Hence, I ran two-day back trajectories to examine only the most recent parcel histories.

Forty-eight hour back trajectories with 1 hr time increments were run for the Wye site, with ending points at 1700 EST. Results from twelve model runs are discussed in the following section, providing qualitative justification for observed pollution levels.

3.8.1 "Clean" Versus "Dirty" Days

The mixing ratio of reactive trace gases such as NO_x vary greatly from day to day, and much of this variation is attributed to the large-scale flow arriving at the measurement site [e.g. Moy et al., 1994]. For the purpose of this study, "clean" and "dirty" days will be characterized by NO_x concentrations relative to mean and median hourly observed levels. At the Wye site during September 1993, the mean (and median) NO_x was 4.59 (3.19) ppbv. Corresponding values for 1995 were 3.24 (2.63) ppbv in June, and 3.71 (2.81) in July.

Tables 3.5 (1993) and 3.6 (1995) list the maximum observed mixing ratios before 1700 EST and average mixing ratios, for the chosen "clean" and "dirty" days. Two sets of averages are given. The first is the daytime average, when photochemistry is most active, while the second covers the period from 0000-1700 EST, after which time photochemistry has ended for the day. Low-NO_x days typically average 1-2 ppbv, with maximum observed [NO_x] less than the monthly average. High-NO_x days tend to have two or more hourly average mixing ratios greater than 10 ppbv, and daily averages are more than 2 ppbv

greater than monthly averages.

The corresponding CO values for these days are also listed in Tables 3.5 and 3.6. While CO and NO_x are both associated with areal sources (e.g. moving vehicles), NO_x is also associated with point pollution sources (e.g. coal burning power plants). Hence the two are not directly correlated, and the relative amounts of the two species can offer insight into the sources of the observed pollution.

3.8.2 Examination of "Clean" and "Dirty" Trajectories

Figures 3.10 (1993) and 3.11 (1995) show the HY-SPLIT model runs grouped by "clean" and "dirty" days. Trajectories for the "clean" days (Figures 3.10(a) and 3.11(a)) tend to originate from the rural southeast or from over the Atlantic Ocean. High-NO_x trajectories tend to come from the industrial midwest, or are affected by the urban centers in the region (Baltimore, Washington, Philadelphia; see Figures 3.10(b) and 3.11(b)).

The trajectories of June 24 and 28, 1995, are examples of clean North Atlantic air affecting the site. The maximum hourly observed [O_3] on these two days was below 40 ppbv. The CO levels of about 130 ppbv are characteristic of clean marine (North Atlantic) air, comparable to levels measured by Dickerson et al. [1995] in Bermuda. Note that the June mean (and median) [CO] is 177 (175) ppbv. The trajectory from September 22, 1993 is a good example of a

"dirty" day. Although the air parcels arriving at the site originated over the Atlantic Ocean, they passed over New Jersey, southeastern Pennsylvania, and near Baltimore. The maximum CO and NO_x on this day both fall in the upper 2.5% of the hourly averages for the entire month.

An example of a high-NO_x day with only moderate CO levels was September 11, 1993. The median [CO] for the month was 196 ppbv, while the average for that day was only 163 ppbv. Levels of NO_x were on average twice the monthly average on this day, implying that stationary pollution sources were more important than moving sources on this day. Without concurrent SO_2 data, however, it is more difficult to make definite statements about source attribution. Still, this back trajectory model clearly demonstrates the need to tie the synoptic scale flow to the observed chemistry at the site.

3.9 Rate of Ozone Formation

Recall the chemical reactions R1.1-R1.3 involving the photochemical triad of NO, NO_2, and O_3:

$$NO + O_3 \rightarrow NO_2 + O_2 \qquad \text{(R1.1)}$$

$$NO_2 + h\nu \rightarrow NO + O \qquad \text{(R1.2)}$$

$$O + O_2 + M \rightarrow O_3 + M \qquad \text{(R1.3)}$$

In polluted environments where there are ppbv or greater levels of NO_x, or in the absence of appreciable amounts of peroxy radicals, reactions R1.1-R1.3 represent a balance between NO_x, O_3, and UV radiation [e.g. Stedman and Jackson, 1975; Poulida et al., 1994]. This is the so-called photostationary state balance, in which net ozone is neither produced nor lost. In steady-state, the ratio Φ is equal to unity:

$$\Phi = \frac{J_{R1.2} \times [NO_2]}{k_{R1.1} \times [NO] \times [O_3]} = 1 \qquad (3.2)$$

where $J_{R1.2}$ is the rate of photolysis of NO_2, and $k_{R1.1}$ is the reaction rate of R1.1.

In more rural areas, levels of peroxy radicals are comparable to NO_x [Chameides and Walker, 1973; Crutzen, 1974; Fishman and Crutzen, 1978], and NO may be converted to NO_2 without consumption of O_3:

$$NO + HO_2 \rightarrow NO_2 + OH \qquad (R1.4)$$

$$NO + RO_2 \rightarrow NO_2 + RO \qquad (R1.5)$$

Reactions R1.4 and R1.5 disrupt the photostationary state balance, and subsequent photolysis of NO_2 leads to O_3 production via reaction R1.3. Equation 3.2 must then be modified to incorporate the net ozone production:

$$J_{R1.2} \times \frac{[NO_2]}{[NO]} = k_{R1.1} \times [O_3] + k_{R1.4} \times [HO_2] \quad (3.3)$$

$$+ \Sigma k_{R1.5} \times [RO_2]$$

According to Atkinson et al. [1989], the rate constants R1.4 and ΣR1.5 are similar. That is, at 298 K, the rates of reaction of NO with HO_2 and various RO_2 (R = CH_3, C_2H_5, and C_3H_7) are all about 8-9×10^{-12} cm^3 $molecule^{-1}$ s^{-1}, so that Equation 3.3 may be expressed as:

$$J_{R1.2} \times \frac{[NO_2]}{[NO]} = k_{R1.1} \times [O_3] + k_{R1.1} \times [HO_2]_{eq} \quad (3.4)$$

where $[HO_2]_{eq}$ represents an effective or equivalent peroxy radical concentration.

Net production of ozone due to the presence of peroxy radicals is represented by positive deviations of Φ from unity:

$$\Phi = 1 + \frac{k_{R1.4} \times [HO_2]_{eq}}{k_{R1.1} \times [O_3]} \quad (3.5a)$$

$$\Phi - 1 = \frac{k_{R1.4} \times [HO_2]_{eq}}{k_{R1.1} \times [O_3]} \quad (3.5b)$$

Finally, the rate at which ozone is formed is:

$$P(O_3) = (\Phi\text{-}1) \times k_{R1.1} \times [NO] \times [O_3] \quad (3.6)$$

In order to quantify the rate of O_3 production at the measurement site, a simple model was developed, a model similar to that described by Poulida et al. [1994]. The model incorporates the photochemical production and depositional loss of O_3 to the surface:

$$\Delta O_3 = P(O_3) - L(O_3) \quad (3.7)$$

where the rate of loss of ozone, $L(O_3)$, is given by:

$$L(O_3) = (v_d/H) \times [O_3] \quad (3.8)$$

where v_d is the dry deposition velocity of O_3 and H is the height of the surface mixed layer. The daytime value of v_d was fixed at 0.6 cm/s according to Delany et al. [1986]. The height of the mixed layer was modeled in a similar fashion to the scheme of deServes and Johansson [1995], with only slight modifications; the boundary layer was 200 m at night and rose linearly from sunrise to solar noon to a maximum of 2000 m. This model does not take into account advection of O_3 to the site or other photochemical loss mechanisms of O_3, but should at least produce first order insight into the rate at which ozone is produced at the

site.

Without measurements of peroxy radical concentrations, the photostationary state ratio Φ requires the photolysis rate of NO_2. Using the empirical formulation of Madronich [1987], $J_{R1.2}$ is given in terms of the following: UV, the output of the solar radiometer in W cm^{-2}; z, the elevation in km above mean sea level; and θ, the solar zenith angle:

$$J_{R1.2} = \frac{1.35\ UV}{(0.56 + 0.03z) \times \cos\theta + 0.21} \tag{3.9}$$

Equation 3.9 holds for zenith angles < 60° and clear skies, with an absolute accuracy of ±10%.

Table 3.7 shows the results from three cloud-free days; September 6 and 13, 1993, and July 20, 1995. Listed are the observed and calculated amounts of O_3 by hour of day. On average, the estimated ozone values on September 6 were 31% too low, on September 13 about 39% too high, and on July 20 about 21% too high, compared to the observed values. Given that the absolute accuracies of the NO and NO_2 measurement techniques are no better than 15-25%, that I have neglected horizontal advection of ozone to the site, and that I have ignored other photochemical losses, the differences between observed and estimated [O_3] are quite reasonable, lending credibility to this simple scheme. To first order at least I am able to model the boundary layer production of ozone. This

also suggests that the reported NO and NO_2 values are within experimental uncertainty of the actual values.

3.10 Estimated Hydroxy Radical Concentrations

One of the consequences of the model described in the previous section is that effective peroxy radical concentrations may be determined as deviations from steady state. Equation 3.5b may be reorganized to give:

$$[HO_2]_{eq} = (\Phi - 1) \times [O_3] \times \frac{k_{R1.1}}{k_{R1.4}} \qquad (3.10)$$

Table 3.8 shows the calculated amounts of effective peroxy radicals for daytime hours, again on September 6 and 13, 1993, and July 20, 1995. Hourly average $[HO_2]_{eq}$ ranges from near 0 to slightly above 100 pptv. At least on September 6 and July 20, there is a maximum occurring around noon. Studies in rural environments have reported similar findings [e.g. Cantrell et al., 1992; Ridley et al., 1992; Poulida et al., 1994], with maximum $[HO_2]_{eq}$ values of about 60-150 pptv occurring around 1030-1230 LT. This adds further evidence to the notion that peroxy radicals along with NO_x play key roles in the photochemical production of O_3.

A recent study by Behmann et al. [1995] found daily maxima of RO_2 on the order of 20-30 pptv. The measurement site was a coastal site in France.

The authors suggested that differences between calculated and observed O_3 values were possibly due to "missing oxidants," such as halogen oxides (most likely BrO), in addition to peroxy radicals.

3.11 Regional Air Quality

As previously discussed, NO_x is crucial to the photochemical production of ozone, and therefore is key to examining air quality. Photochemistry is quite variable on a regional scale, leading to widely varying $[O_3]$ levels. Hence, the measurement of trace gases at one fixed point is most useful when coupled with similar measurements elsewhere. In order to characterize regional air quality, observations at the Wye research site must be compared with other local observations for perspective.

The Air Chemistry Group at the University of Maryland currently maintains an air monitoring site in the Shenandoah National Park (SNP). The Big Meadows site (38.5°N, 78.5°W, 1100 m) has been previously well documented, and was used from 1989-1990 to make measurements of various trace gases [e.g. Poulida et al., 1991; Doddridge et al., 1992]. At present, various hydrocarbons, CO, O_3, NO, NO_y, and SO_2 are among the trace species monitored. K. Hallock provided the SNP data reported in this thesis.

Table 3.9 shows the mean, median, minimum, maximum, and standard deviation of hourly average O_3 mixing ratios for June and July 1995, at the SNP

and Wye sites. While the mean and median [O_3] at SNP was noticeably higher than at Wye, the Wye site saw the higher maximum observed [O_3] values. The Wye site also exhibits a larger variability, as measured by the standard deviation.

Figure 3.12 plots the diurnal variation of O_3 at both sites. On average, the SNP site has a much smaller daily amplitude (difference between minimum and maximum daily values). Poulida et al. [1991] attributed a similar small daily amplitude to the altitude of the SNP site (1100 m). Ozone concentrations at the elevated site are less affected by boundary layer dynamics than a corresponding ground-level site. Ozone concentrations at this mountain site are most affected by large scale transport from the mid- to upper troposphere, and therefore typify regional air quality. In contrast, the near-sea level Wye site is affected by strong local photochemistry, leading to higher concentrations during the day. At night, much of the O_3 is lost via dry deposition at the surface, sometimes resulting in nighttime O_3 levels below 5 ppbv. In the following section, a particular period of interest will be examined in more detail.

3.12 Severe Ozone Episode, July 12-15, 1995

A period of particular interest from the summer of 1995 occurred from July 14-15. The two highest hourly average [O_3] during the year at the Wye site, 161 ppbv and 157 ppbv, were observed during the hours centered around 1330 EST and 1430 EST, respectively, on July 15. The synoptic scale situation

is as follows [Ryan et al., 1996]. Between July 12-15, the southeast U. S. was under a high pressure system. An upper level ridge to the west, combined with downslope flow along the eastern side of the Appalachians, allowed for strong subsidence over the Mid-Atlantic region. A tightened boundary layer, local emissions of ozone precursors, strong photochemistry, and light surface winds led to extremely high observed O_3 levels during this time.

Ozone profiles generated from observations aboard a Cessna 172, upwind of the Baltimore-Washington region (Figure 3.13; data provided by R. Morales, and figure adapted from Ryan et al. [1996]) show that there was significant ozone aloft, which was transported toward the surface in the regions of strong subsidence. This profile was obtained on July 14, taken mid-morning west of Baltimore-Washington. The presence of O_3 precursors and intense photochemistry enhanced the ozone levels downwind of Baltimore-Washington. Figure 3.14 (a) and (b) shows a comparison between the observed time series at the Wye and SNP sites, on the 14th and 15th, respectively. Note that the free tropospheric levels of O_3 seen from the flight data are comparable to the levels observed at the elevated SNP site.

For insight into the air quality of the region in general, it is useful to compare the Wye values with $[O_3]$ from other local surface sites. The United States EPA manages a nationwide network of state-operated O_3 monitoring sites as part of the Aeronometric Information Retrieval System (AIRS) [EPA, 1992].

Four such sites within about a 100-km radius of the Wye site are located in Seaford, DE, and Millington, Fort Meade, and Davidsonville, all located in MD (see Figure 3.15). The Seaford and Fort Meade sites are suburban, while the Millington and Davidsonville sites are quite rural. Table 3.10 gives the location and description of each site. Hourly [O_3] from any of these EPA/AIRS sites can be obtained from an EPA telnet site (nccibm.rtpnc.epa.gov).

The hour by hour comparison of [O_3] from the Wye site and each of the four EPA/AIRS sites is shown in Figure 3.16 for July 14, and Figure 3.17 for July 15. The hours 1030 - 1930 EST are chosen to capture the daily peak at each site. The National Ambient Air Quality Standard (NAAQS) for O_3 is based on exposure to 120 ppbv for one hour. While there were several violations on the 14th (Millington experienced four violations, from 1330 - 1630), each site violated the standard during at least 3 hours on the 15th, with the exception of Seaford with no violations. Fort Meade is the closest station to Baltimore-Washington, and the two highest [O_3] at any of these stations, 174 and 168 ppbv, were observed here. Davidsonville, Millington, and the Wye site are all downwind of Baltimore-Washington as well. Seaford is far enough removed from the urban centers, and the highest observed [O_3] on the 15th was 110 ppbv.

3.13 Summary

Observations of various trace gases have been made at the Wye River

research site from 1993 to 1995. These measurements are serving to develop a chemical climatology of the research site, a site under agricultural, urban, and rural influences. Measurements at one site, however, are most useful in the sense that they are part of a larger "picture." In a regional sense, trace gases such as NO_x and O_3 vary from place to place. Care must be taken when trying to extrapolate one set of measurements, such as at the Wye research site, to a larger region, such as the entire watershed of the Chesapeake Bay.

These observations have also demonstrated the ability of the high sensitivity NO detector to perform in a real-world setting. They do not, however, test the time response of the detector. In the next chapter, eddy flux measurements of NO will be described, demonstrating the need for fast time response.

Chapter 4

Flux Measurements of Nitric Oxide

Eddy correlation is the direct, micrometeorological technique for measuring fluxes of scalar quantities in the atmosphere. After some background information on the technique itself, I will report NO flux measurements made at the Wye research site during late July, 1995. Fluxes of NO at the Wye site will be used to estimate the amount of reactive nitrogen released into the troposphere in late summer as NO from fertilized soils in the Chesapeake Bay watershed region, putting soil emissions in context with man-made inputs of NO_x. The flux measurements reported will be compared with other similar measurements, adding to the sparse and uncertain existing database.

4.1 Eddy Correlation Theory

Priestley [1959] was among the first to outline the theory behind eddy correlation. The instantaneous vertical flux of a scalar quantity, such as the mixing ratio of NO, χ, is given by:

$$F_{NO} = \rho w \chi \tag{4.1}$$

where ρ and w define the density and vertical velocity, respectively, of a turbu-

lent eddy. Any scalar "x" can be expressed as the sum of a time average (or Reynolds average) term <x> and a superimposed fluctuation term x′ , where:

$$\langle x \rangle = \frac{1}{T} \times \int x \, dt' \tag{4.2}$$

T is the averaging period, and dt′ is simply the time variable of integration. The average component of "x" is usually generated by computing a running mean with a recursive filter on the order of 100-200 s [e.g. Baldocchi et al., 1988]. Thus, the eddy flux may be written:

$$F_{NO} = \rho(\langle w \rangle + w')(\langle \chi \rangle + \chi') \tag{4.3}$$

if density fluctuations are neglected.

Since the primed quantities are random, an instantaneous flux is difficult to interpret. The average eddy flux over a given period of time ($\langle F_{NO} \rangle$) is:

$$\langle F_{NO} \rangle = \langle \rho(\langle w \rangle + w')(\langle \chi \rangle + \chi') \rangle \tag{4.4a}$$

where the averaging period is usually on the order of a half hour. The eddies are random, so that $\langle w' \rangle = \langle \chi' \rangle = 0$ (but $\langle w'\chi' \rangle$ is not necessarily zero):

$$\langle F_{NO} \rangle = \langle \rho w \rangle \langle \chi \rangle + \langle (\rho w')\chi' \rangle \quad (4.4b)$$

Finally, if the surface is flat, advective effects can be neglected, and the vertical wind speed averages to zero. Also, since the density of the eddy is constant:

$$\langle F_{NO} \rangle = \langle (\rho w')\chi' \rangle \quad (4.4c)$$

$$= \langle w'(\rho\chi') \rangle \quad (4.4d)$$

Equation 4.4d represents the average vertical flux of concentration (density × mixing ratio). In the ideal sense, the flux is simply a product of the eddy wind speed and eddy concentration components. Practically speaking, there are considerations and difficulties which arise from using this technique. These topics will be discussed in the next section.

4.2 Measurement Considerations

The rate at which flux data are sampled should be at least 2-3 times greater than the highest frequency which contributes to the flux in an appreciable manner [e.g. Baldocchi et al., 1988]. From Chapter 1, any detector making eddy correlation flux measurements must have a response at least on the order of 2u/z, where u is the mean wind speed and z is the measurement height above the zero

plane. During this flux measurement period, the mean and maximum observed hourly averaged wind speeds were 2.37 m/s and 6.51 m/s respectively. This corresponds to a minimum response on the order of 1.3 to 3.6 Hz, assuming a displacement height which is 80% of the 3 m canopy height [e.g. Kaimal and Finnigan, 1994]. Hence, the NO detector, with an upper bound response of about 3.5 Hz is adequate to capture most of the eddy flux, in an average overall sense. The sonic anemometer used during this flux measurement period samples data at a rate of 100 s^{-1} and averages 10 successive samples into 10 Hz data.

In order for eddy fluxes to be applicable to a larger area, not simply the point where measurements are taken, the upwind fetch should be uniform for a distance 100 times the measurement height. Obstacles along the fetch such as trees can introduce spurious vertical motions and, therefore, apparent fluxes. The upwind terrain should be as flat as possible. The Wye site is generally flat (grade < 3%) with a uniform corn canopy which extended > 100 m in any direction from the sampling tower at the time of the NO flux measurements. However, there were two roads and a grove of trees which bounded the corn fields within the 300-600 m fetch requirement.

The orientation of the three-dimensional wind sensor (sonic anemometer) must also be considered. Since it is very difficult to align and level the sensor, and since the terrain is rarely ideally flat, adjustments must be made to reduce $\langle w \rangle$ to zero. The technique of coordinate rotation [Wesely, 1970; Hyson et al.,

1977; Baldocchi et al., 1988] is used. Rotations about the x and z axes are made to force u to be along the mean wind vector in the horizontal (thus eliminating v), and forcing w along the vertical direction, in the frame of reference of the sensor. The fast data acquisition system calculates the two-dimensional coordinate rotation, with corrections typically on the order of 10-15° or less, but occasionally > 50°.

Chemical sensors in general have slower response times than wind sensors. The NO instrument is too bulky to collocate with the anemometer, so only the sample line is placed near the anemometer. Therefore, a delay time of about 2 s, due to the 8 m of sample tubing occurred. Wesely [1983] states that the delay time between two sensors must be no greater than 0.1z/u, or about 0.1 s, for flux estimate accuracy to be within 10%. Lag correlation analysis between the wind and NO signals must be performed to accurately (within ±0.1 s) "remove" the delay between the two signals. That is, it was necessary to determine the time lag such that the correlation between the NO and vertical wind speed signals is maximized, about 2 s. The time delay will be examined in more detail in a later section.

The separation in space of the two sensors is also a consideration. For the two instruments to be measuring the same eddies, Wesely [1983] suggests a separation distance of 0.2z, again for 10% accuracy. At the Wye site, the NO inlet and wind sensor were about 30 cm apart, within this suggested tolerance.

Nitric oxide is a highly reactive gas, which soon after being emitted is titrated by reaction with ozone (R1.1). The lifetime of reaction for the NO-NO_2-O_3 triad, assuming modest levels of ozone (~50 ppbv) and values of the photolysis of NO_2 (5-6 $\times$ 10^{-3} s) is less than 3 minutes. To determine the true NO flux, the rate of chemical loss of NO must really be considered. The measurement of NO and O_3, assuming reaction with ozone is the dominant loss mechanism, at several levels would be needed to characterize this loss, but this is beyond the scope of this thesis.

4.3 Measurement Techniques

Fast wind and temperature measurements are made with an Applied Technologies single-path orthogonal sonic anemometer-thermometer probe [Kaimal and Finnigan, 1994], shown in Figure 4.1. It is capable of measuring both horizontal (u and v) and vertical (w) wind speed components, and temperature, at a rate of 10 s^{-1}. The anemometer consists of three orthogonal transmitter/receiver transducer pairs. Each transducer serves alternately as a transmitter and then a receiver. Sound pulses are sent back and forth along the transducer pair path. The speed of sound depends on the wind speed, so that the transit times along the horizontal path will be different back and forth. The wind speed V in any direction is given by:

$$V = \frac{d}{2} \times (\frac{1}{t_1} - \frac{1}{t_2}) \tag{4.5}$$

where d is the path length (15 cm) and t_1 and t_2 are the transit times along the path. The speed of sound, c, is also a function of ambient temperature, and to a close approximation,

$$c^2 = 403 \times T \tag{4.6}$$

Since the true and virtual temperature are usually about the same (the e/p correction is small, where e is the vapor pressure and p is the ambient atmospheric pressure), and since θ_v' is taken to equal T_v', the sensible heat flux H is:

$$H = \rho c_p \times \overline{w'\theta_v'} \tag{4.7}$$

is calculated, where ρ is the density of dry air and c_p is the specific heat of air at constant pressure.

Fast ozone measurements will briefly be described. The O_3 instrument was provided to the author by Tilden Meyers and Jim Womack of NOAA/Oak Ridge. It consists of a disk coated with a silica gel, soaked in Coumarin I, a laser dye that phosphoresces when it reacts with O_3, emitting blue light. A photomultiplier tube detects the phosphorescent signal, and the output of the sensor

is from -5 to +5 VDC. To calibrate this detector, the output was compared to the output of the ozone instrument described in Section 3.3.2. Unfortunately, the fast O_3 instrument was not working concurrently with the fast NO instrument, so no ozone fluxes were recorded. There was a floating ground problem with the ozone channel of the data acquisition system. That is, the ozone channel was referencing to the ground of the NO channel. Attempts to fix this problem were unsuccessful.

Because the sonic anemometer/data storage system requires analog voltages, the signal leaving the NO detector must be converted from photon counts to voltage. David Auble from NOAA/Oak Ridge provided the author with a pulse-counting-to-voltage circuit, shown in Figure 4.2. The circuit consists of a dual precision, retriggerable and resettable monostable multivibrator (Motorola CD4538), which takes the 220 ns pulses from the NO detector, and an amplifier which allows for proportional 0-5 VDC output.

4.4 Data Processing and Evaluation

All data are sampled at a rate of 100 s^{-1}, then averaged and stored as 10 Hz data. After every 30 min period, all raw data are saved: horizontal wind speed components (u and v), vertical wind speed (w), virtual temperature (θ_v), and the other scalar quantities ([NO], [O_3]). A 200 s running mean is subtracted from the actual signal, and all quantities are stored on a laptop computer in

binary form.

At the end of each 30 minute period, the following information is computed: power spectra of all scalars, including chemical scalars; co- and quadrature spectra between w and each scalar; and lag correlation between w and each scalar. Spectra involving w and [NO] are offset by the appropriate delay time, about 2 s. Additionally, the following average quantities are calculated: wind direction, average horizontal wind speed, friction velocity (u_*), averages and variances for each scalar channel, vertical fluxes, and rotations about the x and z axes. Again, flux quantities are adjusted for delay time.

The friction velocity u_*, a measure of the magnitude of the turbulent intensity at the surface, is defined in the following way:

$$u_* = \langle -u'w' \rangle^{1/2} \tag{4.8a}$$

$$= (\tau_0/\rho)^{1/2} \tag{4.8b}$$

The quantity τ_0 is the momentum flux at the surface, or the surface wind stress, defined such that the sign of the flux of momentum is positive toward the surface. The friction velocity is a scaling parameter, the magnitude of which can be used to determine the atmospheric stability. Light winds tend to yield values of u_* of about 0.1-0.2 m/s, while moderate wind speeds give $u_* > 0.3$-0.4 m/s. If the atmosphere is too convective, the sign of $-u'w'$ is negative, and the friction

velocity is no longer defined, since the fluxes of scalars are defined for neutral stability [R. Valigura, personal communication]. Fluxes calculated when u_* is undefined are then discarded.

Earlier, it was shown that the lifetime of NO with respect to photochemical reactions involving O_3 and NO_2 is less than three minutes typically. An estimate for the turbulent transport time needed for NO to reach the sensor is given by:

$$\tau_{trans} = z/(ku_*) \tag{4.9}$$

where k is the von Karman constant (= 0.4) and z is the height of measurement. Typically, u_* was between 0.2-0.3 m/s at the Wye site, corresponding to transport times of 50-75 s. However, u_* was sometimes less than 0.05 m/s, meaning that transport time to 6 m could be five minutes or longer. Clearly, there is sufficient time for in-air reactions to greatly affect the NO flux, causing divergence in the vertical [Delany et al., 1986; Lenschow and Delany, 1987; Wesely et al., 1989].

The delay time between the NO signal and the vertical wind speed has been mentioned, and a discussion of this delay time determination follows. For the first part of the flux sampling period (before 1500 EST, July 28), the NO detector was sampling through a mass flow controller at the inlet of the detector,

or about 8 m downstream of the sample inlet on the tower. Figure 4.3 shows the lag correlation between NO and w, with a 2.3 s delay in the NO data stream removed. That is, when the NO data stream is shifted by 2.3 s, the correlation between the two data streams is maximized at a lag of 0 s. The standard deviation of the delay times from each 30 min period considered was ±0.1 s. To reduce this delay time, a capillary tube placed at the sample inlet replaced the flow controller for the second part of the flux measurement period. The capillary tube dropped the pressure in the 0.31 cm sample tubing, in effect increasing the pumping speed of the detector. This reduced the delay time of the NO signal to 1.6 s (Figure 4.4). Ideally, the pressure in the sampling line should be near the pressure in the reaction chamber (10 torr), but this is not possible through 8 m of 0.31 cm tubing.

An attempt to measure fluxes of NO_y was made from July 31 to August 1. A small, heated (370°C) molybdenum converter was placed at the sample inlet. Unfortunately, I was not able to determine a consistent additional delay time introduced by the volume of the converter, such that the correlation between the vertical wind speed and the NO_y signal was maximized. Hence, as configured, it was difficult, perhaps not possible, to measure total reactive nitrogen fluxes with a reasonable amount of uncertainty. The results from this NO flux measurement intensive, including this attempt to measure NO_y fluxes, will be briefly described in the following section.

4.5 Results

From July 25-30, 1995, fluxes of NO, along with standard meteorological parameters and the chemical species mentioned in Chapter 3 were measured. The sonic anemometer and the sampling inlet of the NO detector were mounted at about 6 m on the NOAA/ARL tower described in the previous chapter, and the data acquisition system was housed in the same sheds. The corn canopy was about 3 m high at this time. The findings from this flux intensive will be described in the following sections.

4.5.1 Basic Statistics of NO Fluxes

One hundred thirteen half-hour average NO fluxes were computed during this measurement period (Table 4.1). The mean (and median) flux of NO was 7.53 (and 7.61) ng N m^{-2} s^{-1}. The mean and median NO fluxes are reported as positive, since the source is at the surface and the sink is the atmosphere, in general. Two of the 30 minute average flux values were negative, and if the negative fluxes are ignored, the mean (and median) is 7.79 (and 7.64) ng N m^{-2} s^{-1}. Figure 4.5 is a histogram of the 113 flux values. The shaded area corresponds to times when the wind came from over the untilled field, while the unshaded area denotes times when the wind came from the tilled side. Negative fluxes suggest the existence of a compensation point for NO in the atmosphere, a construct which will be discussed in the next section. Table 4.2 lists the half

hour average basic statistics for the chemical species monitored during this flux intensive. The hourly statistics combining the months of July and August are also shown in Table 4.2 for comparison.

Figures 4.6-4.11 show the time series of average NO and sensible heat fluxes for each of the six days. Periods of rain are denoted with solid vertical lines. On July 26, 27, and 30 there is a daily maximum in NO flux around 1000-1200 EST, with a drop off later in the day. This is less evident on the other three days, with the possible exception of July 29. Nighttime NO fluxes are always positive. This suggests that observed levels of nighttime [NO] > 200 pptv are real, and can in part be attributed to soil emissions. Hence, no corrections for nighttime NO artifact signals were made [e.g. Poulida et al., 1994], unlike Doddridge et al. [1992], who measured free tropospheric air at a mountain site and, therefore, removed nighttime signals from their data.

The distribution of NO fluxes appears to be normal, upon first glance. To test the null hypothesis that the flux measurements are indeed sampled from a normal distribution, a χ^2 goodness-of-fit test was performed. For 9 degrees of freedom (10 flux groupings minus 1) and a level of significance of 0.05 (5% probability that I will reject a true null hypothesis), the critical value of $\chi^2_{9,0.05}$ is 16.919. The calculated χ^2 is 13.821, and is given by the following formula, with o_i and e_i respectively the observed and estimated (or calculated) frequencies of occurrence for a given grouping of flux values:

$$\chi^2 = \sum (o_i - e_i)^2 / e_i \qquad (4.10)$$

Because the calculated value is less than the critical value, the null hypothesis is not rejected, and the fluxes are distributed normally. Consequently, it seems reasonable to assume that indeed the NO fluxes arise from random turbulent eddies in the atmosphere. Variability in the soil environment potentially can contribute to the random nature of the NO fluxes, but the soil was mostly dry and cracked, and the corn was also dry. Hence, soil conditions probably did not change much during the period of flux measurements.

Although it appears that this entire distribution of fluxes is normal, Figure 4.5 suggests that the distribution may actually be bimodal. Fluxes of NO for times when the wind came from the untilled side are always between 0 - 4 ng N m^{-2} s^{-1}. However, this only represents 17 of the 113 half-hour fluxes. The only two negative fluxes occurred when the wind came from the tilled side. This is the western field, susceptible to pollution from Baltimore and Washington.

4.5.2 NO Fluxes as a Function of Wind Direction

Table 4.3 lists the mean 30-min average horizontal wind speeds, variance in u, and average NO flux as a function of surface wind direction. All values were binned according to wind direction octant. Fifty of the 113 fluxes were from the WSW direction, and the largest mean wind speed and variance in wind

speed corresponded to this octant. On average, relatively high wind speeds also came from the ENE, but fluxes during the times the wind was from the ENE were only about 0.93 ng N m^{-2} s^{-1}. In general, there is not much variation in wind speed based upon wind direction. However, the largest vertical fluxes corresponded to wind from the tilled side, while the lowest fluxes corresponded to winds from the untilled side.

The origin of the wind direction becomes important, considering the orientation of both the path along which flux measurements are made, and the sonic anemometer itself. The dirt path runs generally SSE to NNW, and the field is tilled to the south and west of the road and untilled to the north and east. The largest fluxes generally are occurring when the wind comes from the tilled side, while the lowest fluxes are observed when the wind passes over the untilled side. These findings suggest that tilling the soil mixes the top layers of soil, removing weeds and cover vegetation which could retain the NO in the soil. Tilling the soil increases the exposed surface area, makes oxygen more readily available for nitrification to occur in the soil, and decreases the surface resistance, allowing for the production of NO in the soil and escape to the atmosphere. The average flux from the tilled side (n = 96) is 8.65 ng N m^{-2} s^{-1}, while the average flux from the untilled side (n = 17) is 1.21 ng N m^{-2} s^{-1}, implying an upper bound of a seven-fold reduction in NO flux due to not tilling the top layers of soil.

Next, the orientation of the sonic anemometer is considered. The prevailing winds in the summer at the Wye River tend to be from the SW [R. Brinsfield, personal communication], so the sonic anemometer was oriented to face the SW. It is possible that the fluxes reported during times when the wind passed over the untilled side may be contaminated by the tower. It is also possible that the trees and road introduce spurious momentum exchange on the tilled side as well. To test the data for reasonableness, the value of u_*/u is calculated. The value for uncontaminated data should equal 0.1 [R. Valigura, personal communication]. The value of u_*/u from the tilled side was 0.1, and the value from the untilled side was 0.07. Hence, it is not possible to conclusively state that these fluxes should be discarded, so they will be kept.

4.5.3 NO Compensation Point

One possible explanation of the negative fluxes observed at the Wye site assumes that nitric oxide is in a steady state equilibrium, governed by the rate of formation in the soil and photochemical destruction after being emitted [e.g. Galbally and Roy, 1978; Delany et al., 1986; Slemr and Seiler, 1991]. Nitric oxide will continue to be emitted (in a net sense) only when the mixing ratio of NO in the atmosphere is less than the partial pressure in the soil; otherwise, deposition occurs. The level at which there is no net destruction or emission is called the compensation point.

Figure 4.12 shows the dependence of the NO flux on ambient [NO] in the atmosphere. A simple linear least-squares fit to the data and interpolation of F_{NO} to zero results in a compensation point of 1.68 ± 1.49 ppbv, based on 51 data pairs with a correlation coefficient, r, of -0.47. The uncertainty defines the central 95% confidence interval of the y-intercept from the simple regression plot. The large uncertainty is reasonable, since the 51 pairs of fluxes and mixing ratios reflect differences in time of day, temperature, and ambient conditions in the atmosphere. Of the 51 data pairs, 45 correspond to times when the mean wind passed over the tilled field and 6 for when the mean wind passed over the untilled side.

In an effort to further investigate the NO compensation point, 10 s^{-1} data for two half-hour periods are plotted. The first period was from 1100-1130 EST on July 26, and the average [NO] during this half hour was 2.25 ppbv (Figure 4.13). The value of [NO] is an estimate, since I do not have a background signal for this half-hour period. The mixing ratios are calculated by subtracting the value corresponding to the 2.5%-ile of observations during the half hour, only an estimate of the background. The 2.5%-ile corresponds to a level of NO much less than 1 ppbv. This period saw levels of NO peaking around 5 ppbv, and for half the period, [NO] was above the compensation level of 1.68 ppbv. Deposition of NO during the first 15 minutes of this period was the dominant mechanism, and the flux from 1100-1130 was -12.33 ng N m^{-2} s^{-1}. It is worthwhile to

note that during the other half-hour period with a negative flux, ambient [NO] was greater than or equal to 1-1.5 ppbv, suggesting that a compensation point of 1.68 ppbv may be an over-estimate, but not by more than 0.5 ppbv or so. Recall from Table 4.2 that the mean (and median) [NO] for the flux intensive project was 0.39 (and 0.17) ppbv.

The second period examined occurred an hour and a half later. From 1230-1300 EST on that same day, the average [NO] was 0.39 ppbv (Figure 4.14). Except for a handful of transient NO spikes, the level of NO during this half-hour period was well below the compensation level. The average flux during this time was positive at 17.67 ng N m^{-2} s^{-1}, as emission of NO dominated over deposition. Other half-hour periods with relatively low ambient [NO] exhibit the same behavior.

The existence of an NO compensation point is one possible explanation for the observed downward fluxes. Rapid in-air chemical reactions at heights of 6 m or less can also alter the flux of NO [Wesely et al., 1989; Gao et al., 1991]. If the photolysis of NO_2 is less important than the photochemical losses of NO, this can cause a reversal in the vertical gradient of NO, resulting in an apparent downward flux above the surface. Again consider the period from 1100-1130 on July 26. The high levels of NO at the sample inlet (6 m) were probably due to advection of fresh pollution to the site. High levels of NO drive the photostationary state ratio down; that is the rate of loss of NO increases (see Equation

3.2). This can result in a negative flux of NO if the in-air reactions dominate over emission at the surface.

4.5.4 Effect of Soil Moisture on NO Fluxes

Past investigators [e.g. Slemr and Seiler, 1984; Anderson and Levine, 1987; Williams and Fehsenfeld, 1991] have examined the influence of soil moisture on NO emissions. Nitric oxide is produced in soils by microorganisms, either as an intermediate step in the process of nitrification (oxidation of soil ammonium to nitrate, a form of nitrogen useful to plants; aerobic process) or denitrification (conversion of nitrate to molecular nitrogen; anaerobic process) [e.g. Lipschultz et al., 1981; Johansson and Galbally, 1984; Firestone and Davidson, 1989]. Microbes require water, but can survive extensive dry periods. Water saturation in soil restricts the diffusion of ammonium and oxygen crucial for nitrification to occur, inhibiting the process of nitrification as a source for NO. Finally, the wetting of dry soil can decrease the stress on soil microbes, and inhibit the diffusion of oxygen through the soil environment allowing for increased denitrification to occur. Hence, the effects of soil moisture on NO fluxes at the Wye site will be discussed.

Table 4.4 lists the rainfall amounts observed from July 25-30, 1995, at the Wye site. The soil was quite dry, as there was little observed rainfall during June and July. The total rainfall from June 6-30 was 43.6 mm, with more than

half occurring during one hour periods in June 11 (14.4 mm) and 24 (9.8 mm). About 66.6 mm of rain was recorded between July 1-30, with the two largest events observed during one hour periods on July 17 (13.2 mm) and 24 (15.8 mm). It should be noted that the average (1941-1985) rainfall at the Wye site is 90 mm in both June and July [R. Brinsfield, personal communication]. During the flux measurement period, the soil surface was visibly hard and dry during the day; however, no reliable soil moisture measurements are available for this time.

Williams and Fehsenfeld [1991] saw large increases in NO fluxes immediately following rain events onto previously dry soils, sometimes by nearly an order of magnitude. From Figures 4.8-4.10 (corresponding to 27-29 July) it appears that NO fluxes are increasing following periods of light rain. Unfortunately, there is a lack of data sufficiently long enough following these rain events to demonstrate a definite short-time increase in the fluxes. Still, it appears that on the 27th and 28th, light rain added to previously dry soils increased NO fluxes by 4-5 ng N m^{-2} s^{-1}, while on the 29th there is an indication that the flux is increasing as well.

Another factor involving soil moisture is the level of the water table. At various places in the field site, the water table is only 1 m deep, and never more than about 4 m deep. This is potentially another source of water for the microbes, which may not have been so moisture-stressed as to stop the denitrifica-

tion and nitrification processes from taking place.

4.5.5 Effect of Temperature on NO Fluxes

Past investigators [e.g. Slemr and Seiler, 1984; Anderson and Levine, 1987; Williams and Fehsenfeld, 1991] have also looked at the influence of soil temperature on NO flux rates. Flux rates tend to increase with soil temperature until biogenic processes become stressed. Beyond some temperature, heat and soil desiccation reduce soil microbial activity, and fluxes no longer increase.

Soil temperature was not recorded during this flux measurement period, so the temperature at 6 m will be used as a proxy. Air temperature was always greater than 25°C for the flux periods reported, and the soil surface temperature is probably about 5°C warmer than the air. Figure 4.15 shows the effect of air temperature on NO flux rate. Little correlation is deduced from this plot ($r = -0.04$), due partly to the already high temperatures, and partly to the fact that air temperature may not be a sufficient substitute for soil temperature. However, if only periods of emission are considered, and taking only air temperatures less than 31°C, a weak linear fit is deduced ($r = 0.26$; Figure 4.16).

From Figure 4.15 there is an indication that the NO flux is beginning to decrease above air temperatures of about 30-32°C. Williams and Fehsenfeld [1991] suggest that for soil temperatures above 35°C, biogenic activity in the soil is suppressed. My findings are consistent with this supposition, assuming

that the soil surface temperature is about 5°C greater than the air temperature at 6 m.

Clearly, soil moisture and temperature are closely tied to each other. They are two variables which need to be monitored carefully for a more complete analysis of fluxes of NO from soils. Additionally, the type and amount of fertilizer applied to the soil, vegetative cover, and time of year strongly influence NO emission from soils. Table 4.5 is a comparison of some spring- and summertime NO fluxes. Two of the measurement sites were cornfields, while the other nine sets of fluxes were taken over grassland. The final two grassland measurement sets were made using the eddy correlation technique, and my flux measurements compare favorably with these reported values. There is a spread covering several orders of magnitude due to varying conditions. Also worth noting is the fact that there are currently few existing eddy correlation NO flux measurements in the published literature.

4.6 Fluxes of Total Reactive Nitrogen

As mentioned in Section 4.4, an attempt was made to measure the flux of total reactive nitrogen, NO_y, by placing a small molybdenum converter at the sample inlet on the NOAA/ARL tower. It was not possible to determine the additional delay between the w and NO_y data streams caused by the converter. The fluxes listed in Table 4.6 are from eight-30 min periods, not accounting for

the additional delay time caused by the converter. Lag correlation analysis was performed on the NO_y and w data streams, and lags ranging from about 0 to 2.2 s were observed. Hence, the fluxes are presented to give an order of magnitude estimate of summertime NO_y fluxes during the evening and morning. By placing a capillary tube upstream of the molybdenum converter instead of using a flow controller at the NO detector, one would reduce the residence time in the sampling tubing, allowing for a better estimate of the lag time.

Recall that NO is generally emitted from the soil, and other NO_y species such as HNO_3 and NO_2 are deposited to the surface. This means that the net flux of NO_y can be upward or downward, depending on the soil environment, boundary layer dynamics, and amounts of ambient reactive nitrogen species. The diurnal variation of the ratio of NO_x to NO_y from September 1993 (Figure 3.8) suggests that deposition of HNO_3 at night is an important mechanism in determining the flux of NO_y. The downward flux of NO_y should dominate the upward emission of NO. Keeping in mind only eight fluxes are reported, the positive sign of the fluxes reported in Table 4.6 may reflect the incorrect delay between the w and NO data streams, and further study is needed to accurately assess the delay caused by the molybdenum converter if NO_y fluxes are to be measured in the future.

4.7 Implications of NO Fluxes From Soils

Having measured NO emissions from soils, it is next logical to see how important these soil emissions are to the total NO_x budget. Nitric oxide is emitted from the soil through the processes of nitrification and denitrification which result from the large amounts of fertilizer applied to agricultural lands. Given a rate of N-based fertilizer application and estimates of the amount of NO emitted as a fraction of the fertilizer applied, a yearly estimate of NO emitted from soils can be determined.

The U. S. average rate of N-based fertilizer application is 140 kg N ha^{-1} yr^{-1} [Lin et al., 1995], while the amount applied at the Wye research site is 159 kg N ha^{-1} yr^{-1} [Staver, personal communication]. Typical losses of NO from agricultural soils as a fraction of the fertilizer applied range from about 0.4% [Harrison et al., 1995] to 0.79% [Anderson and Levine, 1987]. Hence, in the state of Maryland the amount of NO emitted from the soil is about 2-4 ng N m^{-2} s^{-1}. There are 6.35×10^5 ha of harvested land in Maryland [U.S. Dept. of Commerce, 1994], resulting in about 0.4-0.8 Gg N yr^{-1} being emitted from agricultural soils. An estimate of the 1990 anthropogenic NO_x emissions in the state of Maryland [Maryland Dept. of the Environ., 1993] is 106 Gg N yr^{-1}, where about 95 Gg N yr^{-1} come from the following urban and industrial counties: Allegheny, Anne Arundel, Baltimore (County and City), Charles, Frederick, Harford, Howard, Montgomery, Prince Georges, and Washington. The other 11 Gg N yr^{-1} come from the rural counties in Maryland.

It appears that the amount of NO coming from soils contributes little to the yearly NO_x budget in the state of Maryland. However, if I use the mean summertime NO flux measured at the Wye research site, 7.53 ng N m^{-2} s^{-1}, this brings the total NO emitted from soils to 1.5 Gg N yr^{-1}, about 10-15% of the anthropogenic NO_x emitted in the rural counties of Maryland in the summer. This value is more representative of the NO emitted from soils, as most of the NO is released in the summer after fertilization. Taking the five-state region of Pennsylvania, Virginia, Maryland, Delaware, and West Virginia into account increases the NO soil emission to 8.4 Gg N yr^{-1}. The yearly emissions presented here represent an upper limit, as not all harvested land is treated with nitrogen-based fertilizer. For example, only about 20% of soybean fields in the U. S. are fertilized with nitrogen, while about 97% of corn fields are [Lin et al., 1995]. This entire region effects the Chesapeake Bay watershed. Apparently, the amount of NO released into the atmosphere from soils can be significantly reduced by simply not tilling the soil.

Farmers who choose to till their fields do so for weed control, and for the aesthetic value of applying seed and fertilizer to a clean surface [e.g. Phillips and Phillips, 1984]. While the no-till practice of farming does require the increased use of pesticides, many advantages exist. They include drastic reductions in soil runoff, reductions in surface runoff of fertilizer and soil nutrients, and reductions in fuel consumption because large tilling machines are not needed [e.g. Phillips

and Phillips, 1984; Smith et al., 1995]. Crop yields between the two techniques are similar. In particular, Brinsfield and Staver [1991] report that corn yields at the Wye site from 1985-1991 were comparable, with yields from the no-till fields slightly higher. No-till agriculture, then, will decrease pollution (because heavy machinery is not used) and may increase farmer profitability. Reductions in NO emission, then, further strengthen the argument for no-till agriculture.

From Chapter 3, the poorest air quality with respect to high ozone levels in this region occurs during the summer months, due to a combination of meteorology, photochemistry, and availability of precursors. Harrison et al. [1995] showed that about 90% of the NO emitted from fertilized soil is released within 25 days of fertilizer application. Therefore, the highest soil emissions around the Chesapeake Bay will occur in the summer, precisely when conditions are most favorable for photochemical ozone formation. Any reductions in NO_x, including emissions from soils, in this region can improve the quality of the air.

The NO_x emission limit for light-duty vehicles from model years 1980-1993 is 1 g NO_2 per mile, or 0.3 g N $mile^{-1}$ [EPA, 1995]. If the average car in the five-state region is driven 10,000-20,000 miles yr^{-1}, then the average car emits up to 3000-6000 g N yr^{-1}. Assuming that no-till agriculture reduces soil NO emissions by a factor of seven, soil emissions could be reduced by 7 Gg N yr^{-1} if all agricultural soil is not tilled in this region. This would be equivalent to removing 1 to 2 million cars from the roads in the region surrounding the

Chesapeake Bay during the summer months.

4.8 Spectral Analysis of Fluxes

Turbulent eddies in the atmosphere occur over many orders of magnitude in time and space. It is therefore useful to examine the time series of individual species and their cross correlations to see what time and length scales are dominant, and to confirm that flux instruments have sufficient frequency response to measure the flux at these dominant scales.

4.8.1 Power Spectrum Analysis

Power spectrum analysis estimates the variance of a given time series as a function of contributing frequencies. A thirty minute average NO flux calculation involves the product of w' and $[NO]'$ sampled at a rate of $10\,s^{-1}$. To understand the spectral aspects of these scalar time series, the fast Fourier transform (FFT) is used. Implicit in the FFT analysis is the fact that a time series can be expressed as a sum of independent harmonics, and that the variance of the time series is a function of these harmonics. Figure 4.17 shows the variance (or power) of a typical w time series as a function of frequency. The variance is very noisy, so a smoothed-fit curve is superimposed to maintain the general shape of the spectrum but smear out some of the highest frequency details. The spectral data was smoothed with a Stineman weighting function, a discrete func-

tion with unity magnitude at the principal weight and decreasing magnitude away from the principal weight. All additional power spectra will be plotted as smoothed curves.

The non-dimensional frequency relates the temporal domain with the spatial domain:

$$n = 2\pi fz/\langle u \rangle \tag{4.11}$$

where f is the frequency (s^{-1}), z is the measurement height, and <u> is the mean horizontal wind speed. Taylor's "frozen turbulence" theory [e.g. Kaimal and Finnigan, 1994] states that measurements of eddies in time (frequency domain) at a fixed point in space are related to spatial scales (wavenumber domain) if it is assumed that the eddies don't change as the mean wind advects them past the sensor. This allows for the use of the non-dimensional frequency defined in terms of a wavelength scale $\lambda \equiv \langle u \rangle / 2\pi f$.

Figure 4.18 plots the frequency-weighted power spectra of u and w for the half-hour period from 1600-1630 EST on July 25, and Figure 4.19 plots w and NO for that same period. These plots are typical of all periods, so only this one will be discussed in detail. The FFT works best when the number of data points N is a power of 2, so N=2048 was chosen for this project. The frequency band Δf in Figures 4.18 and 4.19 is defined by:

$$\Delta f = 1/(N\Delta t) \tag{4.12}$$

where the time step Δt is 0.1 s (corresponding to the 10 s^{-1} sampling rate). Choosing N=2048 results in 1024 harmonics (N/2), since the amplitude and phase of a given harmonic requires two Fourier coefficients. The highest resolvable frequency f_0 is the Nyquist frequency:

$$f_0 = (N/2)\times(1/(N\Delta t)) = 1/(2\Delta t) \tag{4.13}$$

and equals 5 Hz in the temporal domain.

The frequency-weighted power spectra shown in Figures 4.18 and 4.19 compare favorably with idealized wind speed spectra [e.g. Kaimal and Finnigan, 1994]. The value of the spectra at the very highest frequencies is not real; it is due to the curve-smoothing and should be ignored. A discussion of the shape of the spectra follows [e.g. Tennekes and Lumley, 1972; Kaimal and Finnigan, 1994].

Turbulent eddies arise from instabilities in the large-scale (lowest frequencies) mean flow. Most of the turbulent energy is found in the largest scale eddies. Some of the power in the low frequency end of the spectrum may also be due to contamination from diurnal variations or synoptic scale changes. Further instabilities break up the eddies, and energy cascades toward smaller

scales. Turbulent energy is dissipated at the smallest scales (highest frequencies) through the effects of viscosity. Intermediate between the energy containing range and the dissipation range is the inertial subrange. As the spectrum approaches the highest frequencies (n ~ 1-10), it falls off as -2/3 in log-log representation (Figure 4.18). This -2/3 slope, deduced from dimensional arguments [e.g. Tennekes and Lumley, 1972], was observed by Kaimal et al. [1972] in the 1968 Kansas campaign.

The NO power spectrum from Figure 4.19 also exhibits an energy-containing region and at least the beginning of an inertial subrange. However, there was noise at the highest frequencies. Part of this is due to the fact that the frequency response of the detector is about 3-3.5 Hz. Electrical noise was a problem with the pulse-counting-to-voltage converter and the data logging system, which showed up in the NO and O_3 channels at high frequencies and did not show up in the wind speed channels. This implies that although the spectra for NO were less than ideal, the NO signal at high frequencies was not correlated with the w signal at high frequencies. Rather, the variance in the NO signal at high frequencies was real and due to electrical/instrumental noise. The consequence of this will be further discussed in the next section.

4.8.2 Cospectrum Analysis

The cospectrum between two scalar time series is the real component of

the cross spectrum. The cross spectrum is a measure of the correlation between the two time series as a function of frequency, since in general two time series are not correlated equally at all frequencies. The cospectrum is given by the product of the deviations from the means of two time series as a function of frequency. It is therefore a measure of the frequency dependence in the vertical NO flux, in the case of w and NO.

Figure 4.20 shows a typical frequency-weighted cospectrum between w and NO for the same time period mentioned in the previous section. Most of the power corresponds to time scales on the order of 3-30 s. There is little or no contribution to the NO flux above frequencies above n~5-10. Thus, the noise in the NO signal is not contributing appreciably to the NO flux. Unfortunately, this means that the fluxes do not reflect any real contributions of the very highest frequencies.

To make sure that the NO flux was due to the NO signal itself and not background artifact signals, the instrument was operated in background mode for a half-hour period. The cospectrum between w and NO background signal is shown in Figure 4.21. Below frequencies of n~5-10, there is little correlation between the NO and w signals, and the area under the curve is about zero. Therefore, the background signal is not contributing significantly to the NO flux below n~5-10.

4.9 Summary

Nitric oxide fluxes were measured at the Wye research site during late July 1995, and fluxes were reported for a six-day period from July 25-30. The average (and median) flux was 7.53 (and 7.61) ng N m^{-2} s^{-1}, based upon 113 half-hour averages. The fluxes reported here do not cover a wide range of temperature or soil moisture conditions, but are representative of late summer values. The NO flux values in the literature are very widespread, and my values fall within the ranges of fluxes measured under similar conditions. Few NO flux measurements made with the eddy correlation technique exist, and my values add to the small database. Clearly, there is a great need for more research in the area of eddy correlation measurements of NO, including the area of soil emissions.

These NO fluxes, measured along a dividing line between a tilled and untilled field, appear to depend on the wind direction. That is, the fluxes from the untilled field are considerably less than those from the tilled side. Not tilling the soil may reduce the NO being emitted to the soil by as much as a factor of six. NO soil emissions in the state of Maryland make up about 1-2% of the total NO_x budget. The NO emitted from soil may be equal to about 10-15% of the total man-made NO_x emitted in the rural counties in Maryland.

For the Chesapeake Bay area, though, soil emissions may be relatively significant, contributing as much as 8.4 Gg N yr^{-1} to the region. By simply not

tilling the agricultural soil, NO emissions can potentially be drastically reduced expending no effort, in addition to reducing local pollution and potentially increasing farmer profitability. If the entire region around the Chesapeake Bay switched to no-till agriculture, the reductions in NO emissions (by a factor of seven) would be equivalent to removing 1 to 2 million cars from the roads during the smog season. This would help reduce the photochemical formation of ozone during the summer months and improve air quality to the Chesapeake Bay region.

Chapter 5

Recommendations and Discussion

This dissertation has described the development and characterization of a fast response and high sensitivity NO detector. The instrument has a 20 pptv detection limit for a 1 s accumulation time. Its response time is 0.1-0.2 s to a step change, and 0.28±0.05 s to a sinusoidally varying input signal. The instrument has been used at a site on Maryland's Eastern Shore from 1993 to 1995 to help make air quality measurements. Measurements of nitric oxide are important because nitrogen oxides are critical to the photochemical production of ozone. The site experienced the influence of agricultural and urban emissions, and at other times saw relatively clean air originating from over the Atlantic Ocean. Ozone measurements at the Wye research site were compared with other sites in the Chesapeake Bay region during a high ozone episode, highlighting the role of the urban areas to the photochemical formation of ozone, and demonstrating that the relatively rural Eastern Shore of Maryland can be subject to elevated ozone levels. Ozone episodes occur in the summer as a result of meteorology, availability of precursors, and sunlight.

To understand the role of NO soil emissions, eddy correlation flux measurements were made at the site during the summer of 1995 for a six day period. The average NO flux from a fertilized corn field, about 6 weeks after fertiliza-

tion, was found to be 7.53 ng N m^{-2} s^{-1}. An upper limit on the emissions from agricultural soils in the region surrounding the Chesapeake Bay is estimated to be 8.4 Gg N yr^{-1}. It was also determined that the practice of not tilling soil may reduce NO emissions by up to a factor of seven. This is equivalent to removing about 1 to 2 million cars from the road, with respect to emissions of NO_x, during the photochemical smog season, assuming that all the NO is emitted from soils during the summer months. This would reduce the amount of precursors of O_3, leading to improved air quality in the mid-Atlantic region, with the potential to increase farmer profitability. Reduction in NO emissions from soils is another advantage of this agricultural practice over conventional tilling.

5.1 Improvements to the NO Detector Design

In Chapters 3 and 4, I demonstrated that the NO detector was capable of making high sensitivity measurements. It can be used for making fast response eddy correlation measurements, and is robust enough to run unattended for months at a time in the field. It has a wide dynamic range, capable of monitoring clean rural air, or air under urban influence. Still, there are modifications which would enhance its performance.

It has been shown in the past [e.g. Steffenson and Stedman, 1974] that the chemiluminescent signal is proportional to the amount of ozone generated. The detector currently has an ozone generator which is capable of producing

about 2% O_3 with an oxygen feed. Ozonology (Illinois) produces a corona discharge custom ozone generator capable of making about 5% O_3. It is a large (50 mm diameter, 30 cm long) glass cylinder with a stainless steel tube inside, similar to but larger than the ozonizer found in Thermo Environmental's (Massachusetts) Model 14B NO-NO_x Analyzer. This design has been tested [W. Luke, personal communication] up to oxygen flows of about 200 cc/min. This ozonizer has the potential to increase the chemiluminescent intensity by a factor or 2-2.5, assuming the reaction chamber geometry, vacuum pump, and sample inlet flows are kept the same.

Another problem with detecting the chemiluminescent signal is that the PMT is about 5 cm away from the end of the reaction chamber. The weak signal falls off with the square of the distance, and the photon collection efficiency is reduced. Products for Research can custom manufacture a shorter PMT housing, reducing the distance between the signal source and the PMT. A longer socket assembly would also reduce this distance.

Also, the time delay for a given length and diameter of sample tubing, and pumping speed must be determined in the laboratory. For the flux measurements presented in this dissertation, the NO data stream was shifted such that the correlation between the vertical wind speed and [NO] was maximized at zero lag. An attempt to quantify this delay was tried in the field by filling a balloon with calibration gas, and then popping the balloon near the sonic anemometer

and NO inlet. However, I was unable to obtain a reproducible delay time. Agreement between the delay time determined from the lag correlation analysis and from a real determination would be highly desirable.

Finally, the apparatus used for the sinusoidal input response time determination did not generate a true sinusoidal signal. It produced a signal equivalent to a sinusoid in an rms sense. A better sinusoidal input could be generated using a wheel with a notch of varying width, widest at the top and narrower approaching the bottom, with only a small amount of aluminum keeping the wheel intact at the bottom.

5.2 Unattended Air Quality Monitoring

Chapter 3 describes the findings from long-term chemical and meteorological measurements at a site on the Eastern Shore of Maryland. It is an interesting site, because it is under agricultural, rural, and urban influence at different times. In July 1995, this site, downwind of Baltimore and Washington, saw some of the highest hourly averaged O_3 levels in this region. At other times during the summer, clean marine air arrived at the site, resulting in low levels of NO_x and CO. Back trajectory analysis was incorporated with chemical measurements to determine air mass origins.

The existing data set of reliable measurements of ozone precursors, in particular NO_x, is rather limited away from urban areas. I showed in Chapter 3

that the EPA-approved method for determining compliance of air quality with respect to NO_x, the molybdenum converter technique, is simply not sufficient for areas away from cities. It is critical to be able to measure sub-ppbv levels of NO and NO_2 with a method free from large interferences. The photolytic converter technique should be used to monitor NO_x where PAN and HNO_3 levels can be comparable to or larger than levels of NO_2.

Oxides of nitrogen, O_3, and CO are all important trace species which play key roles in air quality. Sulfur compounds are also important, as they contribute to the problem of acid rain. Sulfur dioxide has not been measured at the Wye site, but future research will include SO_2 measurements. In Chapter 3, I used back trajectories to show that air with high NO_x levels often originated from the industrial Midwest, or passed directly over urban areas. Coal-burning power plants also produce high levels of SO_2, as coal in the eastern part of the country tends to be rich in sulfur [e.g. Finlayson-Pitts and Pitts, 1986]. Knowledge of NO_x and SO_2 simultaneously would strengthen the argument that air coming from the Midwest can be influenced by the existing matrix of point sources of pollution, namely power plants. Low mixing ratios of SO_2 combined with high NO_x and CO would suggest the dominance of moving sources (e.g. cars).

5.3 Flux Measurements

The flux intensive from July 25-30, 1995 contributed to the few pub-

lished eddy correlation NO flux measurements. However, this is only a brief period in late summer. It was hot, and what little rain was available probably did little but dampen the soil surface. If flux measurements are to be studied in a temporal context, there must be varying weather and soil conditions. To describe variations throughout the year, measurements should be made for about two weeks during each season. Seasonal flux measurements could be extrapolated to better estimate a yearly budget for NO soil emission.

The site at the Wye River is fertilized twice a year with nitrogen-based fertilizer, in May and June. To investigate the role of fertilizer, flux measurements should be made prior to and immediately after application. Additionally, it may be important to look at the role of vegetation on NO emission. Vegetation restricts the turbulent eddies at the soil surface. The vegetation also reduces the soil temperature and alters the local soil environment [e.g. Slemr and Seiler, 1984], and provides surfaces for the removal of NO. Hence, it may be useful to quantify the reduction in flux by measuring before and after the corn is planted. Corn grows rather quickly, so it will only be a couple of weeks between no corn canopy and a canopy several 10's of cm high.

The issue was raised in Chapter 4 that some of the reported NO fluxes may have been artifacts of a sonic anemometer incorrectly aligned with the mean wind flow. Varying the orientation so that the anemometer sometimes faces the wind passing over the tilled side, and sometimes faces the untilled side will

allow for better testing the theory that tillage practices affect the NO flux. An omnidirectional anemometer could also remove the dependence on wind direction.

Nitric oxide emitted from the soil is a result of either denitrification or nitrification by microbes. Nitrous oxide (N_2O) is also an intermediate in these processes [e.g. Firestone and Davidson, 1989]. Concurrent measurements of N_2O would support the idea that the observed NO fluxes were indeed due to soil processes. Nitrous oxide is long-lived in the atmosphere, and is a greenhouse gas and a source of stratospheric NO [e.g. Cicerone, 1989].

Another issue raised in Chapter 4 involves the rapid reactions between NO, NO_2, and O_3 which alter the NO flux even at a height of only 6 m. To address this, NO fluxes should be made at more than one height. Vertical measurements of fluxes could help determine when these reactions are significantly altering the flux, in conjunction with concentrations of NO, NO_2, and O_3 relative to their photostationary state values [e.g. Gao et al., 1991] .

Table 2.1. Nitric oxide detector characterization.

Sample Flow Rate	700 - 1000 cc/min
Oxygen Flow	250 cc/min
O_3/O_2 (by volume)	~2%
Ozonizer High Voltage	6650 VAC
Typical Sensitivity	~ 1 - 2 counts s^{-1}/pptv
Detection Limit	20 pptv @ 1 s accumulation time
Response Time - step input	~ 0.1-0.2 s
Response Time - sinusoidal input	~ 0.28±0.05 s

Table 3.1. Trace gas species monitored at the Wye site, with dates of measurement.

Year	Chemical Measurements	Dates
1993	NO, NO_x, NO_y, O_3, CO, UV flux	Sep. 2 - 28
1994	NO, NO_x, O_3, CO, UV flux	Aug. 27 - Oct. 10
1995	O_3, CO	Jan. 6 - Sep. 21
	NO	Mar. 18 - Aug. 3
	NO_x	Jun. 10 - Aug. 3
	NO_y	Aug. 3 - Sep. 21
	UV flux	Mar. 18 - Sep. 21

Table 3.2. Basic statistics for reactive nitrogen species, O_3, and CO at the Wye site for (a) 1993 (Sep. 2-28), and (b) 1994 (Aug. 27 - Oct. 10), in ppbv. All values reported hereafter are hourly averages.

(a) 1993 (Sep 2-28)

	Daytime NO	NO_2	NO_y	O_3	CO
Mean	0.56	4.20	7.67	28	211
Median	0.10	3.05	5.24	26	196
Minimum	0.00	0.52	1.07	1	95
Maximum	14.78	20.68	48.66	76	628
16.5%	0.03	1.21	2.97	11	142
83.5%	0.76	7.39	12.14	45	274
2.5%	0.01	0.75	1.75	1	108
97.5%	2.90	13.40	27.45	66	495

(b) 1994 (Aug 27 - Oct 10)

	Daytime NO	NO_2	O_3	CO
Mean	0.54	6.28	27	247
Median	0.12	4.38	25	231
Minimum	0.00	0.00	1	109
Maximum	10.89	36.88	86	588
16.5%	0.01	1.53	11	175
83.5%	8.59	11.94	43	323
2.5%	0.00	0.01	3	143
97.5%	3.96	17.80	64	432

Table 3.3. Basic statistics for (a) daytime NO and (b) NO_2 at the Wye site for 1995, by month in ppbv.

(a) NO

	March	April	May	June	July
Mean	2.37	1.47	1.16	0.52	0.50
Median	1.65	0.77	0.63	0.43	0.25
Minimum	0.02	0.00	0.00	0.03	0.02
Maximum	13.30	16.18	10.59	2.32	4.60
16.5%	0.40	0.16	0.14	0.18	0.12
83.5%	3.71	2.80	2.04	0.89	0.76
2.5%	0.10	0.03	0.01	0.07	0.12
97.5%	7.82	6.85	5.43	1.59	3.21

(b) NO_2

	June	July
Mean	2.84	3.27
Median	2.37	2.44
Minimum	0.18	0.14
Maximum	15.22	16.39
16.5%	1.11	1.03
83.5%	4.11	5.08
2.5%	0.39	0.59
97.5%	9.39	12.43

Table 3.4. Basic statistics for (a) O_3 and (b) CO at the Wye site for 1995, by month in ppbv.

(a) O_3

	Jan	Feb	Mar	Apr	May	Jun	Jul	Aug	Sep
Mean	21	20	30	40	46	39	55	46	40
Median	20	21	31	39	44	35	50	42	37
Minimum	1	1	1	7	8	10	9	4	2
Maximum	44	40	58	78	96	106	161	124	105
16.5%	10	11	19	29	30	21	25	25	22
83.5%	31	28	40	52	60	60	78	67	56
2.5%	2	2	5	17	21	13	14	12	9
97.5%	36	34	52	68	76	83	125	92	83

(b) CO

	Jan	Feb	Mar	Apr	May	Jun	Jul	Aug	Sep
Mean	249	284	259	226	212	177	210	168	159
Median	244	262	244	216	207	175	206	157	152
Minimum	125	158	134	132	127	100	107	78	100
Maximum	511	893	635	593	471	396	479	382	364
16.5%	155	215	202	187	171	133	154	124	124
83.5%	325	347	307	258	246	214	261	214	186
2.5%	131	185	160	169	143	111	128	100	109
97.5%	430	530	443	360	313	277	3353	274	272

Table 3.5. Maximum and hourly average [NO_x] and [CO] for (a) "Clean" and (b) "Dirty" days at the Wye site, 1993, in ppbv. Averages are for daytime (0930-1630 EST) and 0030-1630 EST.

(a) "Clean" Days

Day		Maximum	0930-1630	0030-1630
9/13	NO_x	2.58	1.80	1.66
	CO	---	---	---
9/26	NO_x	3.65	2.21	2.12
	CO	239	211	186
9/27	NO_x	3.28	2.18	2.31
	CO	209	136	167

(b) "Dirty" Days

Day		Maximum	0930-1630	0030-1630
9/11	NO_x	16.38	10.83	8.50
	CO	201	159	163
9/12	NO_x	10.55	5.78	6.43
	CO	221	177	191
9/22	NO_x	20.89	8.45	10.81
	CO	394	310	327

Table 3.6. Maximum and hourly average [NO_x] and [CO] for (a) "Clean" and (b) "Dirty" days at the Wye site, 1995, in ppbv. Averages are for daytime (0930-1630 EST) and 0030-1630 EST.

(a) "Clean" Days

Day		Maximum	0930-1630	0030-1630
6/24	NO_x	2.49	1.47	1.48
	CO	160	129	128
6/28	NO_x	2.37	1.37	1.55
	CO	141	130	119
8/01	NO_x	1.65	0.70	1.01
	CO	210	192	177

(b) "Dirty" Days

Day		Maximum	0930-1630	0030-1630
6/14	NO_x	13.43	3.08	6.90
	CO	232	181	196
7/19	NO_x	20.44	5.56	10.15
	CO	275	225	224
7/24	NO_x	16.06	1.21	5.40
	CO	298	166	211

Table 3.7. Estimated (and observed) [O_3] for September 6 and 13, 1993, and July 20, 1995 at the Wye Site, in ppbv.

Time	September 6	September 13	July 20
830	-- (--)	-- (--)	63 (60)
930	25 (34)	33 (39)	66 (72)
1030	23 (48)	48 (40)	73 (75)
1130	33 (53)	56 (42)	86 (76)
1230	39 (58)	64 (46)	97 (77)
1330	40 (60)	73 (50)	106 (71)
1430	44 (66)	75 (53)	109 (81)
1530	56 (62)	84 (53)	112 (95)
1630	55 (66)	82 (51)	117 (89)

Table 3.8. Effective peroxy radical concentrations ($[HO_2]_{eq}$) based on O_3 production rates at the Wye site, for Sep. 6 and 13, 1993, and July 20, 1995, in pptv.

Time	September 6	September 13	July 20
830	--	--	45
930	16	48	18
1030	~0	76	36
1130	91	55	117
1230	80	67	104
1330	12	76	78
1430	31	26	42
1530	104	70	38
1630	~0	~0	50

Table 3.9. Comparison of $[O_3]$ basic statistics for (a) June 1995 and (b) July 1995, between the SNP* and Wye research sites, in ppbv.

(a) June 1995

	SNP	Wye
Mean	57	39
Median	57	35
Minimum	18	10
Maximum	95	106
Standard Deviation	13	20

(b) July 1995

	SNP	Wye
Mean	61	55
Median	61	50
Minimum	33	9
Maximum	98	161
Standard Deviation	12	29

* SNP data provided by K. Hallock, Dept. of Chemistry, University of Maryland.

Table 3.10. Chosen EPA/AIRS [EPA, 1992] O_3 monitoring sites. SEA = Seaford, MIL = Millington, FTM = Fort Meade, DAV = Davidsonville.

Site	Location	Location Setting/Land Use
SEA	38.64° N, 75.61° W	suburban/residential
MIL	39.31° N, 75.80° W	rural/agricultural
FTM	39.06° N, 76.73° W	suburban/commercial
DAV	38.90° N, 76.65° W	rural/agricultural

Table 4.1. Basic statistics of NO fluxes (F_{NO}) with and without negative values, in ng N m^{-2} s^{-1}.

	all fluxes	$F_{NO} > 0$ only
Mean	7.53	7.79
Median	7.61	7.64
Minimum	-12.33	0.00
Maximum	21.67	21.67
Standard Deviation	5.07	4.68

Table 4.2. Basic statistics of chemical concentrations, all in ppbv for (a) July 25-30 (30-min averages), and (b) July and August combined (hourly averages). August NO and NO_2 data is only Aug 1-3.

(a) July 25-30

	CO	O_3	Daytime NO	NO_2
Mean	195	58	0.39	3.10
Median	183	54	0.17	2.07
Minimum	58	7	0.00	0.04
Maximum	416	172	5.21	18.50
16.5%	144	30	0.06	0.81
83.5%	246	80	0.60	4.97
2.5%	111	17	0.02	0.44
97.5%	335	142	1.94	12.12

(b) July/August (combined)

	CO	O_3	Daytime NO	NO_2
Mean	185	51	0.49	3.12
Median	175	47	0.24	2.32
Minimum	78	4	0.00	0.14
Maximum	479	161	4.08	16.39
16.5%	130	25	0.10	0.88
83.5%	236	74	0.85	5.13
2.5%	104	14	0.01	0.58
97.5%	316	116	2.11	11.40

Table 4.3. Average horizintal wind speed (ms^{-1}), variance in wind speed (m^2s^{-2}), and NO flux (ng N $m^{-2}s^{-1}$) for each wind direction octant.

Wind Direction	u	σ_u^2	NO Flux	Number
NNE	2.31	0.91	2.12	4
ENE	2.42	0.97	0.93	13
SSW	1.54	0.25	4.12	3
WSW	2.66	1.31	9.50	50
WNW	2.35	0.95	7.98	43

Note: There are no flux data for times when the wind was from the ESE, SSE, and NNW directions.

Table 4.4. Rainfall amounts, in mm, observed during the July 1995 Wye flux measurement period.

Day	Time (EST)	Rainfall Amount
25th	0400-0500	0.2
27th	2100-2200	0.4
	2200-2300	1.4
	2300-2400	0.6
28th	0500-0600	0.2
29th	1600-1700	0.8
	1700-1800	0.2

Table 4.5. Compilation of spring- and summertime NO flux measurements over (a) corn, and (b) grassland. Fluxes are in ng N m^{-2} s^{-1}. Eddy correlation measurements are denoted with an asterix. Over corn, average fluxes are also reported in parentheses.

(a) Corn

Location	Dates	NO Flux Range	Reference
Jamestown, VA	Jul - Aug, 1984	1.6 to 19.5 (5.2)	1
Rock Springs, PA	Aug, 1986	1.6 to 338 (94)	2

(b) Grassland

Aspendale, Australia	Nov, 1976	0.6 to 2.6	3
Mainz, Germany	Jul, 1983	-0.1 to 2.9	4
Bennett, CO	May & Jul, 1985	0.001 to 16.03	1
Boulder, CO	Aug, 1985	0.28 to >2	5
Nunn, CO	Jul, 1988	1.15 to 52.9	6
Venezuela	Jan, 1990	0.4 to 3.0 (dry soil) 5 to 25 (after rain)	7
Boulder, CO	Aug, 1991	0.9 to 6.62	8
Boulder, CO*	Jun - Jul, 1983	~ -20 to 30	9
NE Illinois*	Spring, 1984	1.4 to 4.2	10

References: 1, Anderson and Levine, 1987; 2, Williams et al., 1988; 3, Galbally and Roy, 1978; 4, Slemr and Seiler, 1991; 5, Parrish et al., 1987; 6, Williams and Fehsenfeld, 1991; 7, Rondon et al., 1993; 8, Willliams and Davidson, 1993; 9, Delany et al., 1986; 10, Wesely et al., 1989

Table 4.6. Estimated net fluxes of total reactive nitrogen, NO_y, from July 31 to August 1, 1995, at the Wye site. Fluxes are in ng N m^{-2} s^{-1}. Positive net fluxes are upward.

Day	Time (EST)	Flux
July 31	1600	0.88
	1630	2.44
	1700	2.62
	2200	0.83
	2230	0.15
August 1	730	2.22
	800	-1.32
	830	4.09

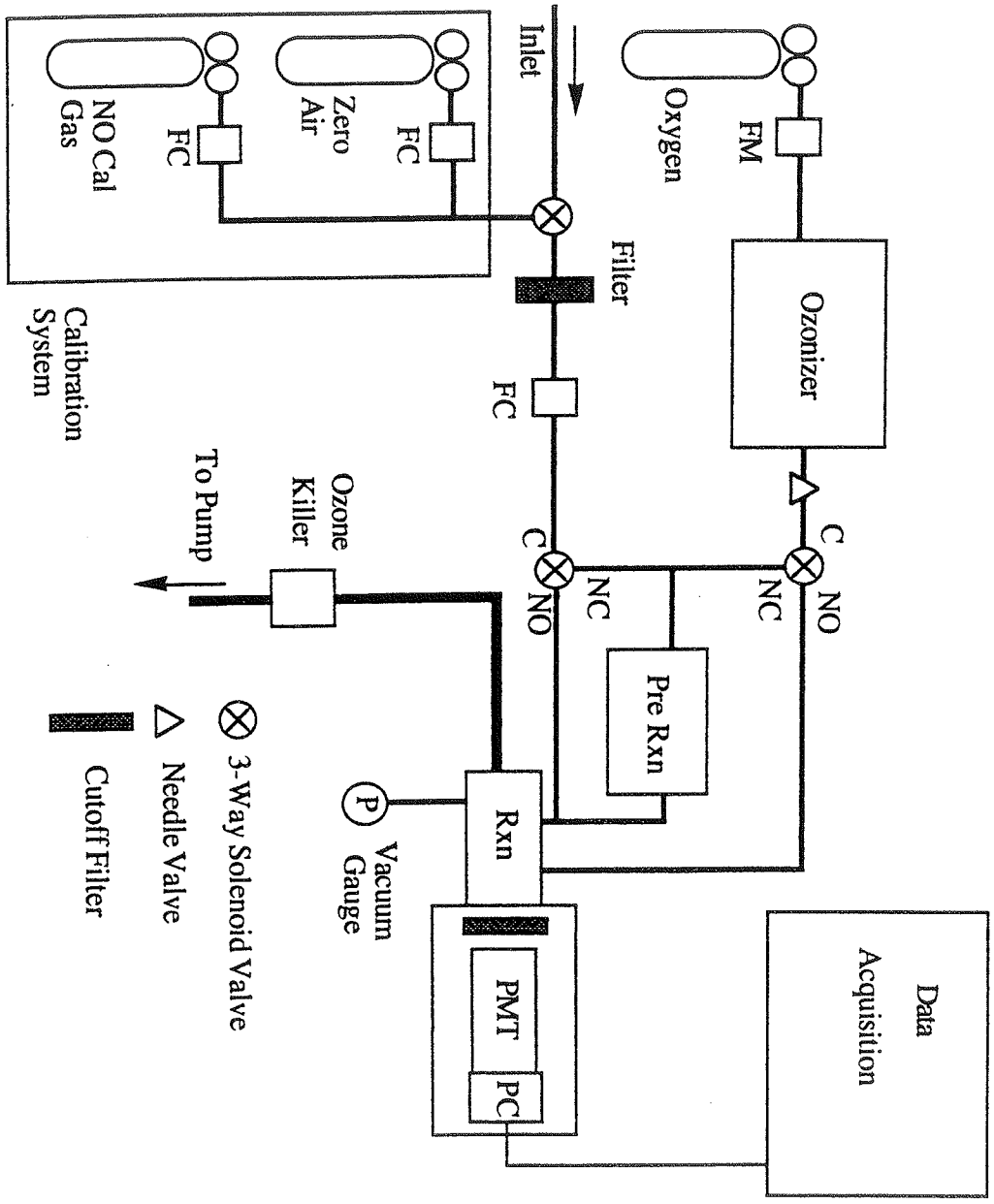

Figure 2.1. Schematic of the NO detector. PC = photon counting unit; FC = mass flow controller; FM = mass flowmeter; RXN = reaction chamber; Pre RXN = prereactor; PMT = photomultiplier tube.

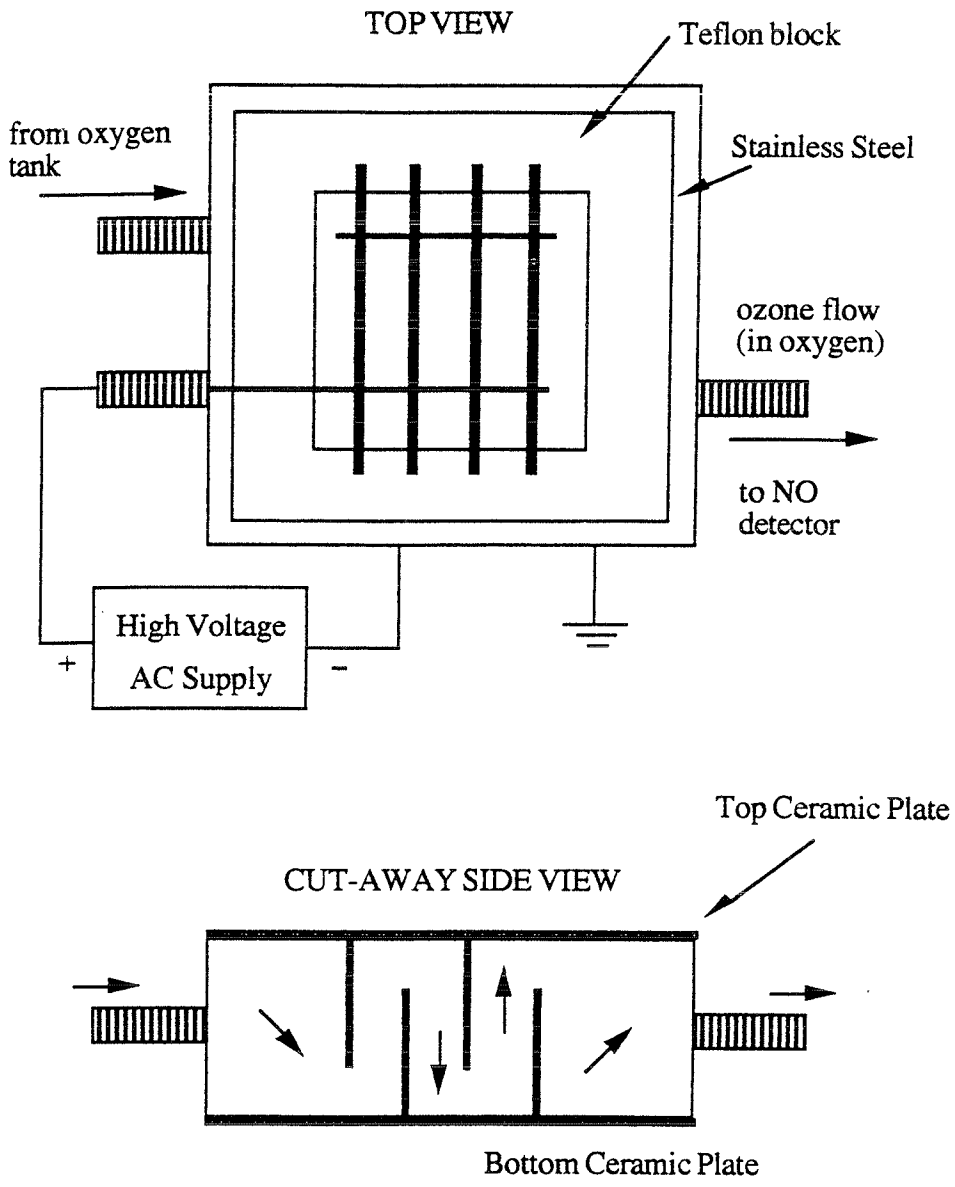

Figure 2.2. Schematic of the ozonizer. Top view shows electrical connections to the four stainless steel plates. Side view shows the ceramic wafers, and the path of ozone/oxygen flow through the block.

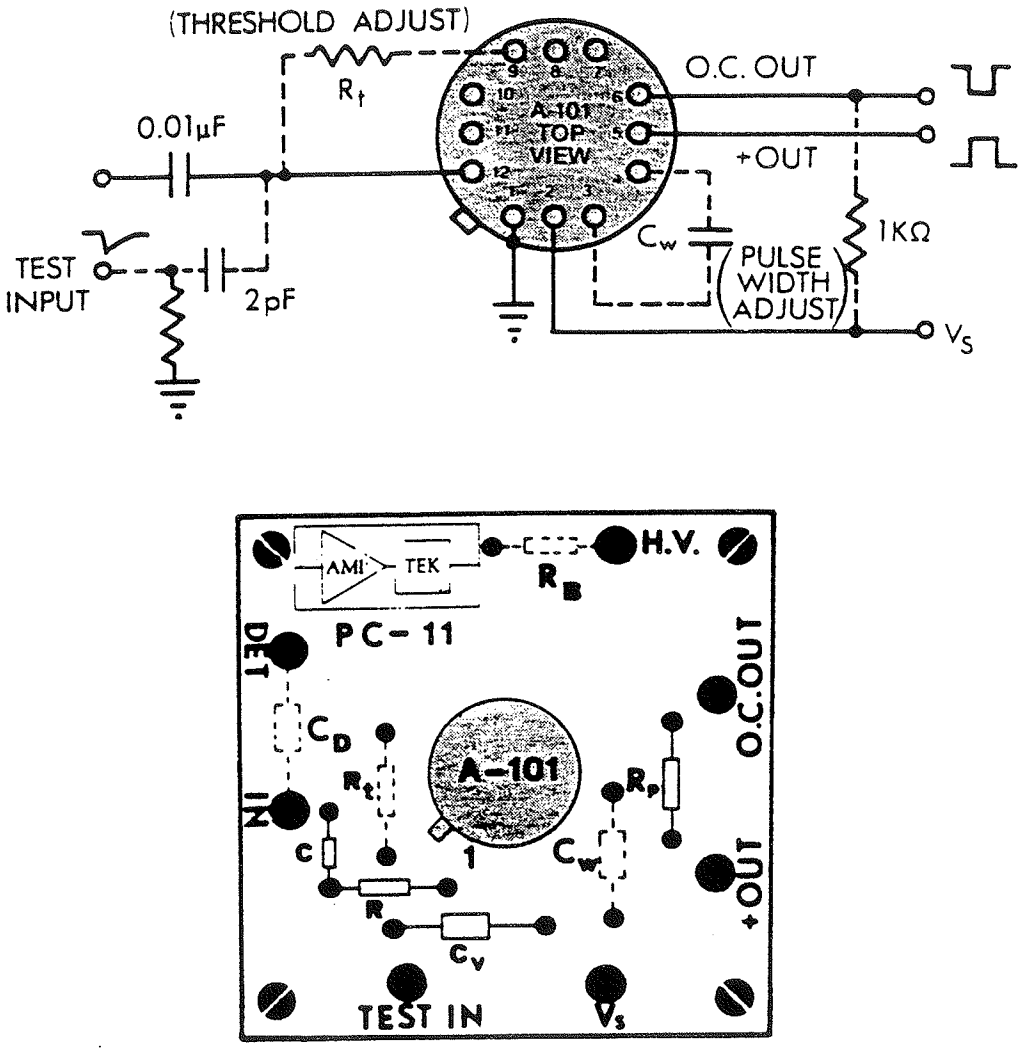

Figure 2.3. Photon counting unit with printed circuit board. Pins: 1, ground; 2, +5V supply; 3 & 4, open (default output pulse of 220 ns); 5, output; 6-8, 10 & 11, open; 9, open (default minimum input threshold for maximum output); 12, input from PMT. Courtesy of Amptek, Inc. (Bedford, MA).

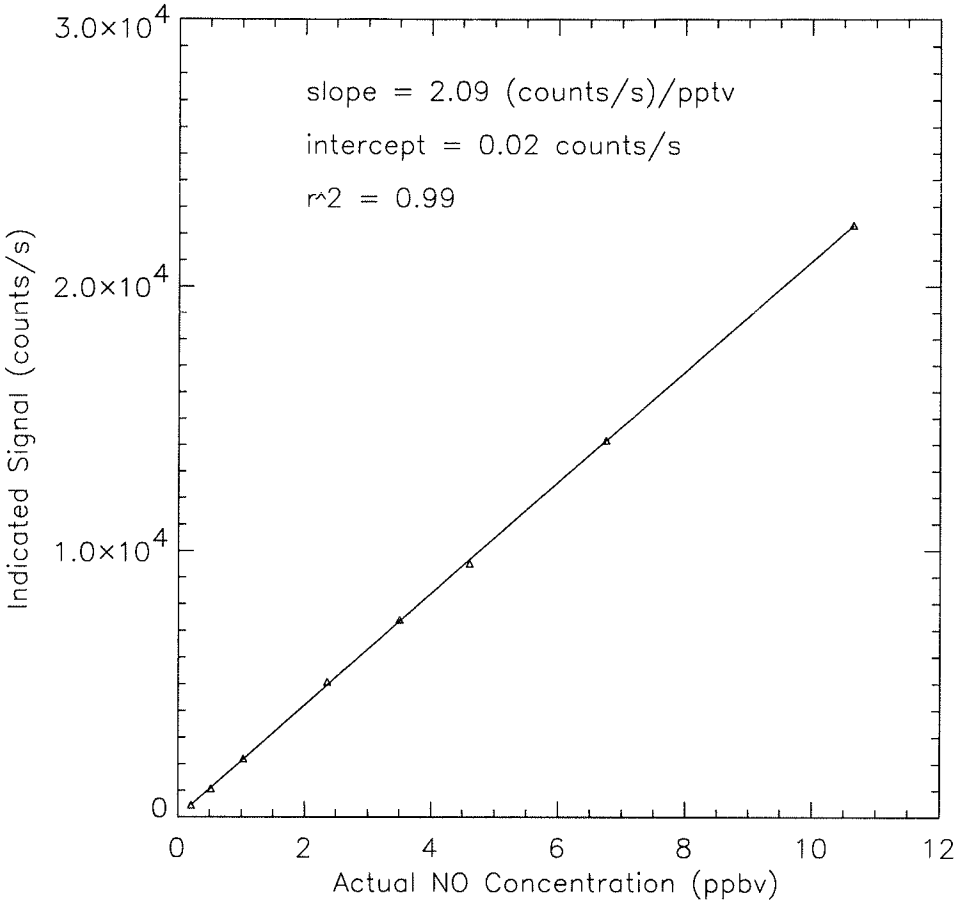

Figure 2.4. A sensitivity curve for the NO detector. In this example, the sensitivity is 2.09 counts s^{-1}/pptv.

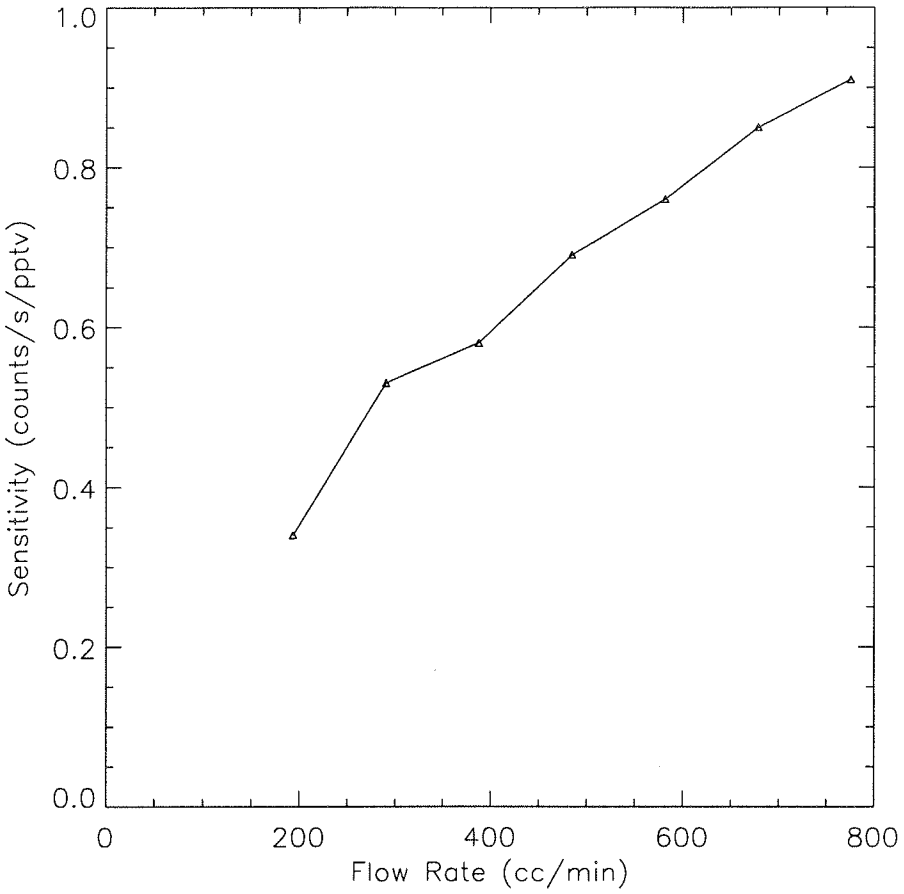

Figure 2.5. Effect of inlet flow rate on the NO detector sensitivity. The actual [NO] for this determination was 4.84 ppbv.

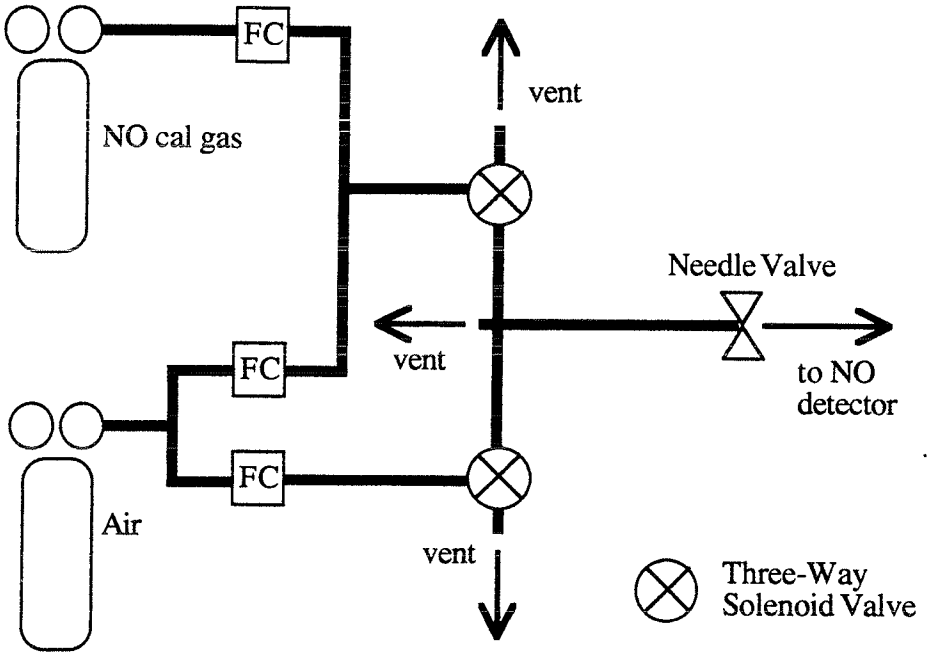

Figure 2.6. Schematic for the determination of the time response to a step change in concentration. FC = mass flow controller.

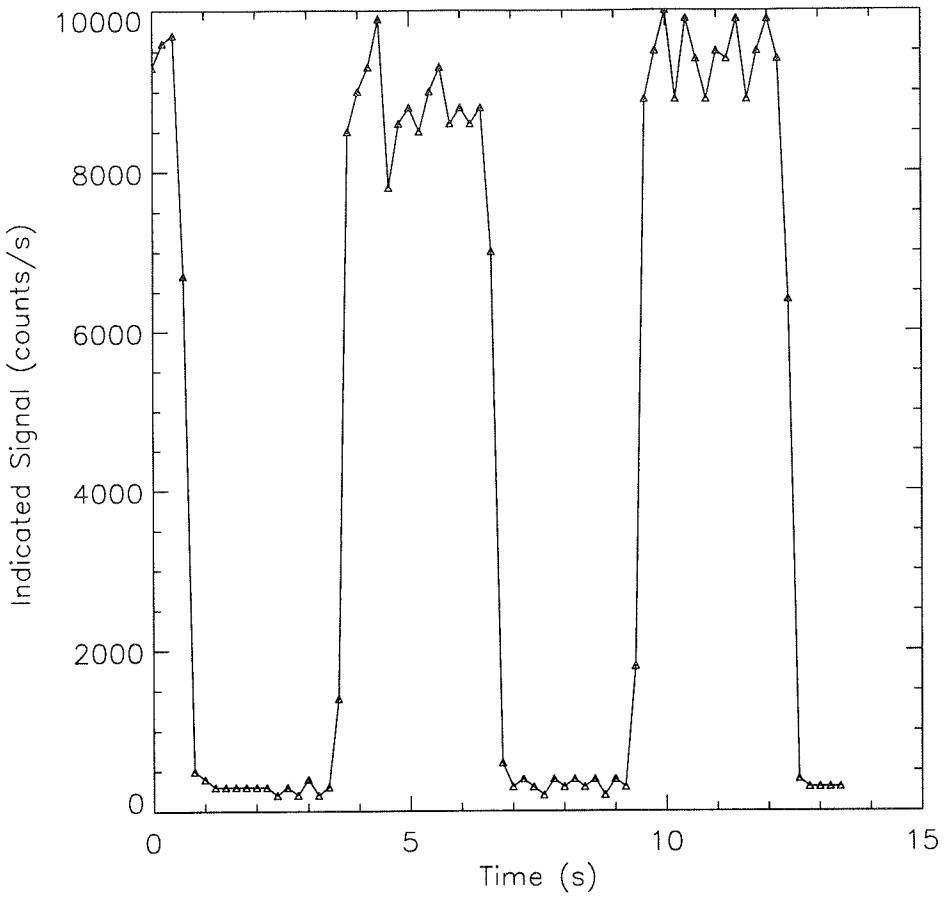

Figure 2.7. Output of the NO detector from a series of step changes in concentration, in 0.2 s increments.

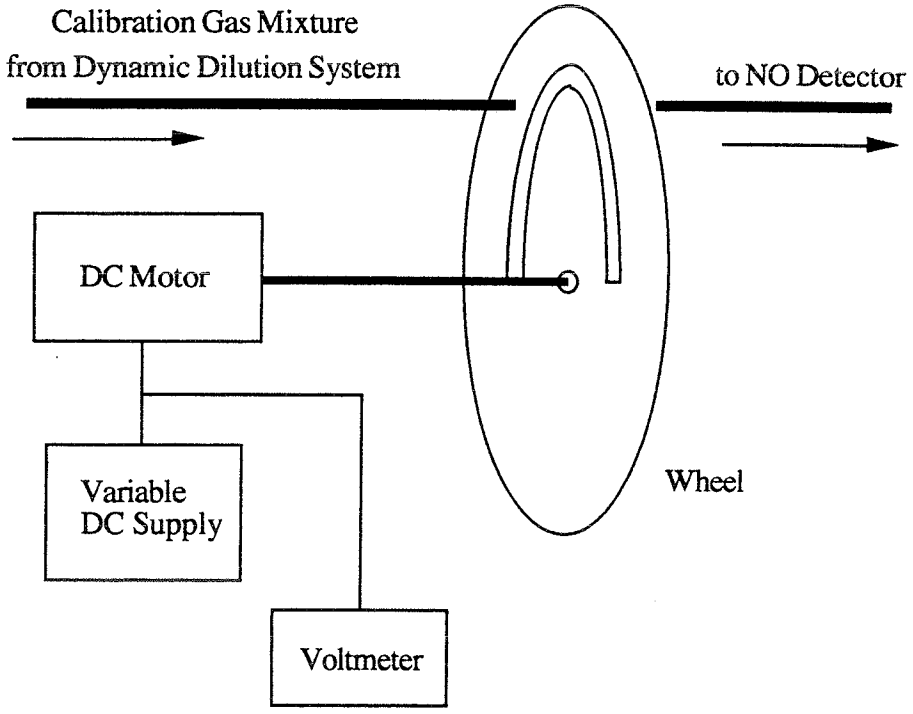

Figure 2.8. Apparatus for the generation of a sinusoidal input into the NO detector.

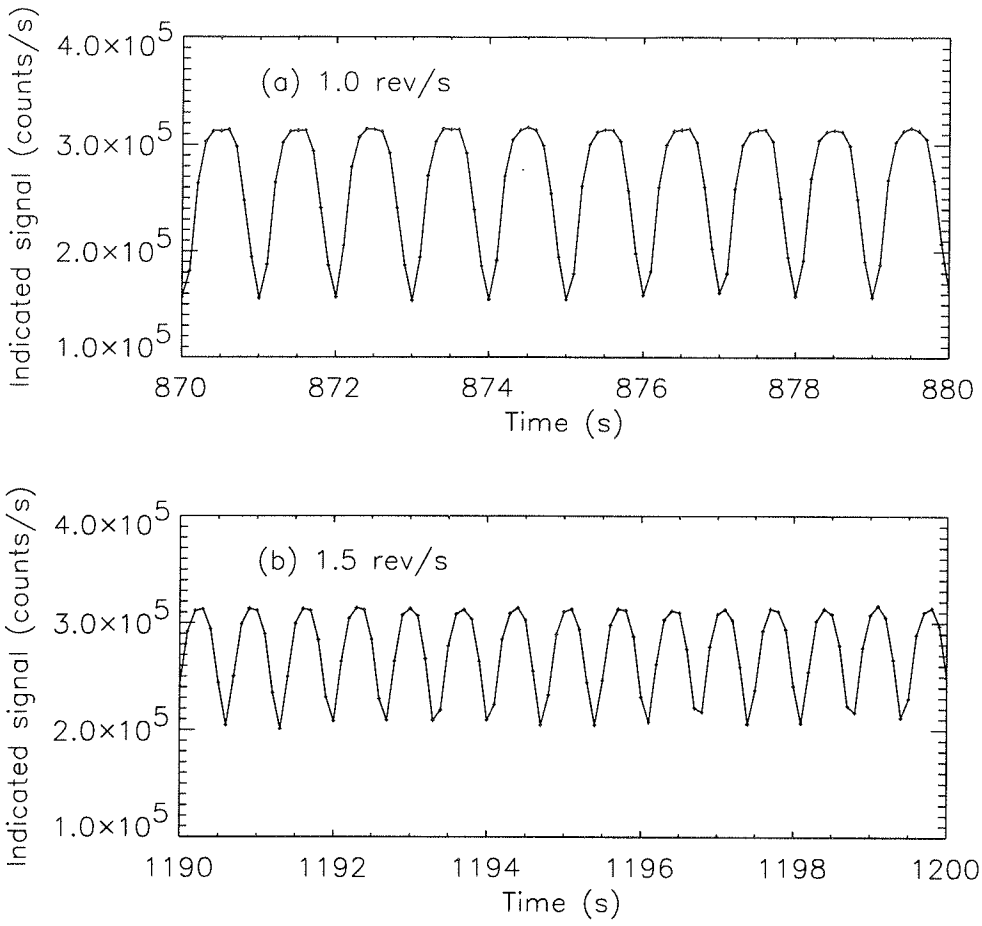

Figure 2.9. Output of the NO detector when the input concentration is modulated sinusoidally at (a) 1.0 revolutions s^{-1} and (b) 1.5 revolutions s^{-1}, in 0.1 s increments.

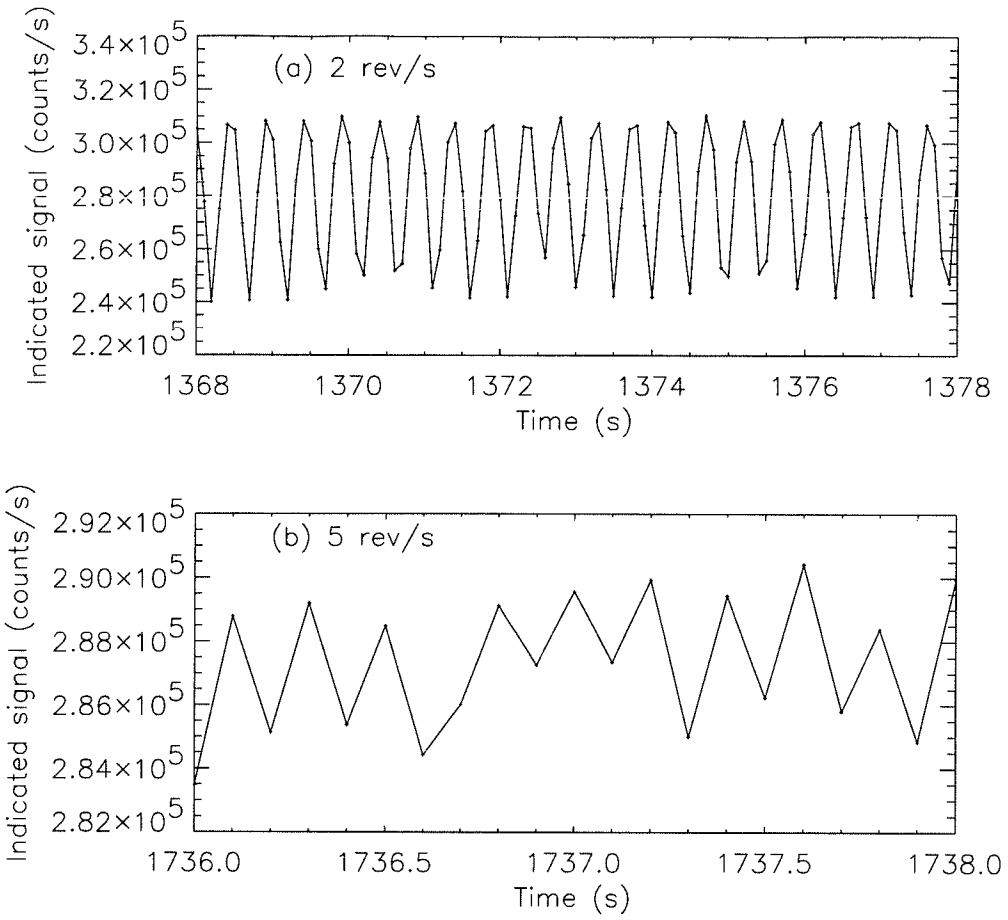

Figure 2.10. Output of the NO detector when the input concentration is modulated sinusoidally at (a) 2 revolutions s^{-1} and (b) 5 revolutions s^{-1}, in 0.1 s increments.

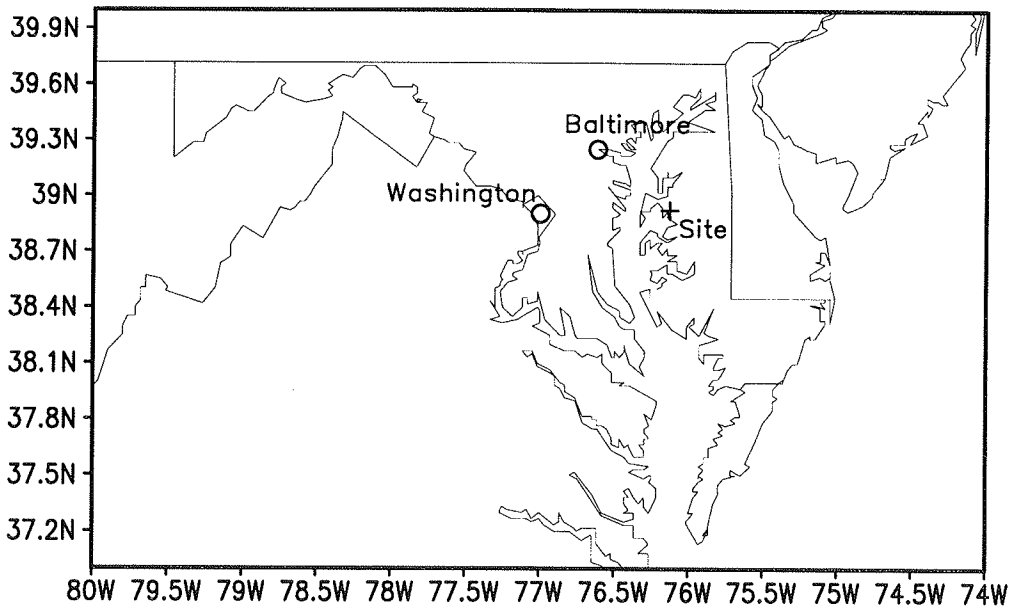

Figure 3.1. Regional map showing the Wye research site in relation to the Baltimore-Washington urban corridor.

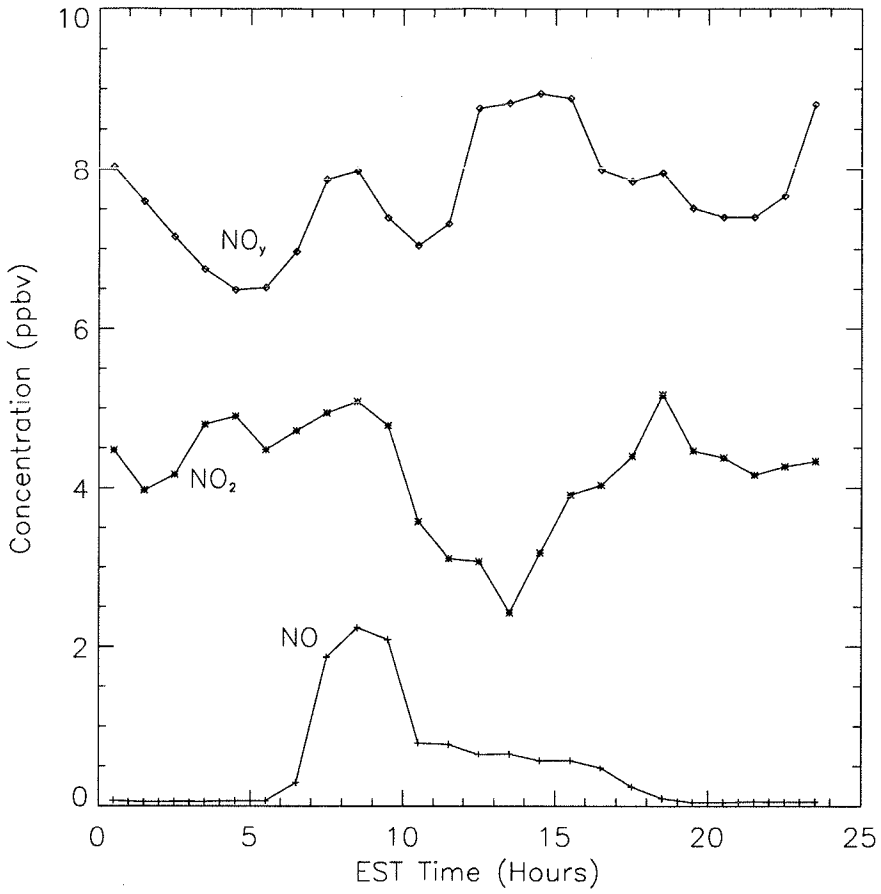

Figure 3.2. Diurnal variations of NO, NO_2, and NO_y at the Wye site, September 2-28, 1993. Values reported are in ppbv.

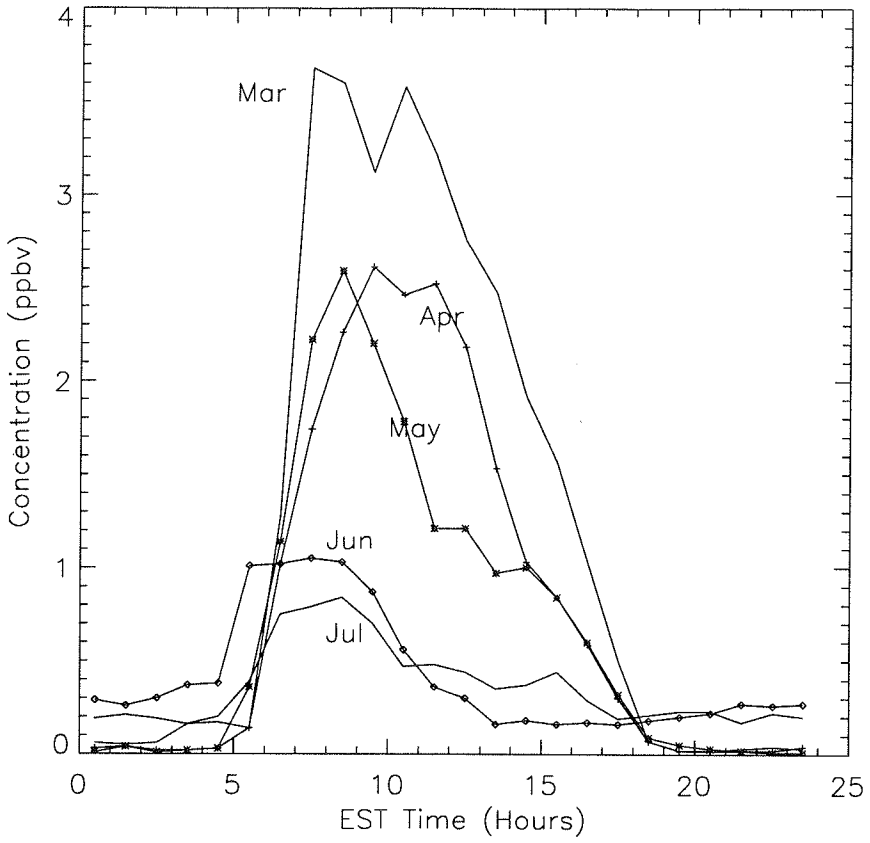

Figure 3.3. Diurnal variation of NO at the Wye site in 1995 by month.

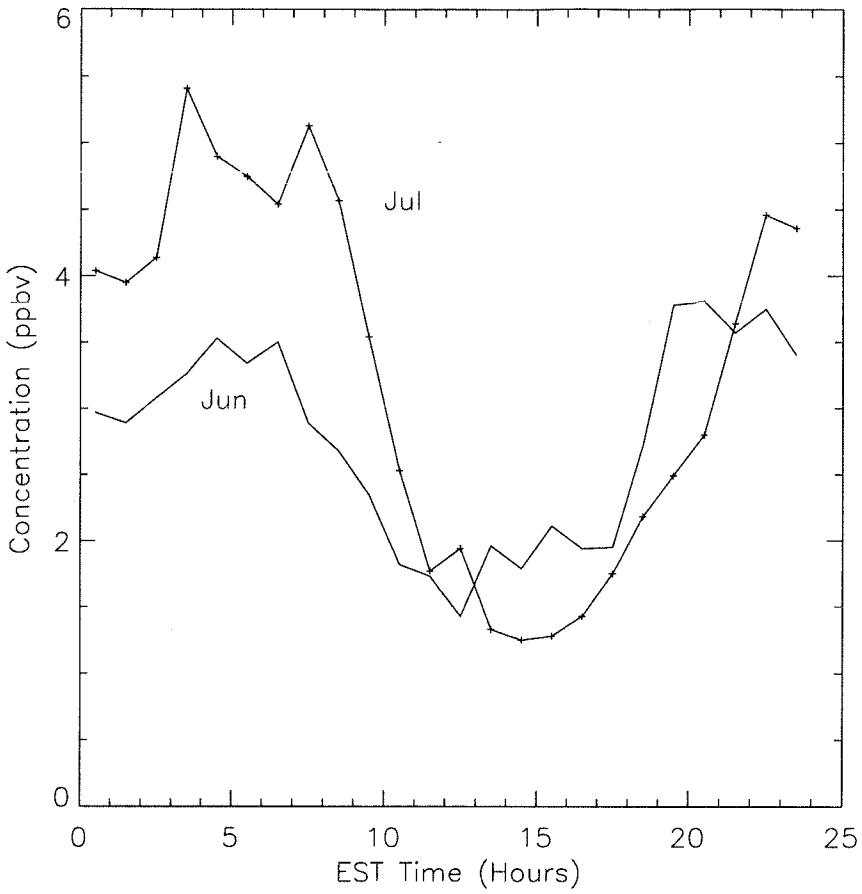

Figure 3.4. Diurnal variation of NO_2 at the Wye site in 1995 by month.

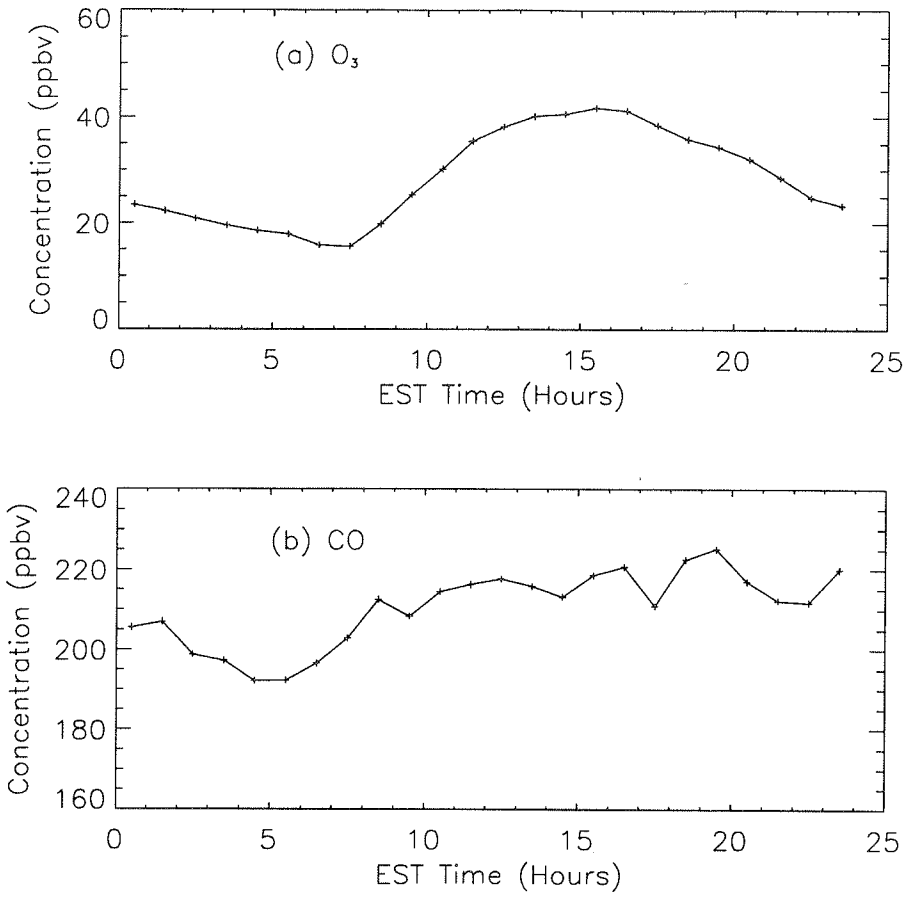

Figure 3.5. Diurnal variations of (a) O_3 and (b) CO at the Wye site, September 2-28, 1993.

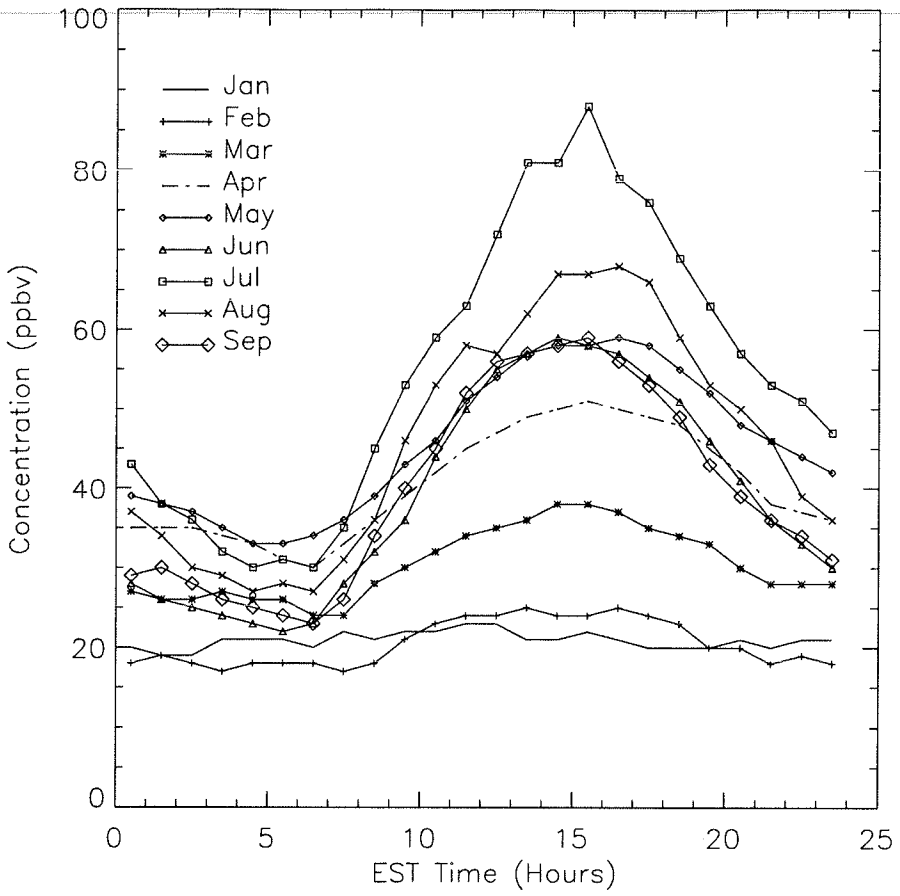

Figure 3.6. Diurnal variation of O_3 at the Wye site in 1995 by month.

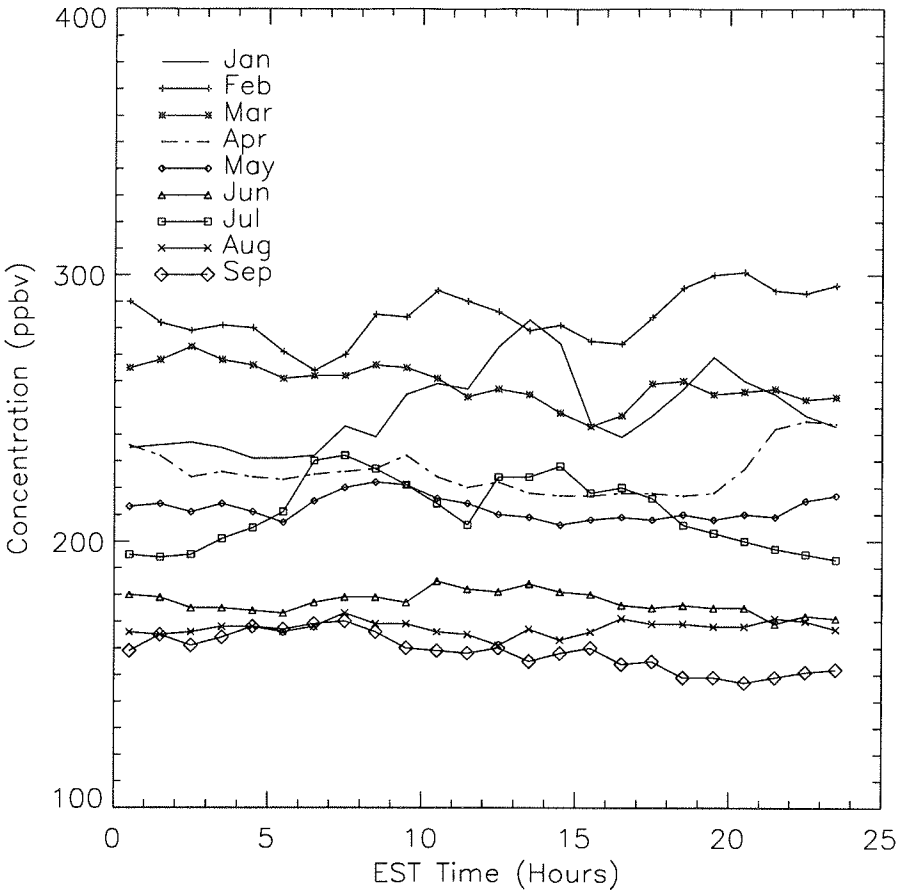

Figure 3.7. Diurnal variation of CO at the Wye site in 1995 by month.

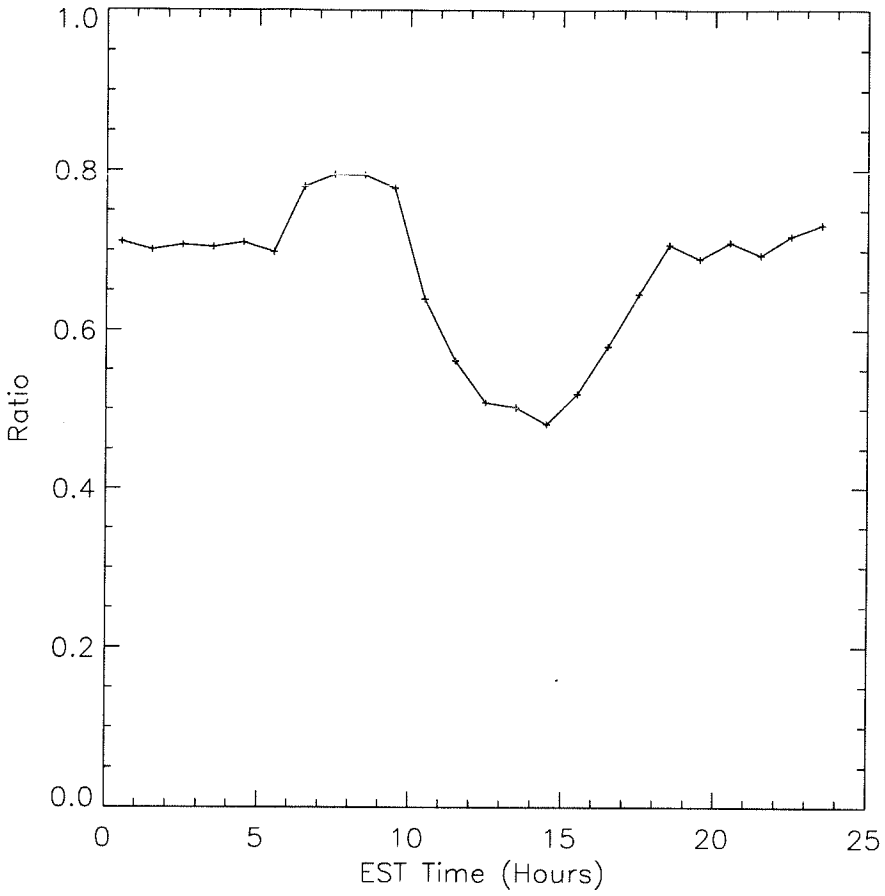

Figure 3.8. Diurnal variation of $[NO_x]/[NO_y]$ at the Wye site, September 2-28, 1993.

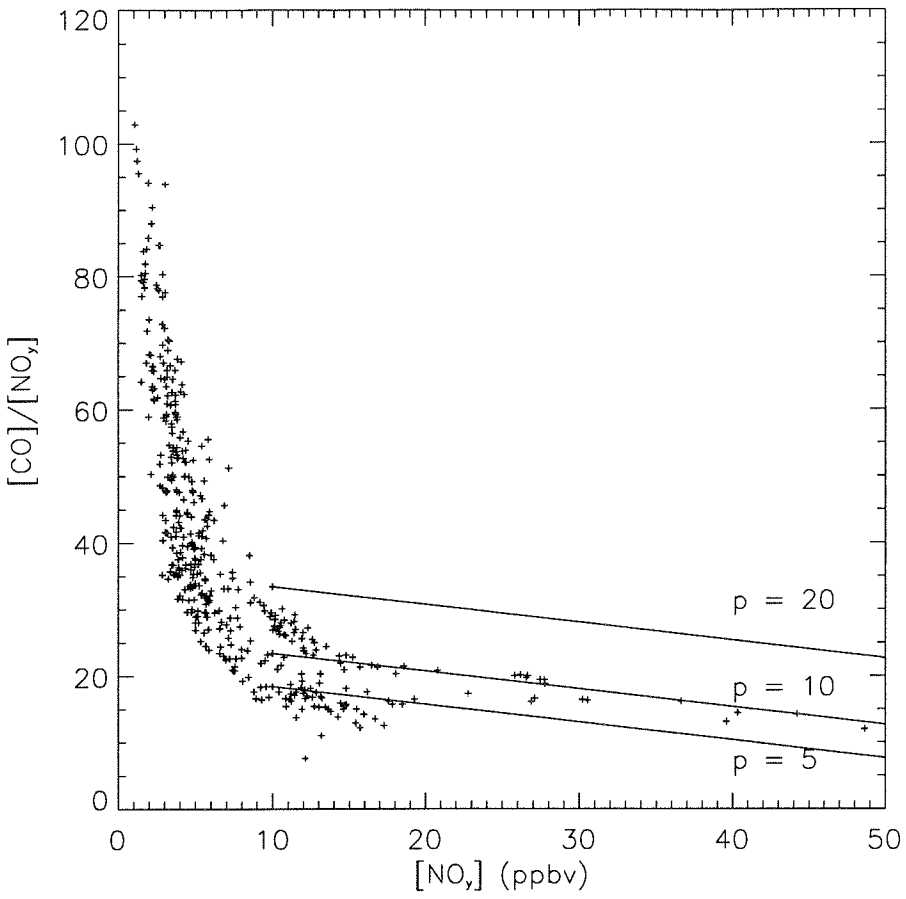

Figure 3.9. [CO]/[NO_y] as a function of [NO_y] during September 1993 at the Wye site. Also plotted for comparison are the expected curves for the [CO]/-[NO_x] molar emissions ratios, p, of 5, 10, and 20.

Figure 3.10. Back trajectories at the Wye site from 1993 for (a) "Clean" and (b) "Dirty" days.

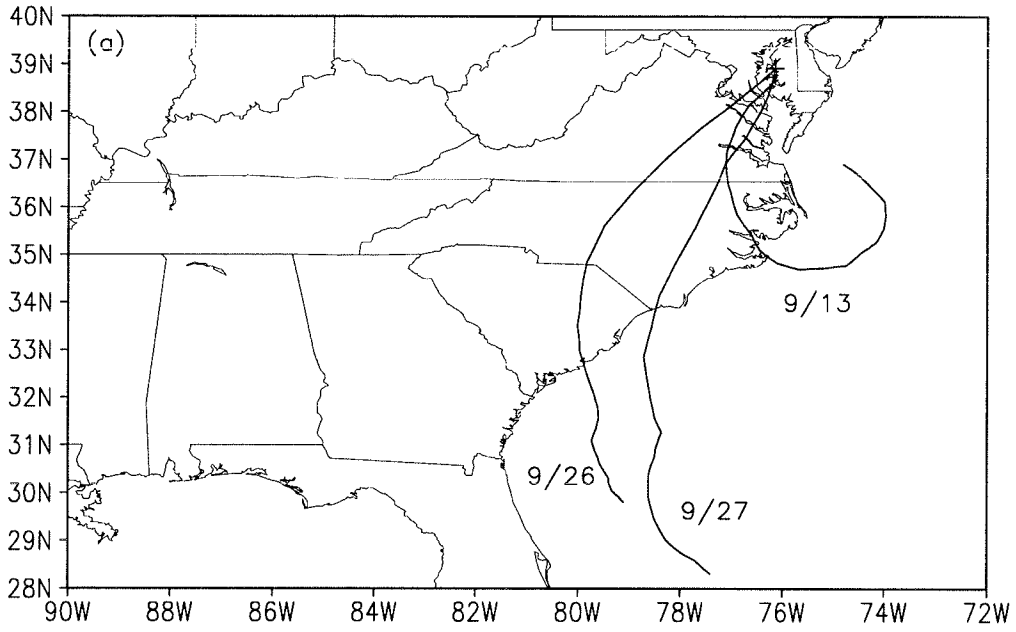

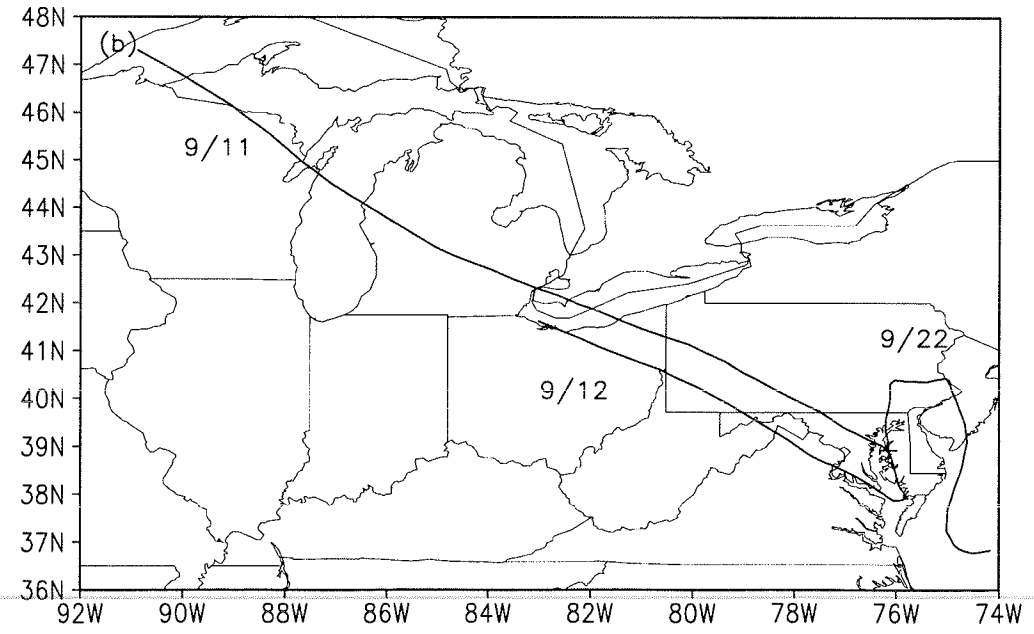

Figure 3.11. Back trajectories at the Wye site from 1995 for (a) "Clean" and (b) "Dirty" days.

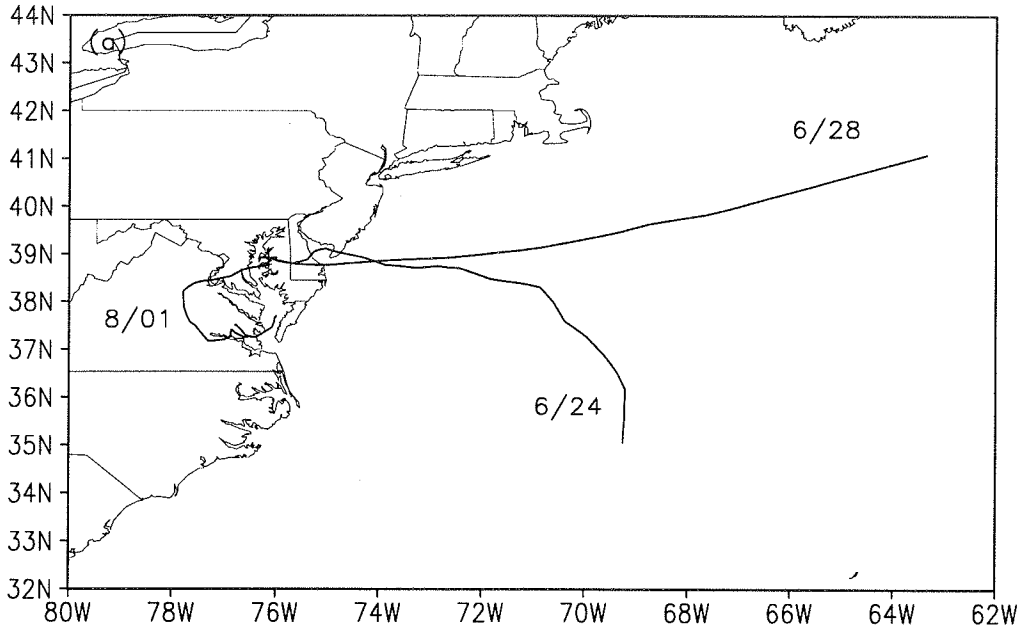

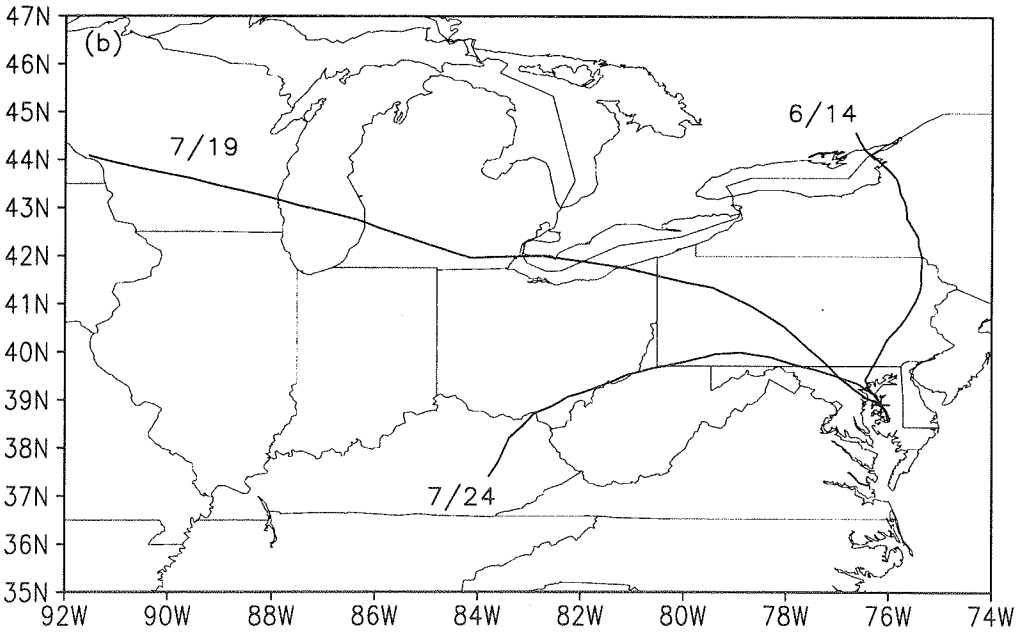

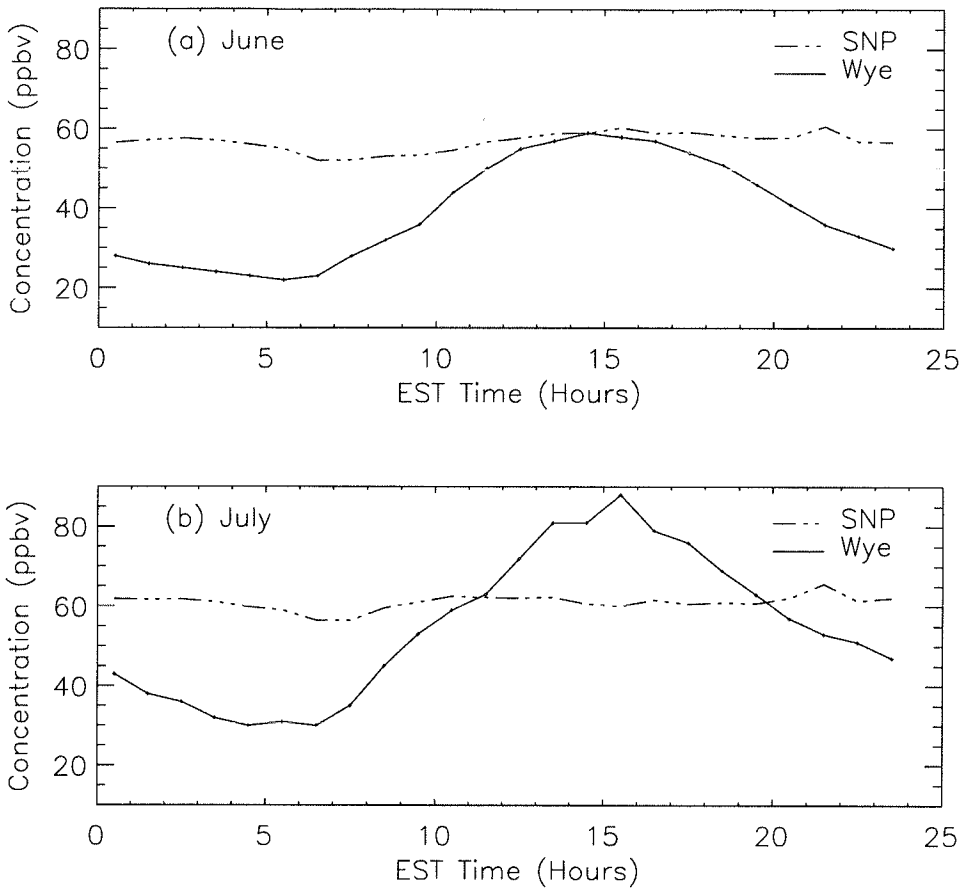

Figure 3.12. Comparison of the diurnal variation of O_3 at the SNP and Wye sites for (a) June and (b) July, 1995. SNP data provided by K. Hallock, Dept. of Chemistry, University of Maryland.

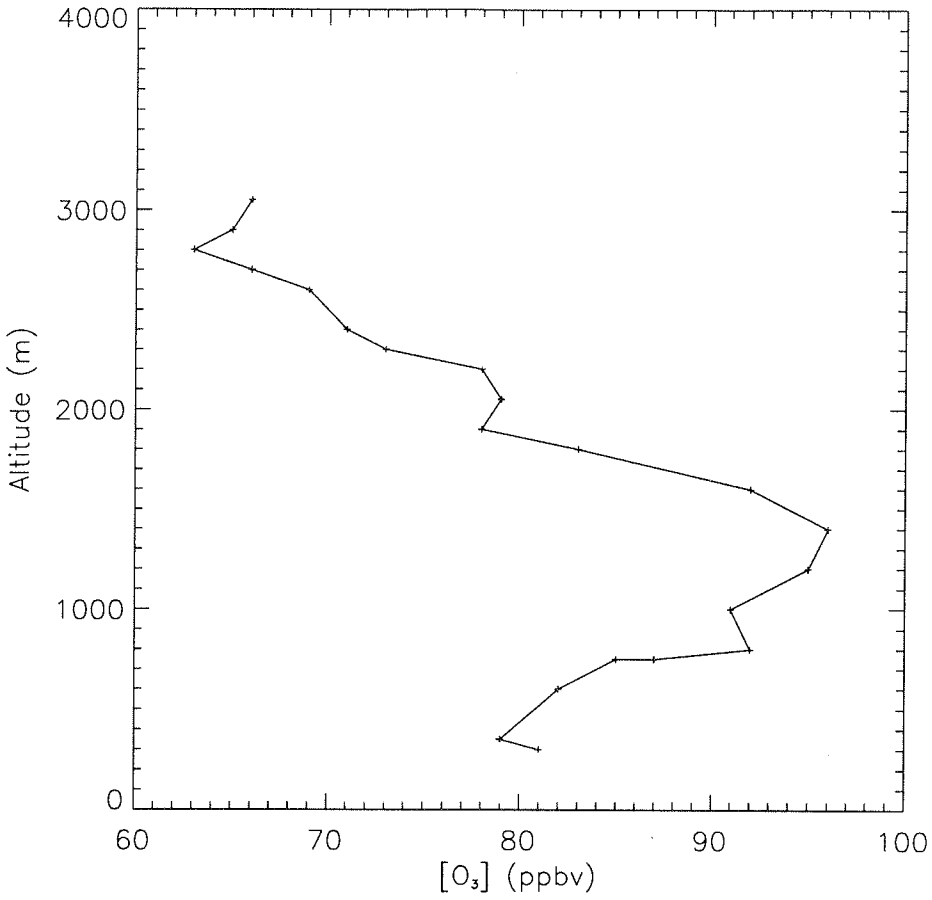

Figure 3.13. Ozone profile near Mt. Airy, Maryland from July 14, 1995. Time is about 1000 EST. Figure adapted from Ryan et al. [1996].

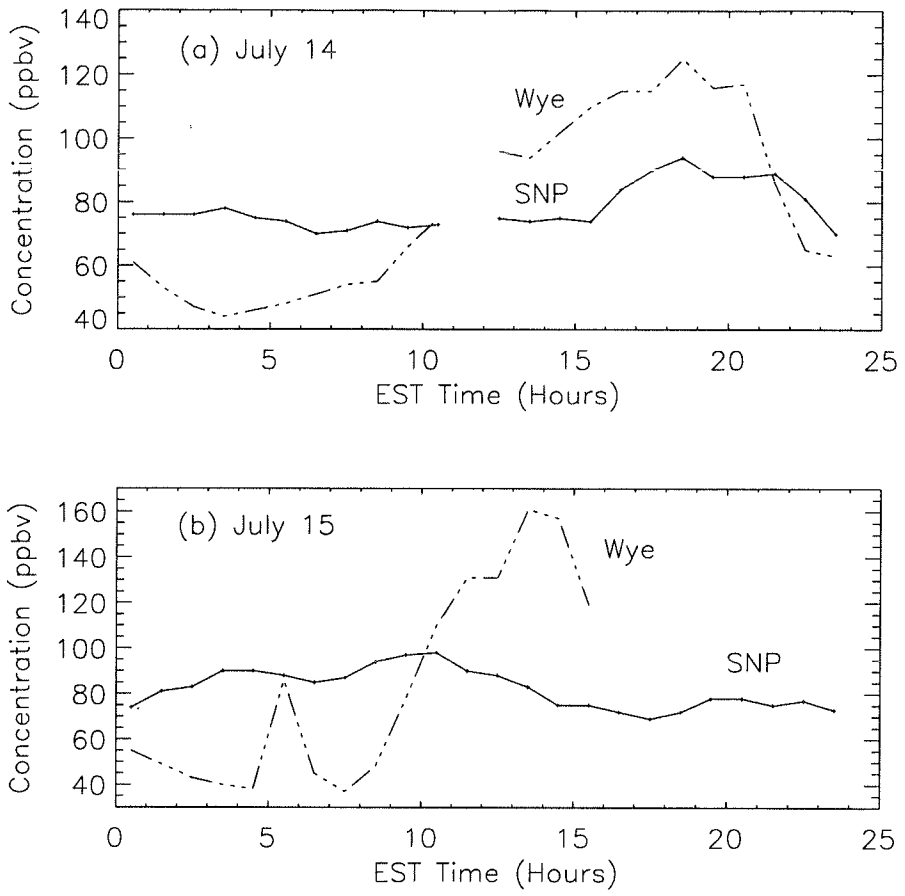

Figure 3.14. Comparison of O_3 hourly average time series at the SNP and Wye sites for high [O_3] days in July, 1995: (a) 14th and (b) 15th. SNP data provided by K. Hallock, Dept. of Chemistry, University of Maryland.

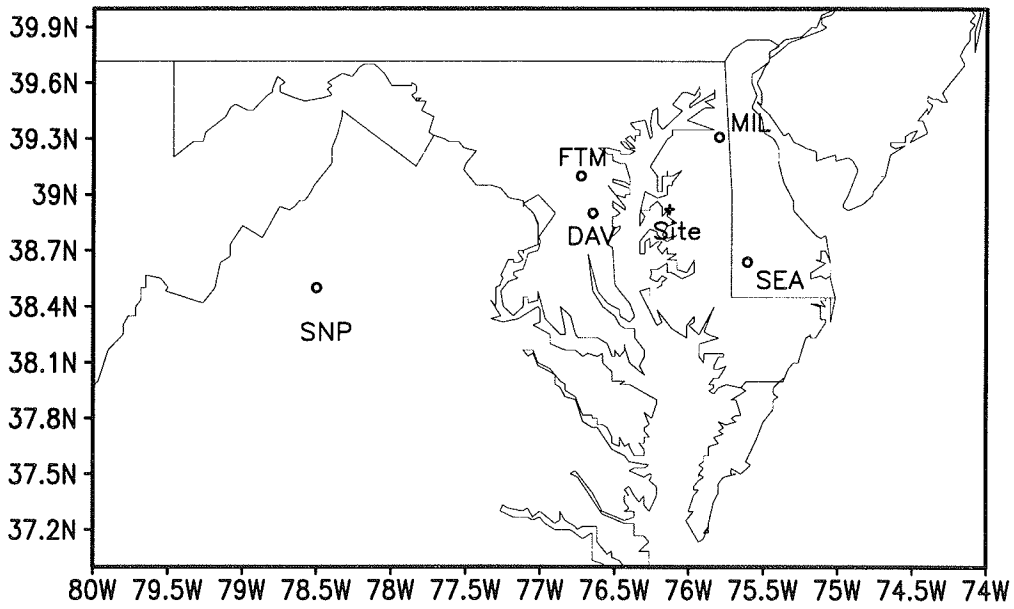

Figure 3.15. Map showing EPA/AIRS [EPA, 1992] stations in relation to the Wye site. MIL = Millington, MD; SEA = Seaford, DE; FTM = Ft. Meade, MD; DAV = Davidsonville, MD. SNP site is also shown.

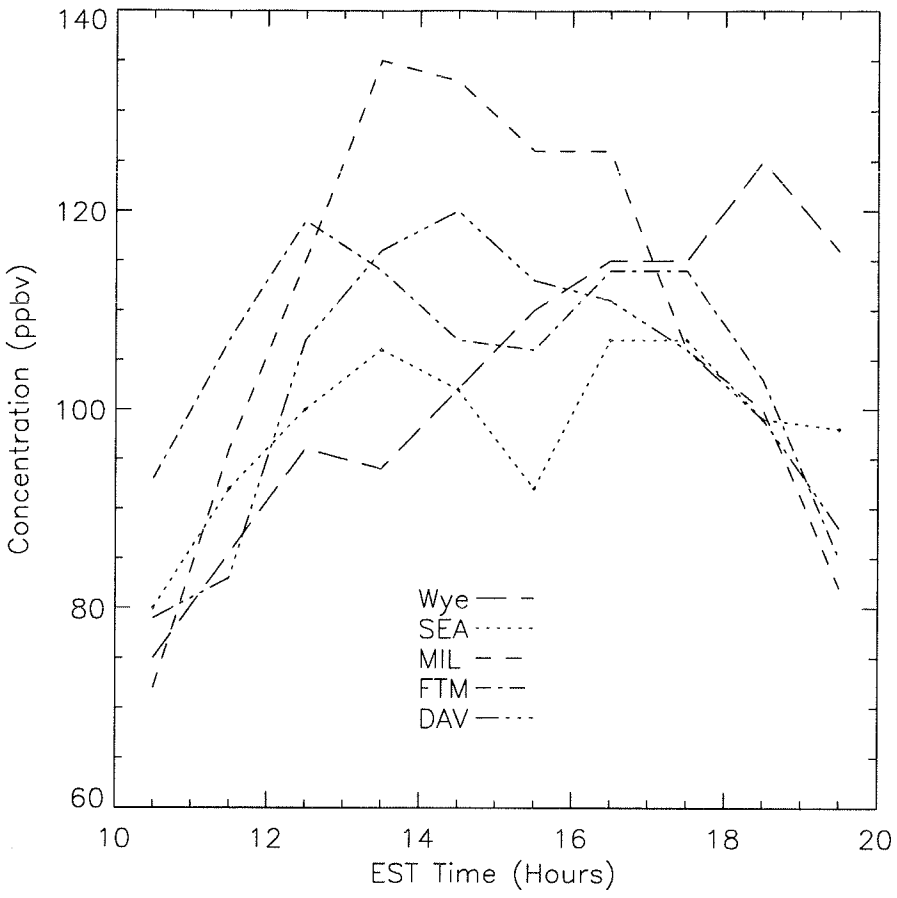

Figure 3.16. Hourly average [O_3] at the Wye site and four EPA/AIRS [EPA, 1992] sites for July 14, 1995. Abbreviations are as in Figure 3.15.

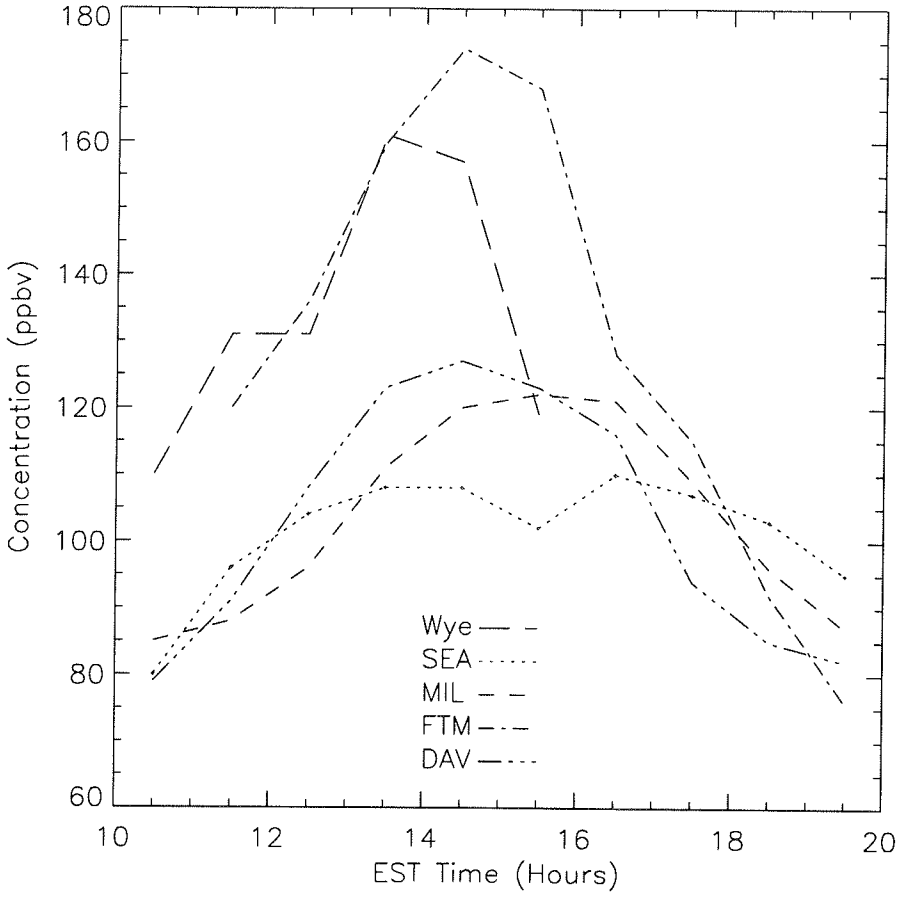

Figure 3.17. Hourly average [O_3] at the Wye site and four EPA/AIRS [EPA, 1992] sites for July 15, 1995. Abbreviations are as in Figure 3.15.

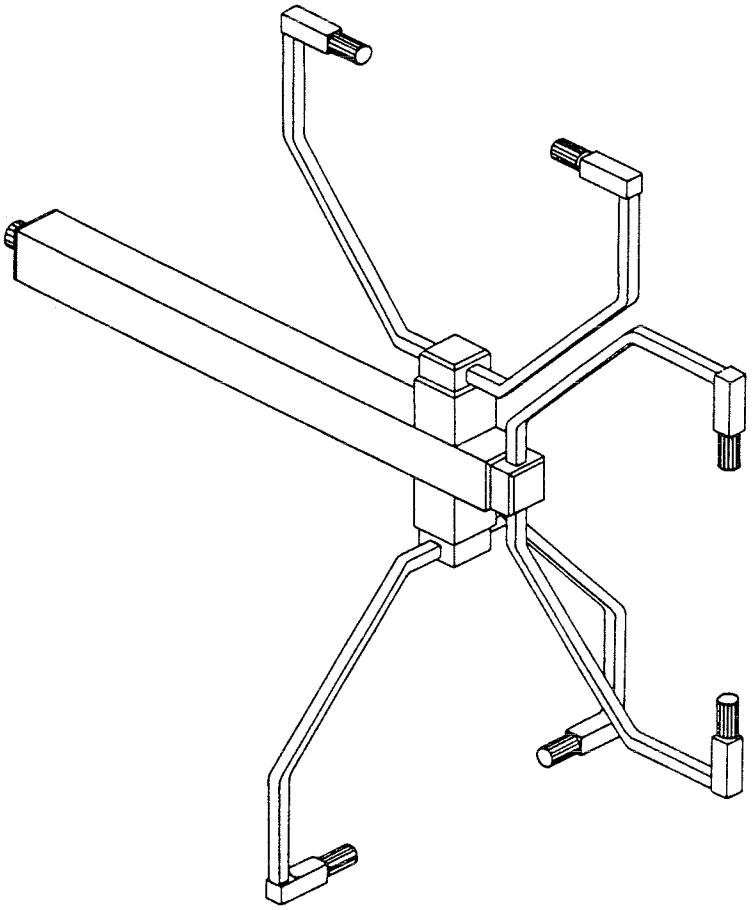

Figure 4.1. Applied Technologies sonic anemometer. Figure is taken from Kaimal and Finnigan [1994].

Figure 4.2. Pulse counting-to-voltage converter, courtesy of David Auble of NOAA/Oak Ridge.

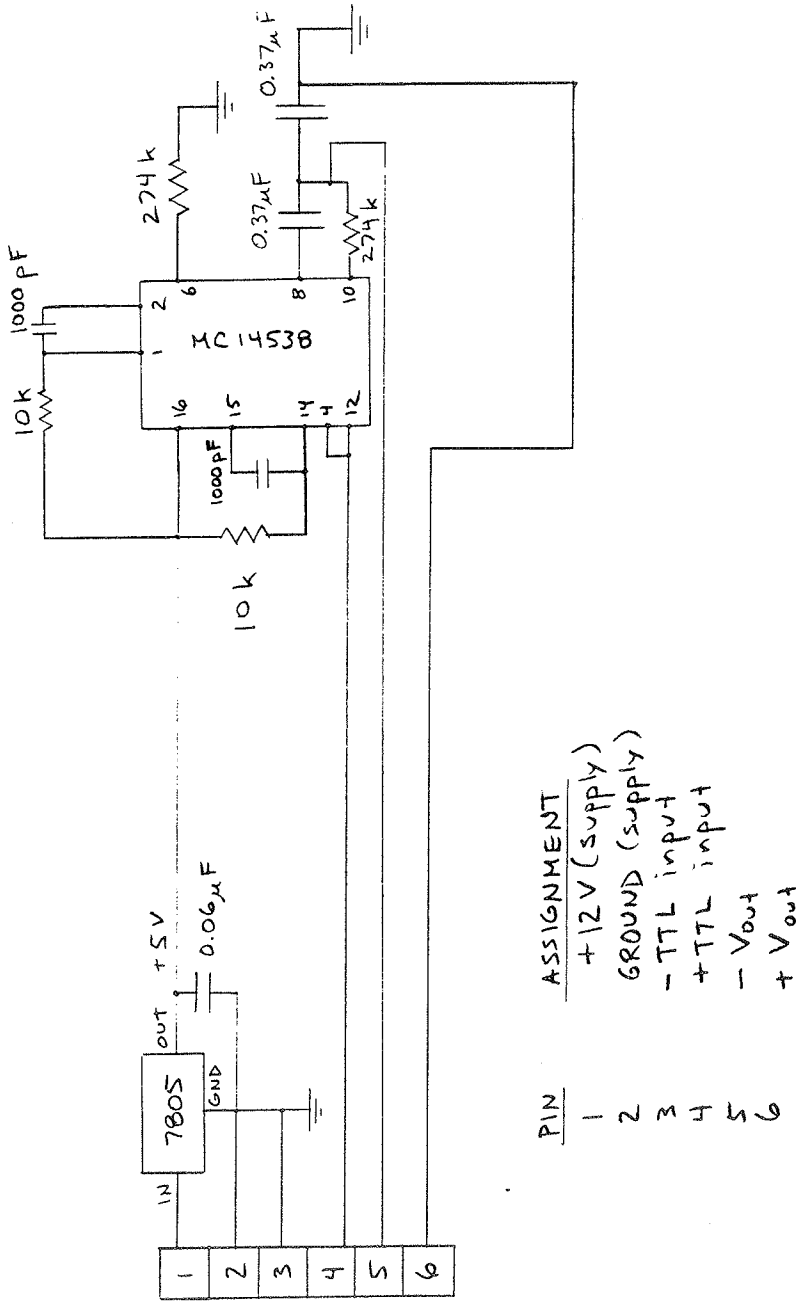

Figure 4.3. Lag correlation between w and NO data streams before 1500 EST on July 28, with a 2.3 s delay in the NO signal removed to maximize the correlation at zero lag. Dark line is a smooth curve fit (Stineman weighting function).

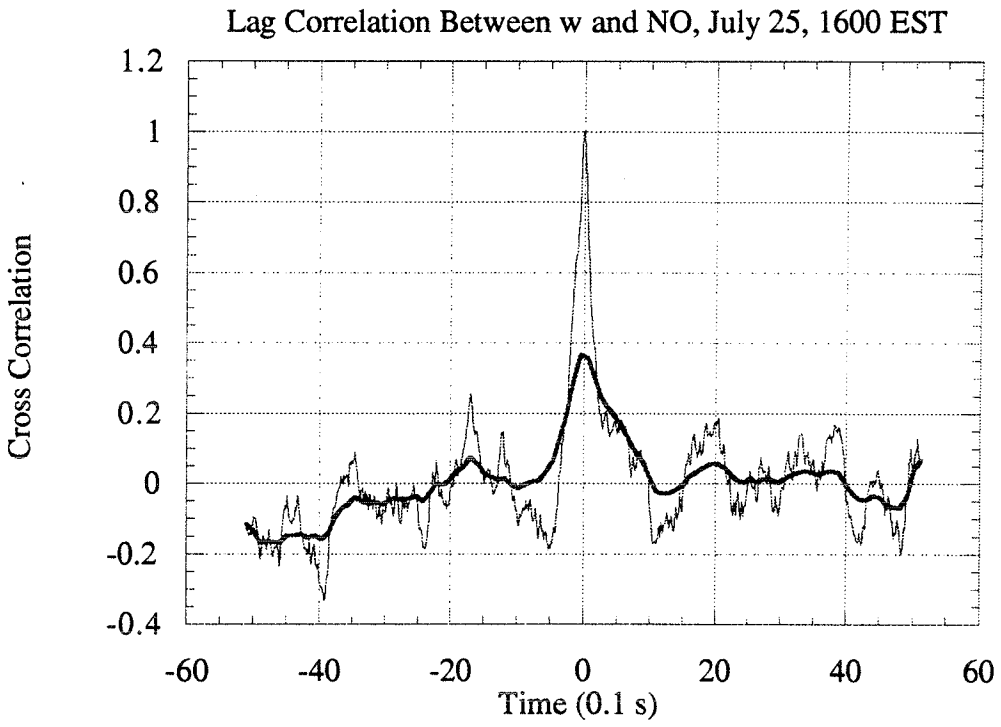

Figure 4.4. Lag correlation between w and NO data streams after 1500 EST on July 28, with a 1.6 s delay in the NO signal removed to maximize the correlation at zero lag. Dark line is a smooth curve fit (Stineman weighting function).

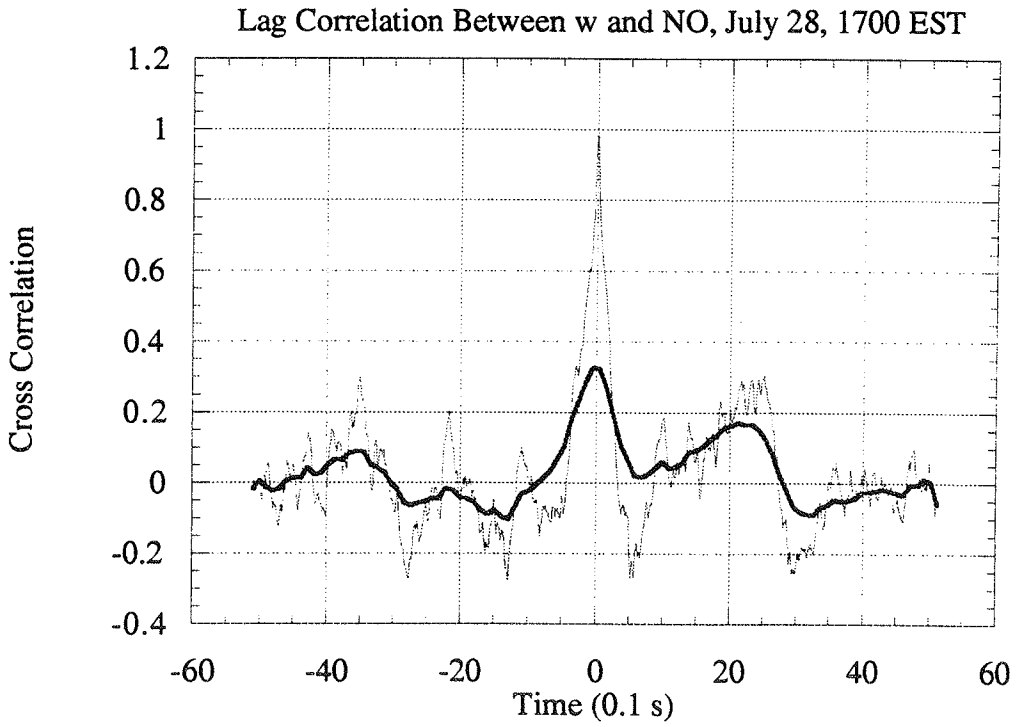

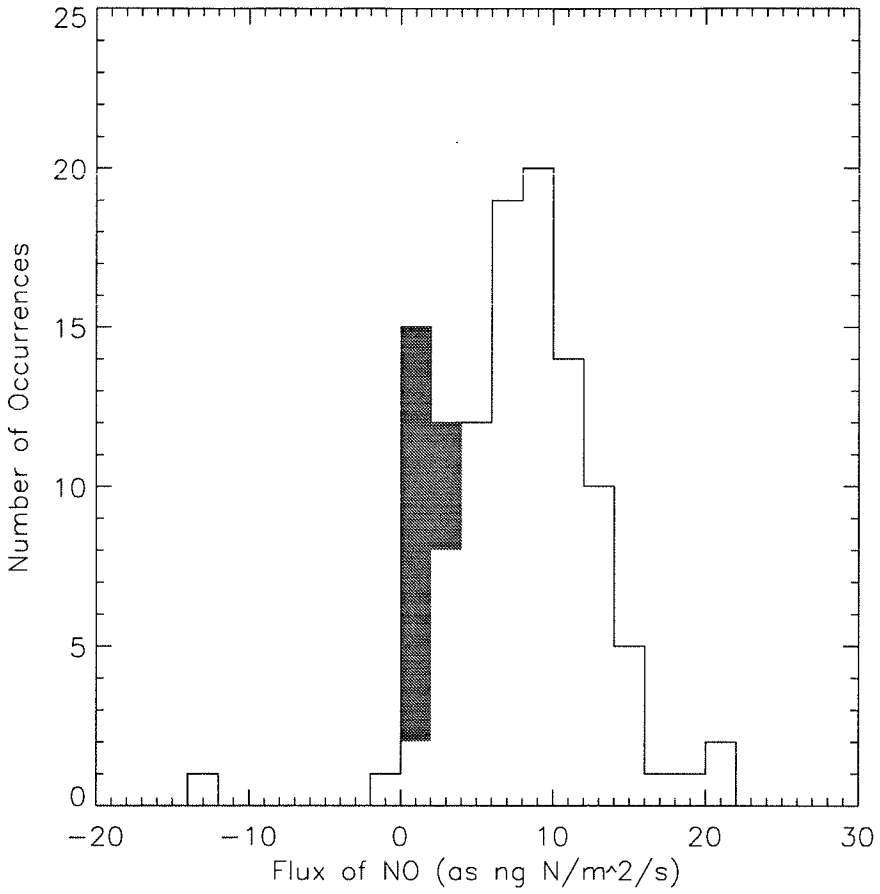

Figure 4.5. Histogram of 30-min average NO fluxes from July 25-30 at the Wye site, in ng N m^{-2} s^{-1}. Shaded area corresponds to times when wind passed over the untilled side, unshaded area corresponds to times when wind passed over the tilled side.

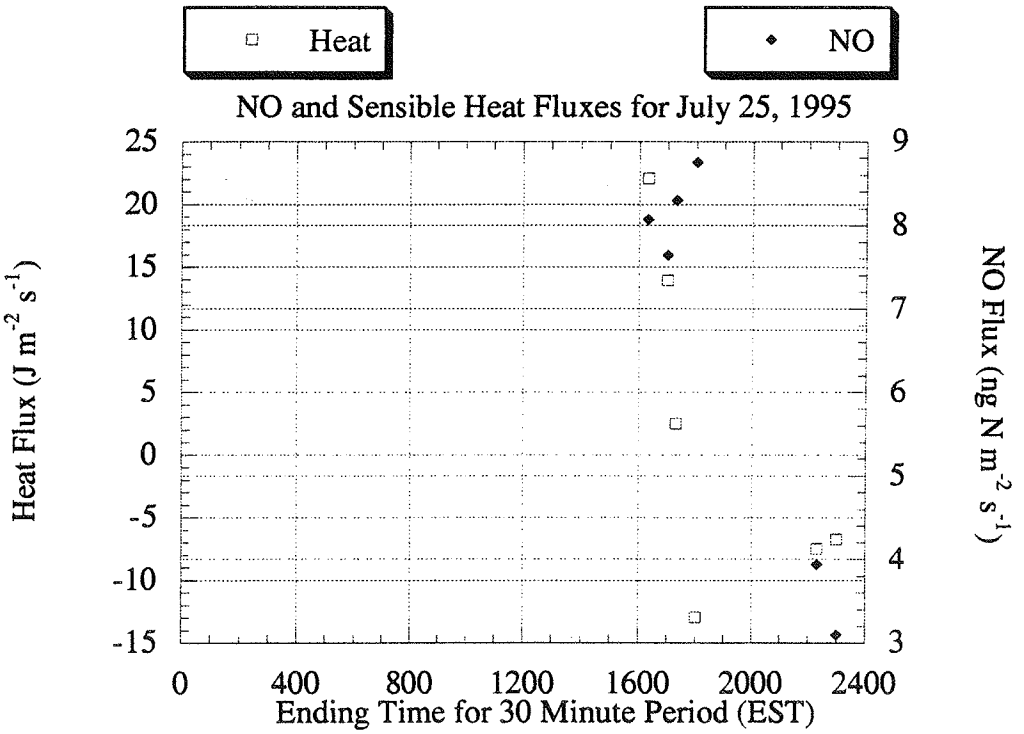

Figure 4.6. Time series of NO and sensible heat fluxes from the Wye site on July 25. Units are reported on the y-axes.

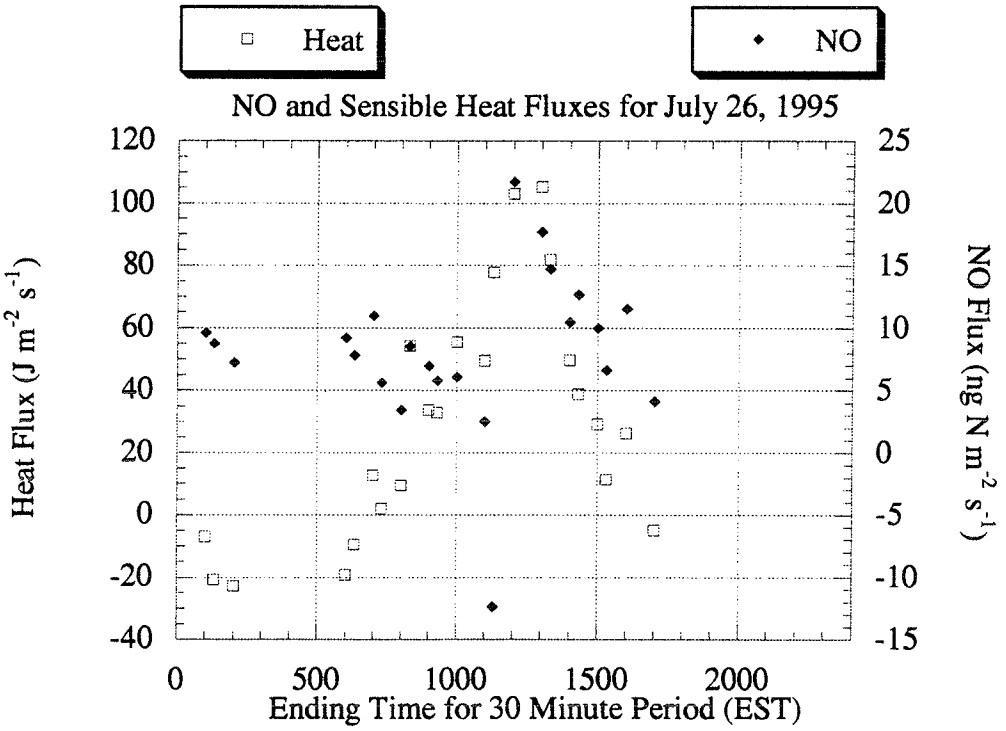

Figure 4.7. Time series of NO and sensible heat fluxes from the Wye site on July 26. Units are reported on the y-axes.

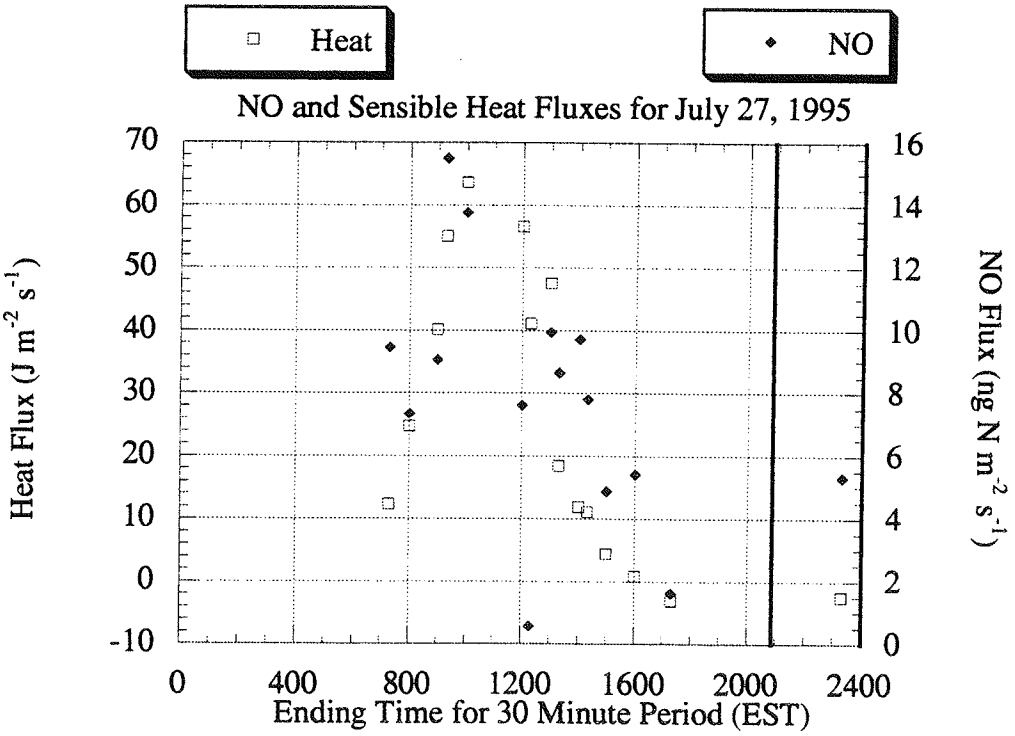

Figure 4.8. Time series of NO and sensible heat fluxes from the Wye site on July 27. Units are reported on the y-axes. Solid vertical lines denote times when rain occurred.

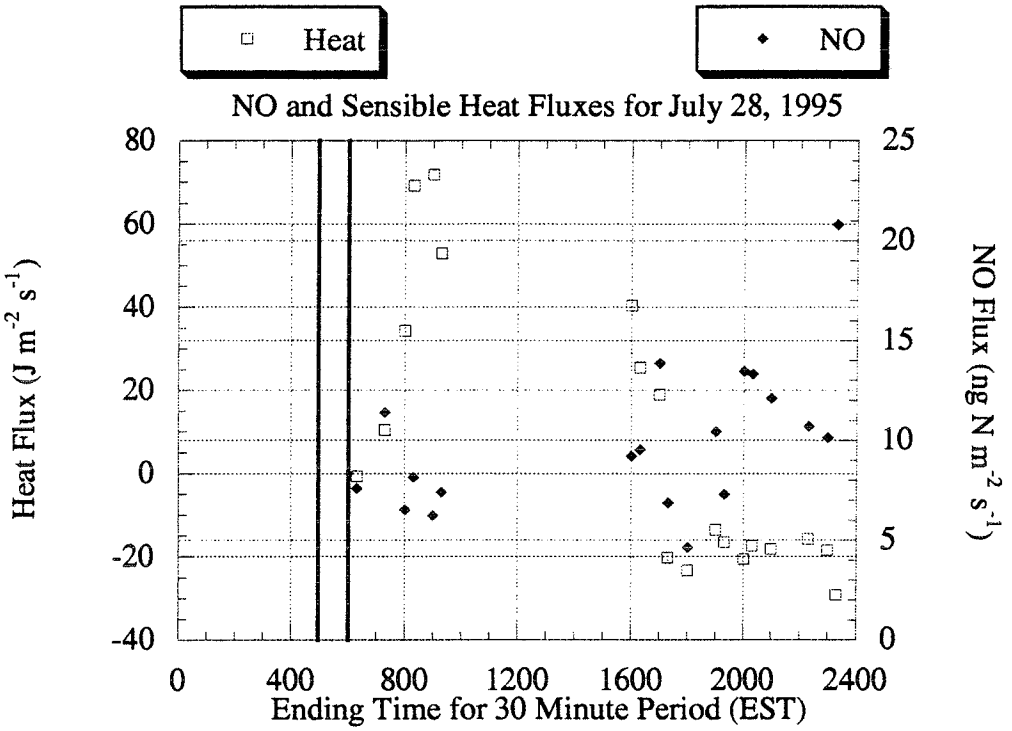

Figure 4.9. Time series of NO and sensible heat fluxes from the Wye site on July 28. Units are reported on the y-axes. Solid vertical lines denote times when rain occurred.

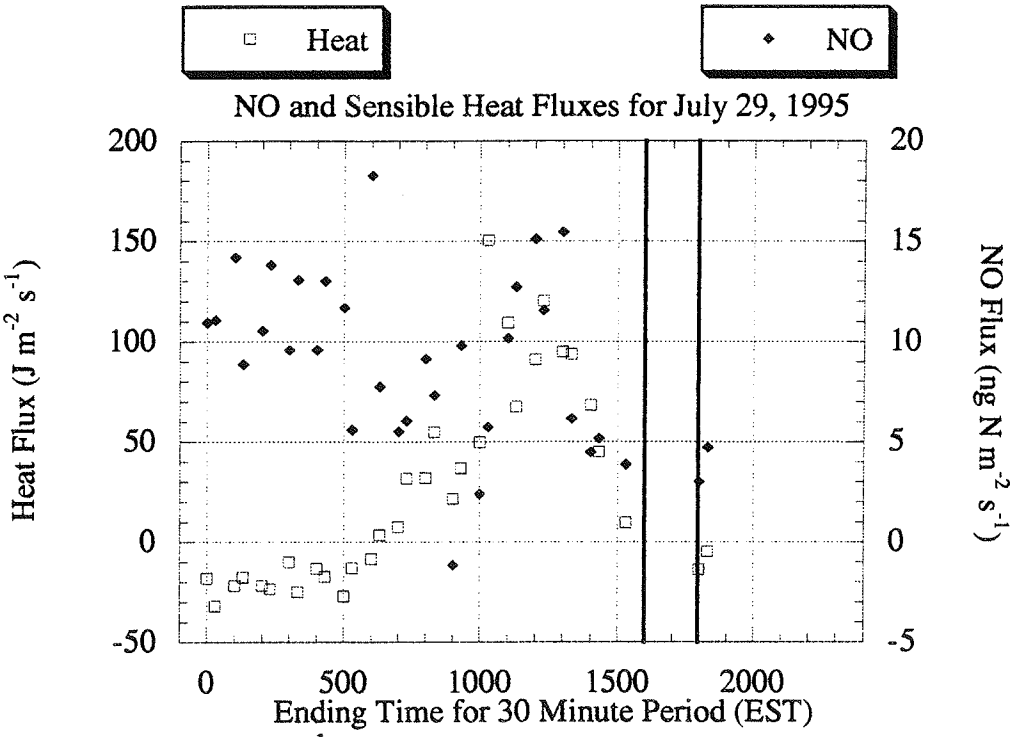

Figure 4.10. Time series of NO and sensible heat fluxes from the Wye site on July 29. Units are reported on the y-axes. Solid vertical lines denote times when rain occurred.

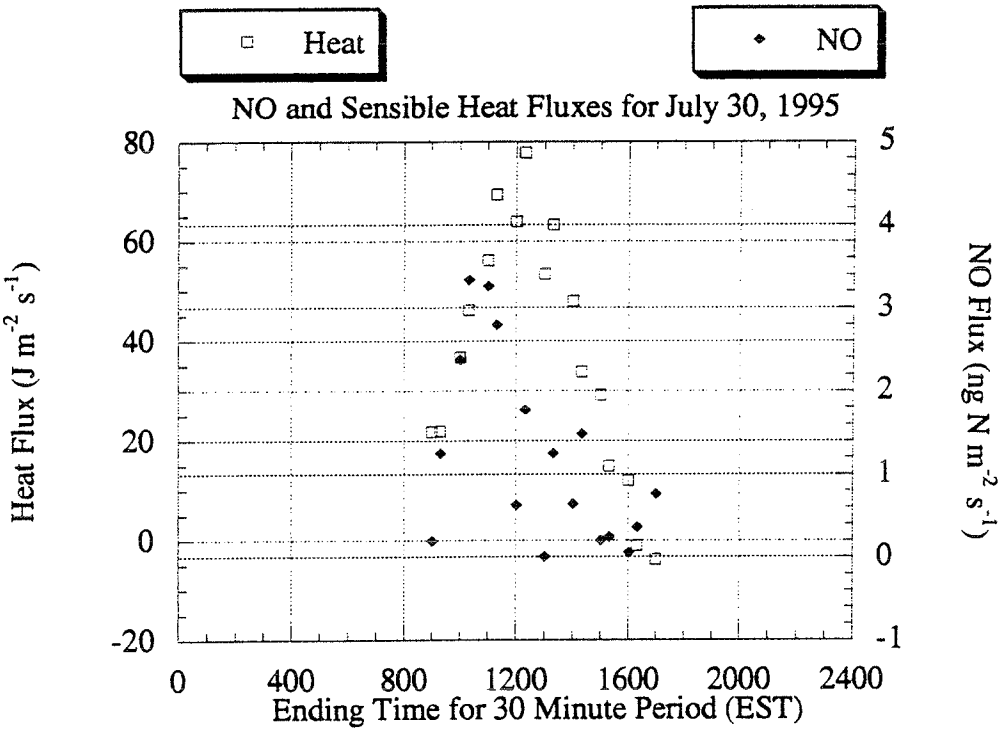

Figure 4.11. Time series of NO and sensible heat fluxes from the Wye site on July 30. Units are reported on the y-axes.

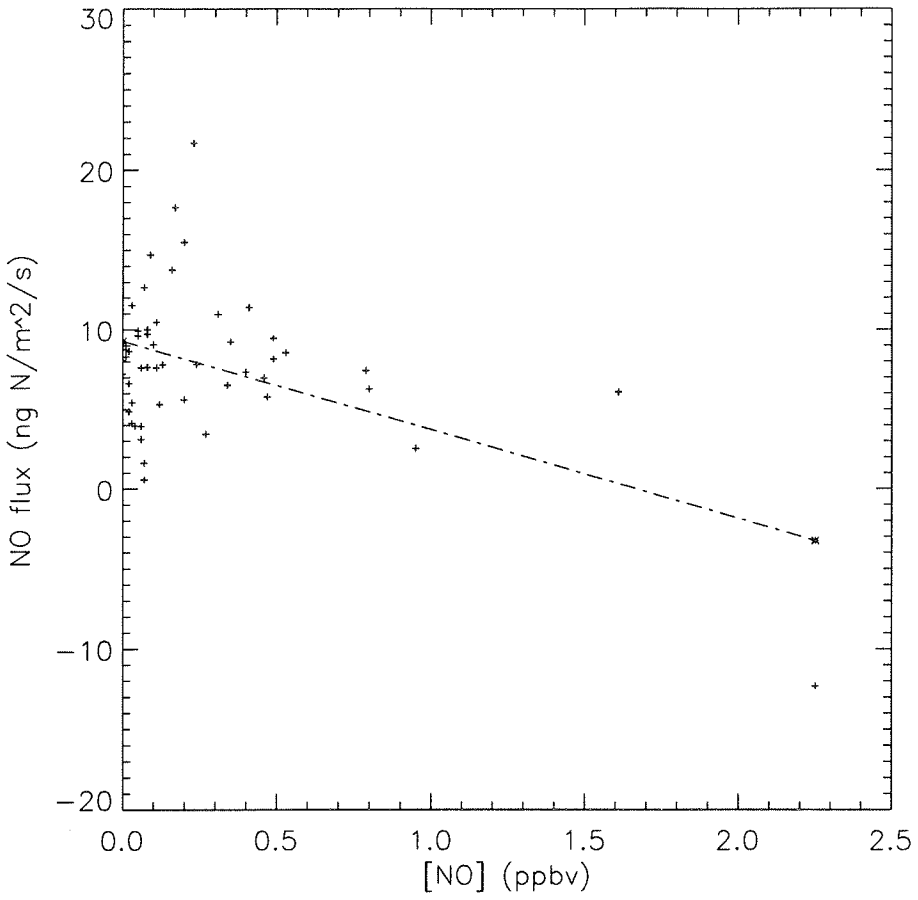

Figure 4.12. NO flux as a function of ambient NO mixing ratio. Also plotted is a linear least-squares fit line (r = -0.47).

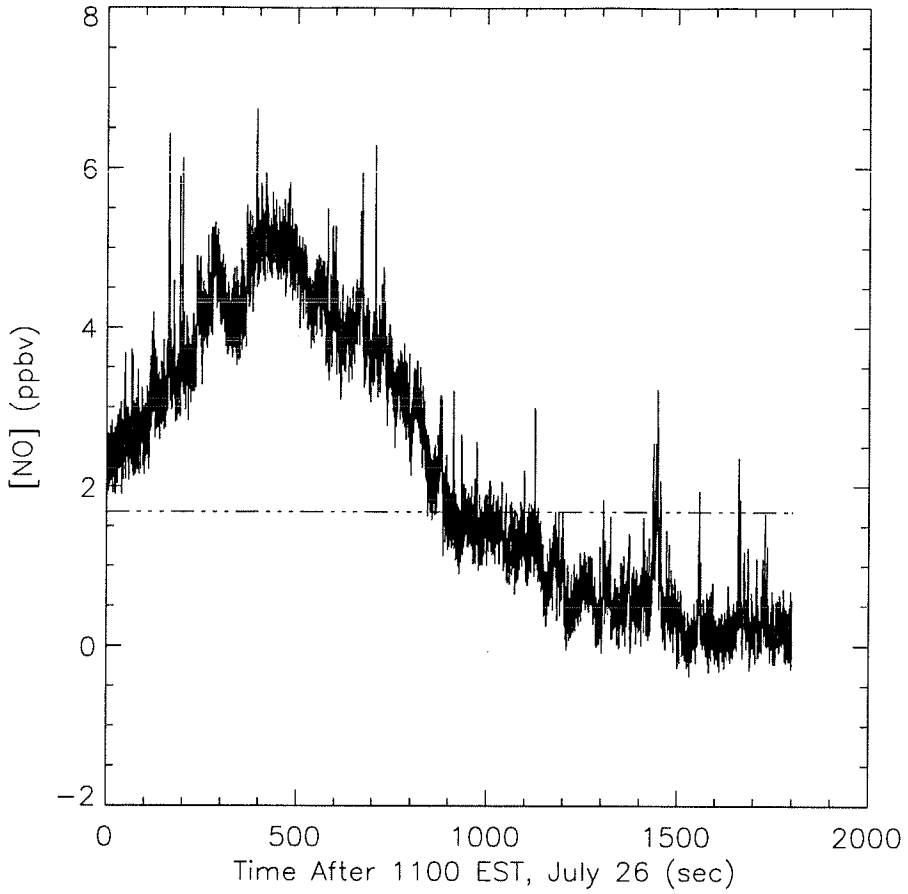

Figure 4.13. Time series of 10 s^{-1} [NO] data for 1100-1130 EST on July 26. The compensation point of 1.68 ppbv is also plotted. Average [NO] was 2.25 ppbv.

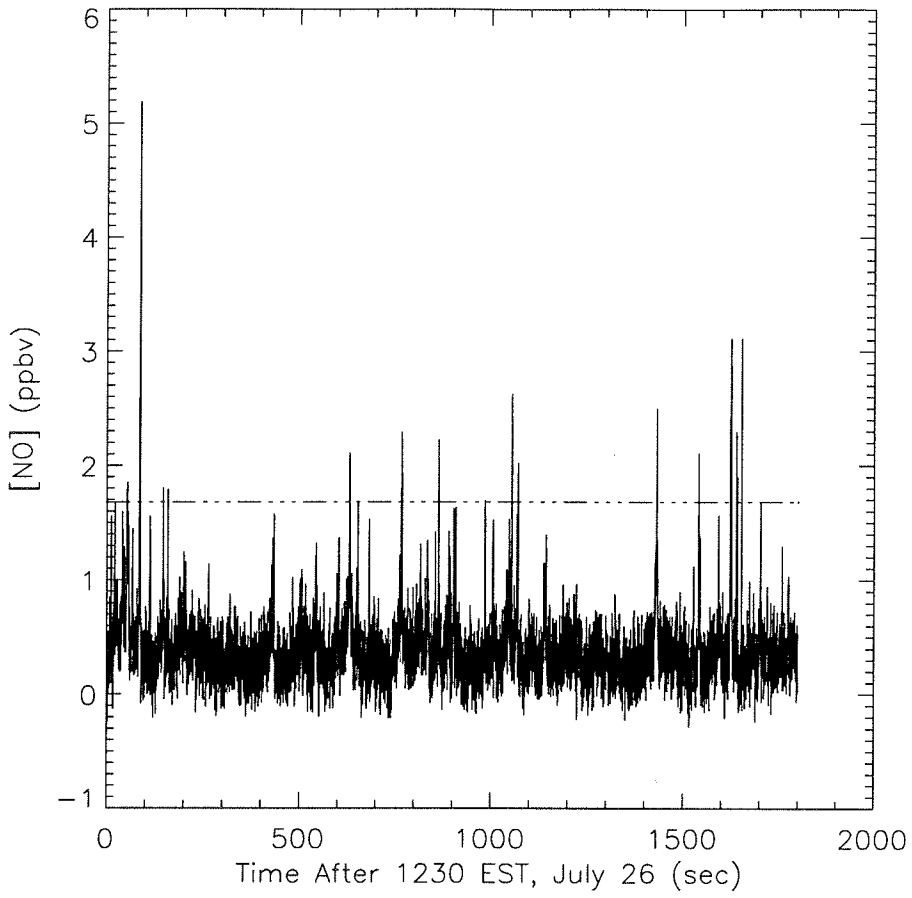

Figure 4.14. Time series of 10 s^{-1} [NO] data for 1230-1300 EST on July 26. The compensation point of 1.68 ppbv is also plotted. Average [NO] was 0.39 ppbv.

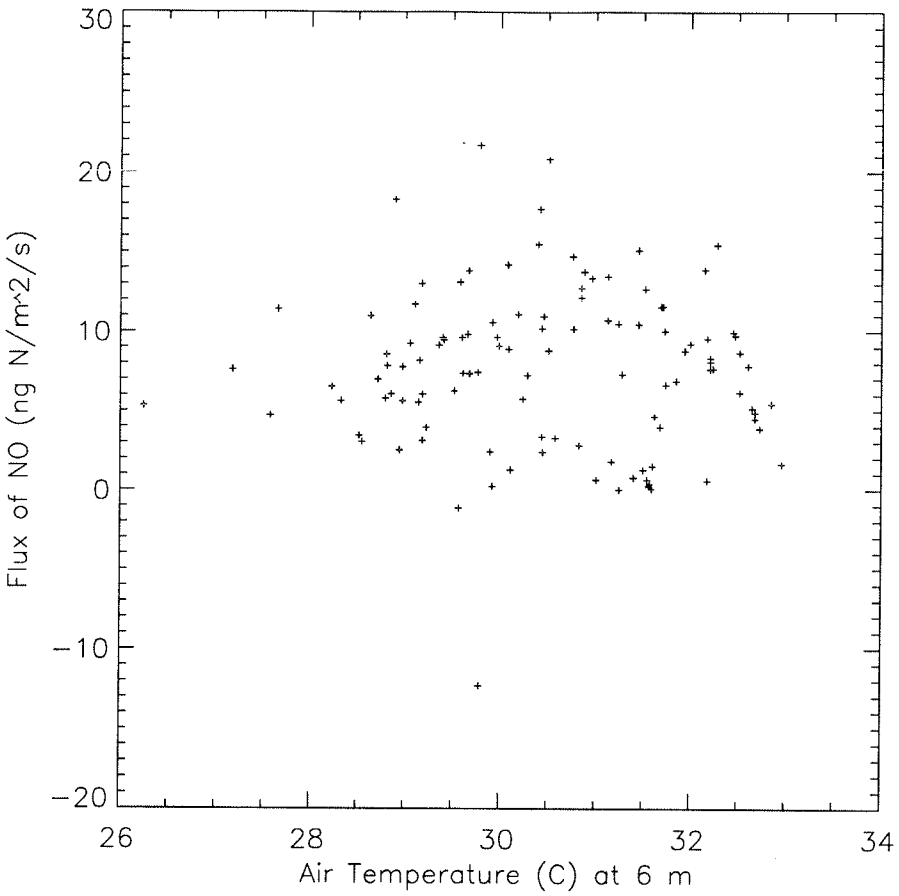

Figure 4.15. NO flux plotted as a function of ambient air temperature at 6 m.

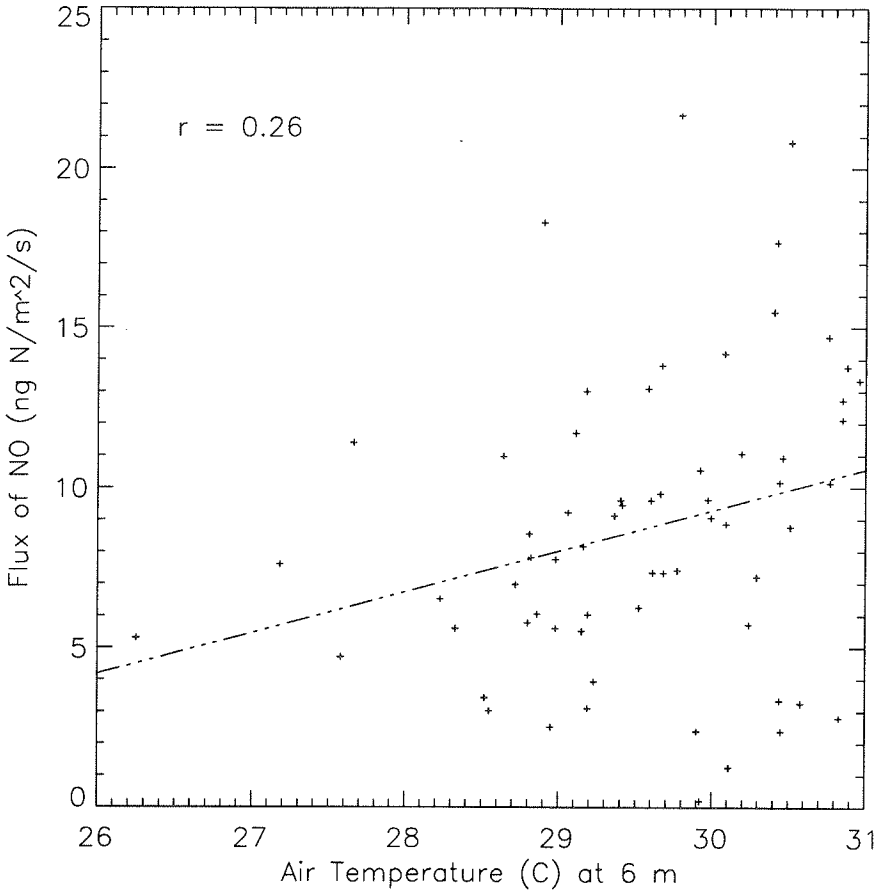

Figure 4.16. NO emission fluxes plotted as a function of ambient air temperature below 31°C. A linear least-squares fit (r = 0.26) is also plotted.

Figure 4.17. Typical frequency weighted power spectrum of vertical wind speed, w. The dark line is a smoothed fit. The non-dimensional frequency is defined as $n = 2\pi fz/u$: f, cyclical frequency; z, sampling height = 6 m; u, mean wind speed. For this half-hour period (July 28, 1700-1730 EST), u = 2.68 m s^{-1}.

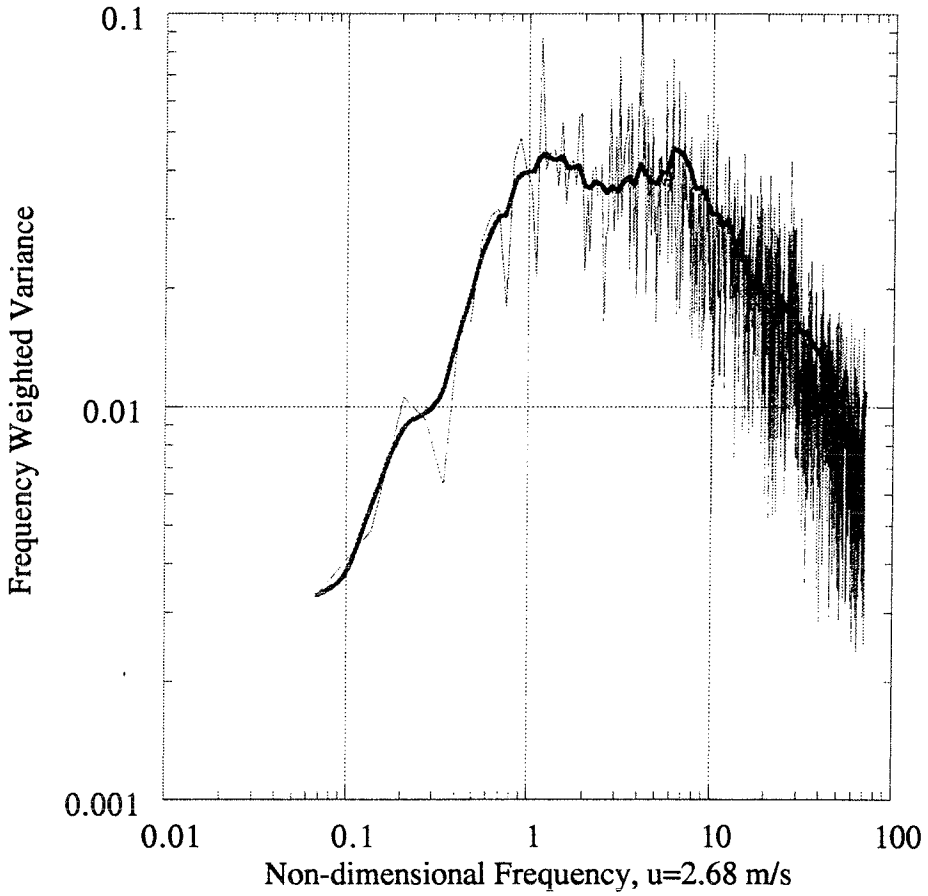

Figure 4.18. Typical frequency weighted power spectra of u and w. Smooth fit curves are shown. For this half-hour period (July 25, 1600-1630 EST), u = 2.52 m s^{-1}. A log-log -2/3 slope line is shown for the inertial subrange.

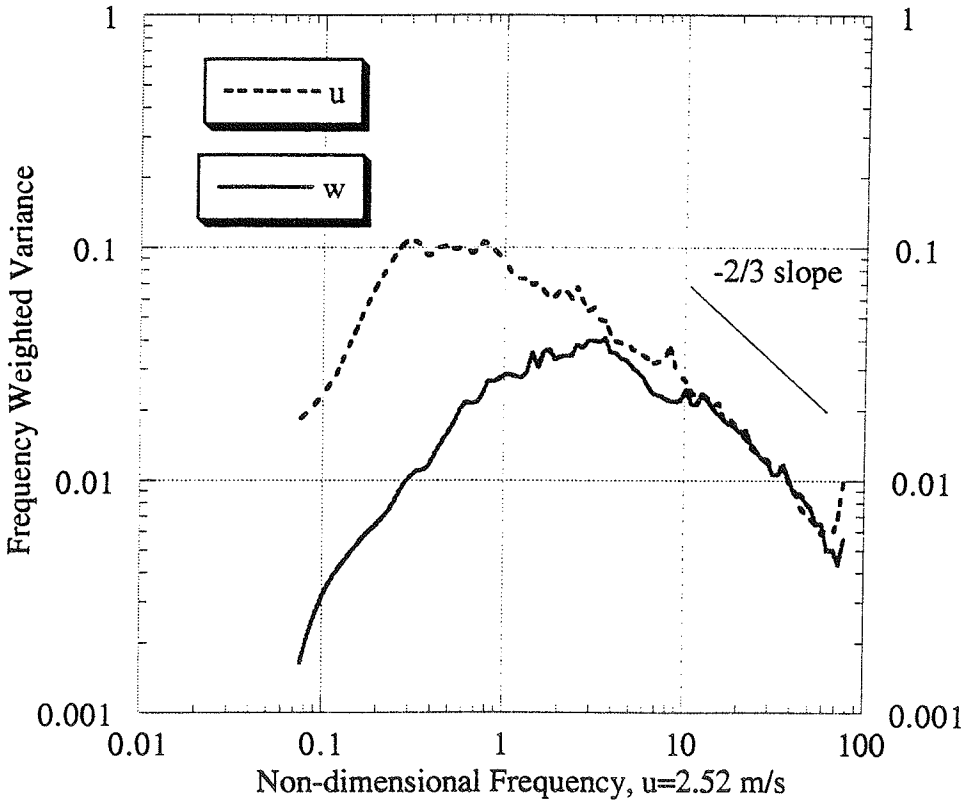

Figure 4.19. Typical frequency weighted power spectra of w and NO. Smooth fit curves are shown. For this half-hour period (July 25, 1600-1630 EST), u = 2.52 m s^{-1}.

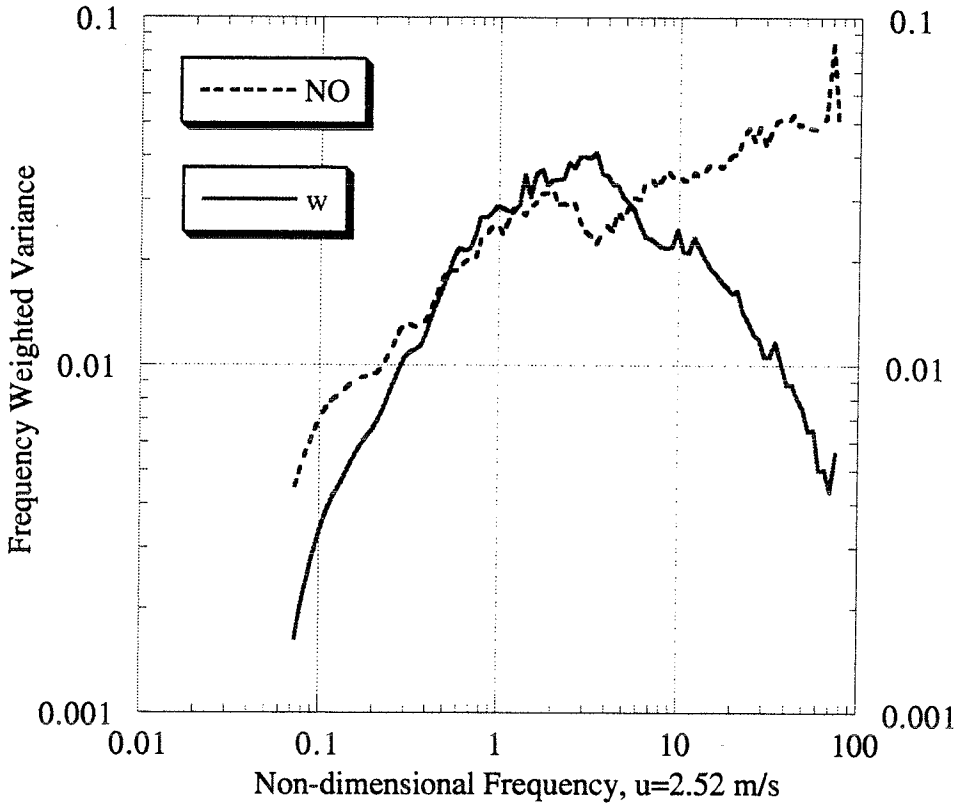

Figure 4.20. Typical frequency weighted cospectrum between w and NO. Smooth fit curve is shown. For this half-hour period (July 25, 1600-1630 EST), u = 2.52 m s^{-1}.

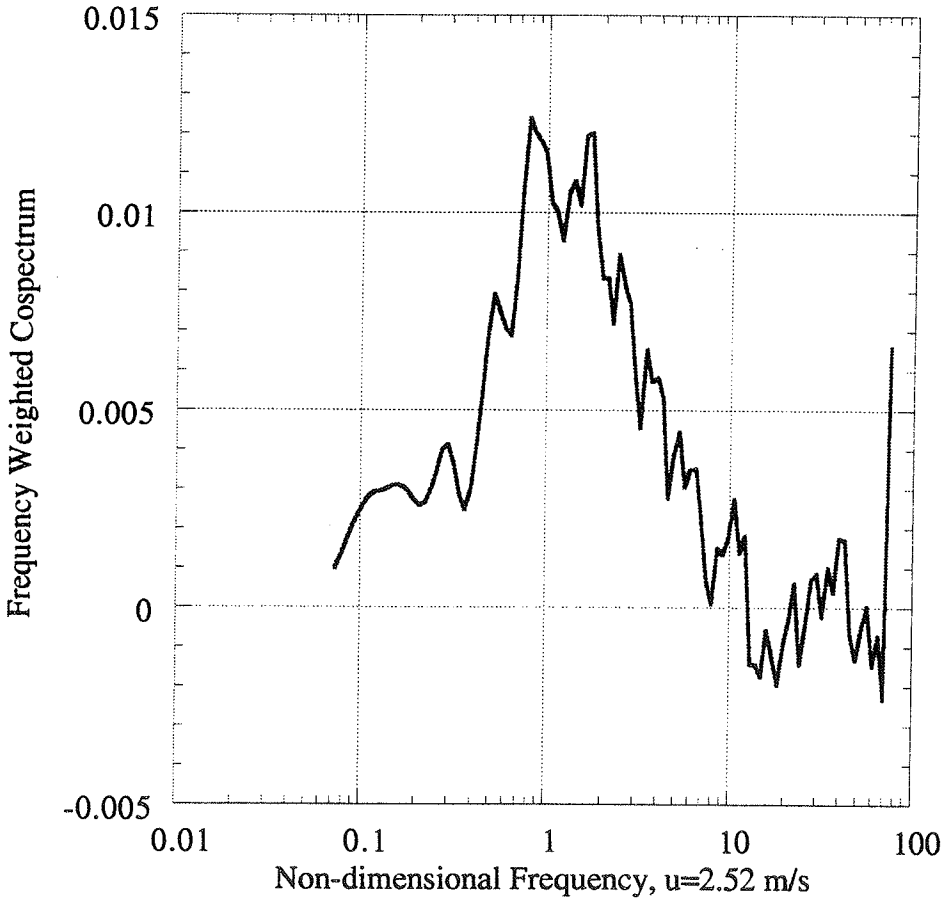

Figure 4.21. Frequency weighted cospectrum between w and background (BG) NO signal. Smooth fit curve is shown. For this half-hour period, u = 3.20 ms^{-1}.

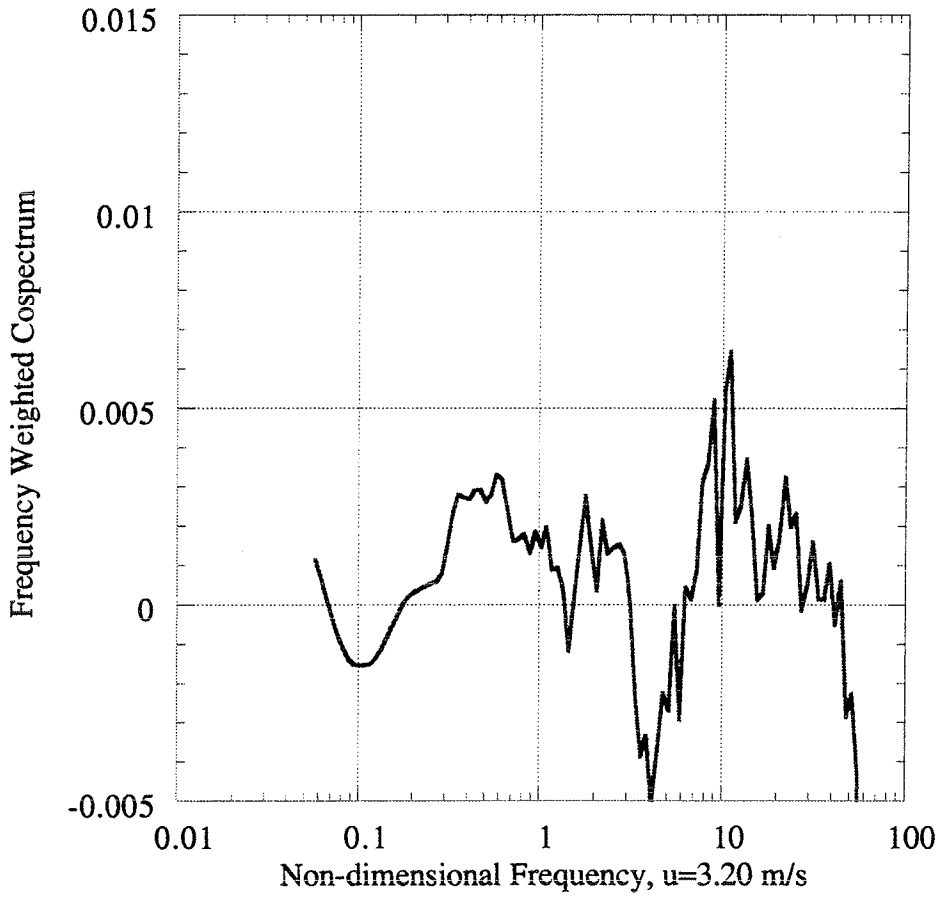

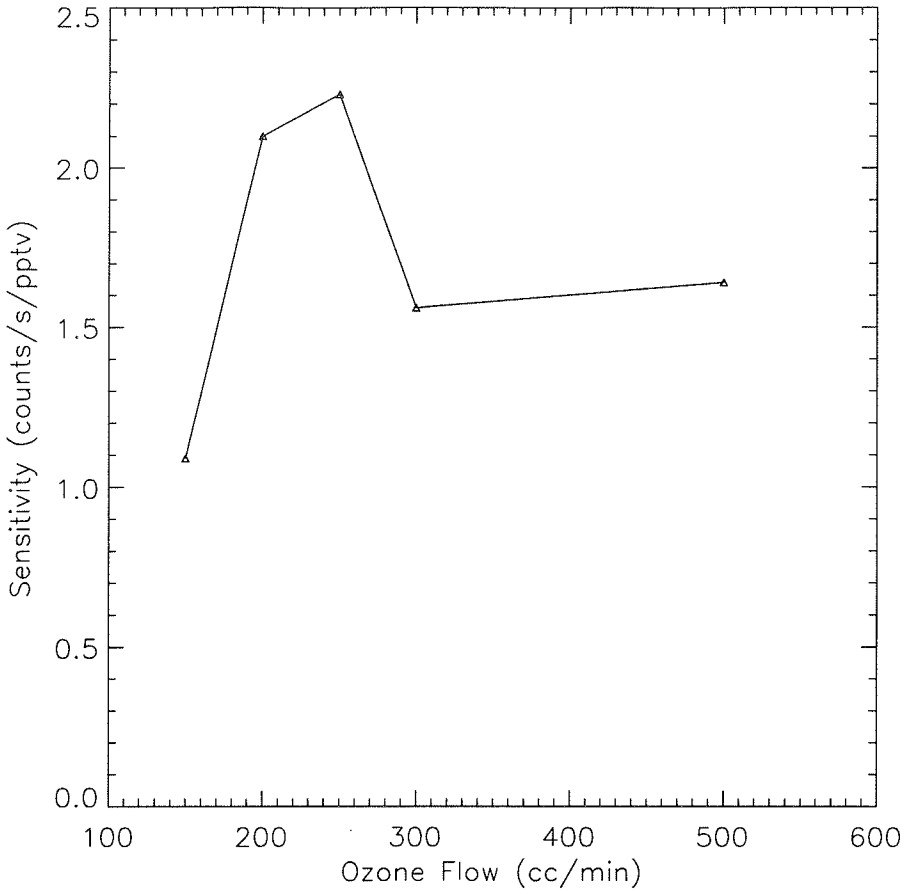

Figure A.1. Sensitivity of the NO detector as a function of O_2/O_3 flow into the ozonizer.

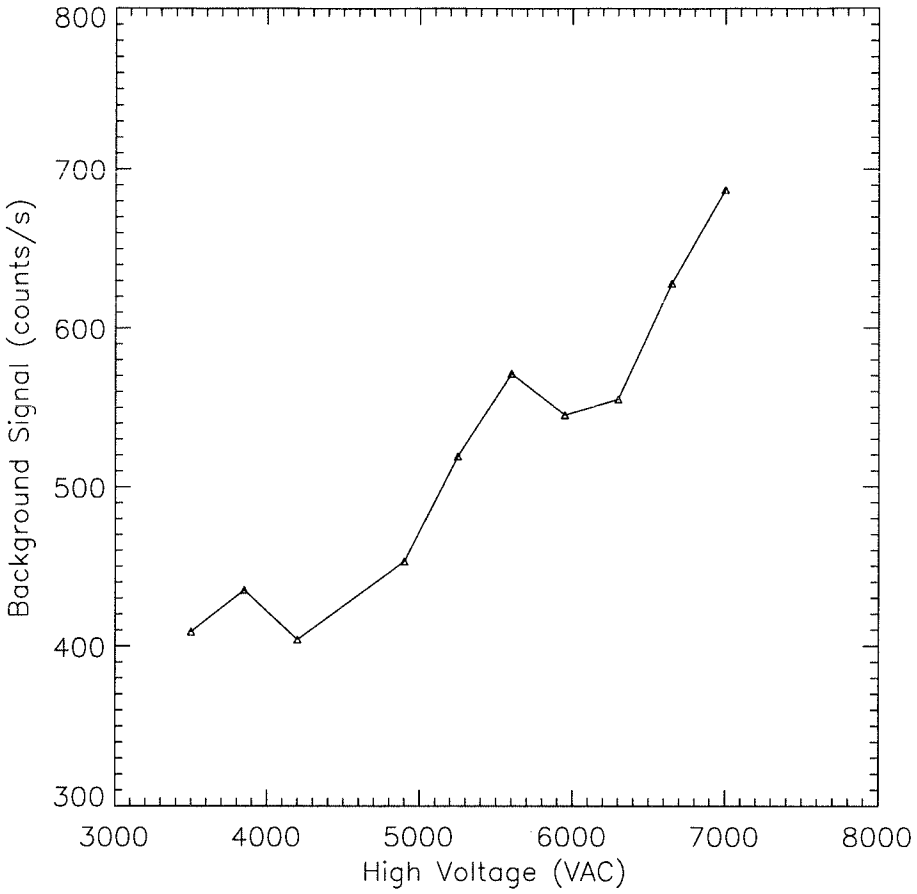

Figure A.2. Background signal of the NO detector as a function of ozonizer high voltage.

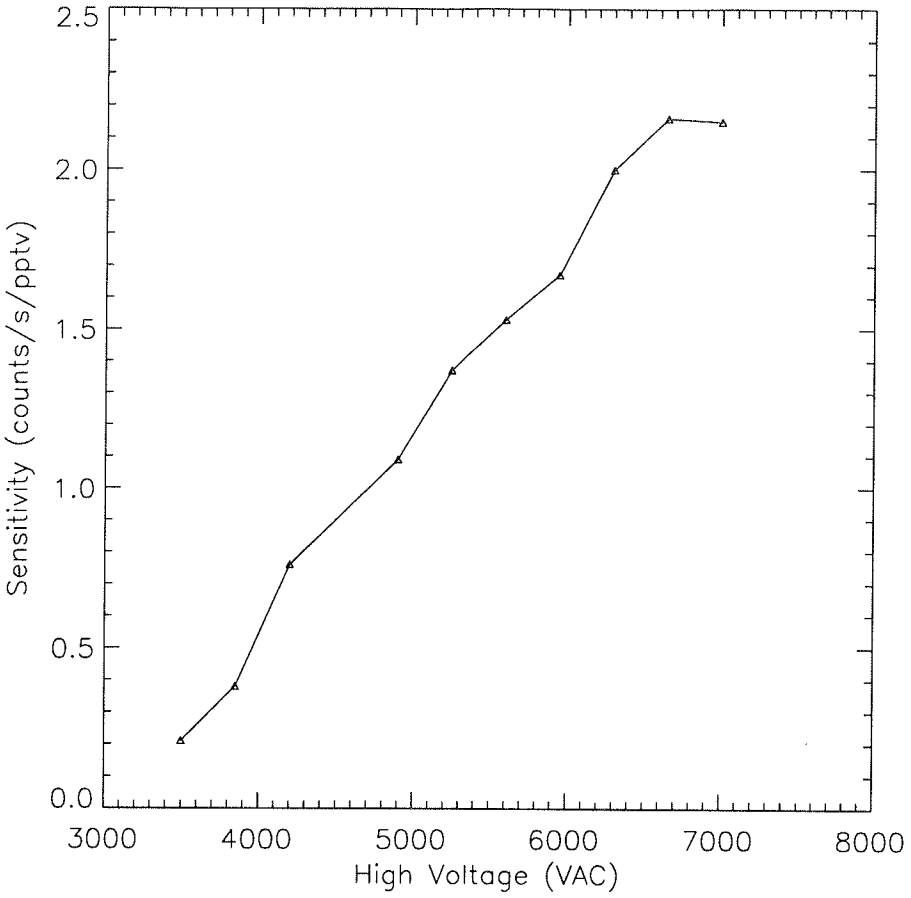

Figure A.3. Sensitivity of the NO detector as a function of ozonizer high voltage.

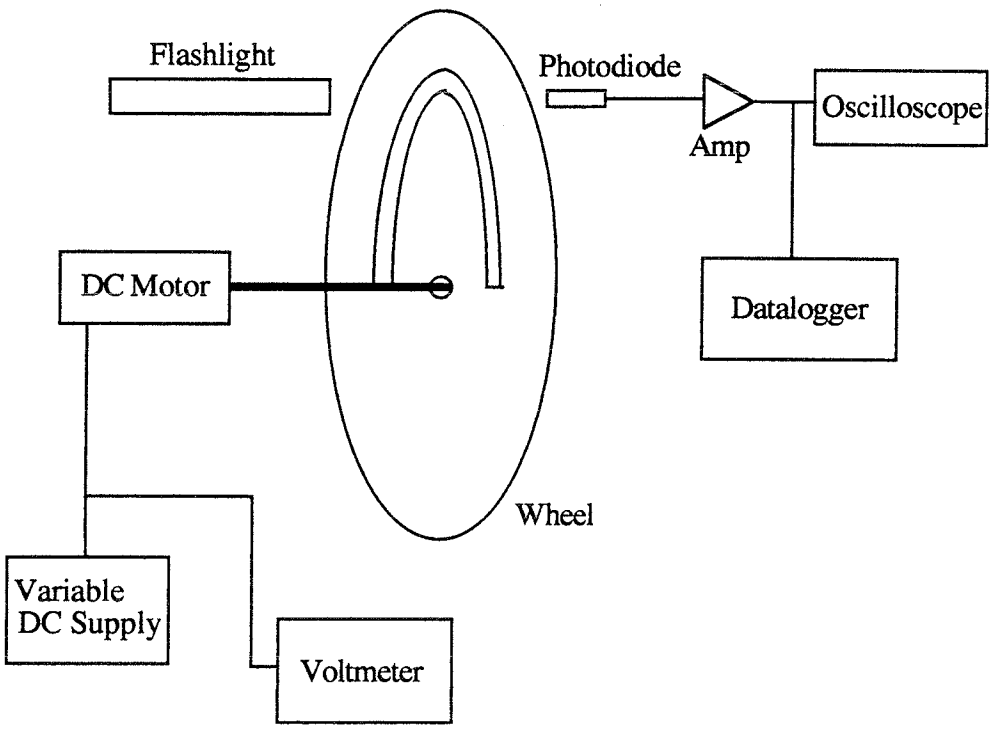

Figure B.1. Apparatus for calibration of the DC motor and wheel, used for the sinusoidal input response time determination.

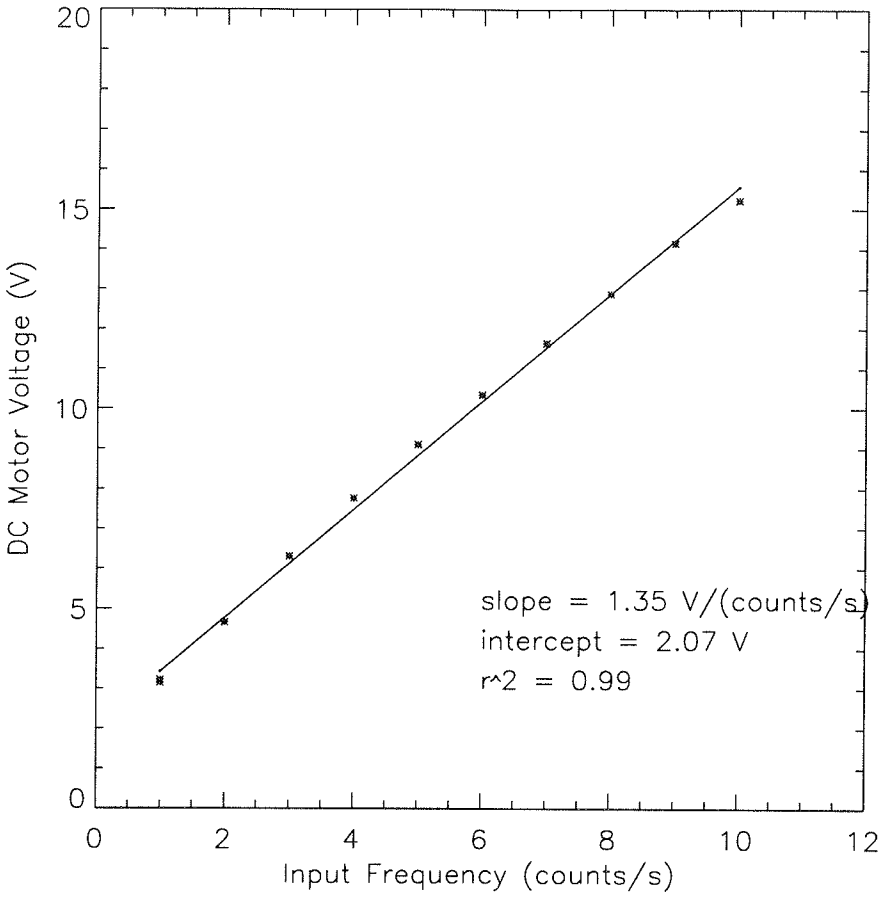

Figure B.2. Calibration curve for the DC motor.

Appendix A

Optimization of the Ozonizer

The design of the ozonizer for the NO detector is shown schematically in Figure 2.2, and the only variables easily changed are the flow of oxygen into the ozonizer, delivery pressure of the oxygen feed, and the high excitation voltage. These variables greatly influence the level of background noise and sensitivity of the instrument, and therefore must be chosen to optimize performance.

First, for a given NO mixing ratio ([NO] = 2.32 ppbv), the flow of oxygen was varied from 150 cc/min to 500 cc/min with a mass flow controller, keeping the high voltage set at 6500 VAC. The sensitivity of the NO detector is plotted in Figure A.1 as a function of O_2 flow. A peak is evident at a flow of 250 cc/min. At lower flows, the ozonizer simply does not make enough O_3, and at higher flows the increased pressure quenches the NO_2 chemiluminescence. Keeping the flow of O_2 constant at 250 cc/min, the inlet pressure was adjusted from just slightly above ambient pressure to about 1 atm above ambient. However, at pressures greater than just above ambient, the sensitivity of the NO detector dropped off significantly, again a result of quenching.

In order to examine the effects of excitation voltage, keeping the calibration gas flow constant and O_2 flow set at 250 cc/min, the high voltage was varied from 3500 VAC to 7000 VAC. With the instrument in background mode,

the signal was plotted as a function of high voltage setting in Figure A.2. As expected, background electrical noise increases with high voltage setting. Next, the sensitivity of the instrument was determined as a function of ozonizer high voltage (Figure A.3). Around 6650 VAC the sensitivity begins to level off, so that increasing the high voltage beyond this point will not improve the signal-to-noise ratio.

Appendix B

Calibration of the Wheel Used for the Time Response Determination

Chapter 2 of this dissertation included a section on the NO detector's response to a sinusoidal input. Before the time response determination was made, the DC motor and wheel had to be calibrated. Given a rate of revolution of the wheel, the DC supply voltage had to be found. Figure B.1 is a schematic of the calibration system.

The motor used was a Pittman Model GM8712D690, 740 rpm at 19.1 V (nominal), with a 10:1 gearbox ratio. The aluminum wheel was fastened to the motor arm. On one side of the wheel was a flashlight, and on the other was a photodiode. The photodiode signal due to the flashlight was too small to resolve with a voltmeter alone, so it was sent to a low offset, low noise precision amplifier (Analog Devices OP27) before being sent to the data acquisition system.

The motor was given power, and the input voltage was varied until the datalogger was recording a given number of pulses in one second. This number of pulses corresponded to the number of times the photodiode detected a signal from the flashlight through the notch in the wheel. Put another way, it was the frequency of the wheel in revolutions per second (rps). The supply voltage was then varied and recorded so that the frequency ranged from 1 to 10 rps. The

calibration curve is shown in Figure B.2, with $r^2 = 0.99$.

References

Anderson, I. C., and J. S. Levine, 1987: Simultaneous field measurements of biogenic emissions of nitric oxide and nitrous oxide. J. Geophys. Res., **92**, 965-976.

Atkinson, R., D. L. Baulch, R. A. Cox, R. F. Hampton, Jr., J. A. Kerr, and J. Troe, 1989: Evaluated kinetic and photochemical data for atmospheric chemistry: Supplement III. J. Phys. Chem. Ref. Data, **18**, 881-1097.

Bakwin, P. S., S. C. Wofsy, S.-M. Fan, M. Keller, S. E. Trumbore, and J. M. daCosta, 1990: Emission of nitric oxide (NO) from tropical forest soils and exchange of NO between the forest canopy and atmospheric boundary layers. J. Geophys. Res., **95**, 16,755-16,764.

Baldocchi, D. D., B. B. Hicks, and T. P. Meyers, 1988: Measuring biosphere-atmosphere exchanges of biologically related gases with micrometeorological methods. Ecology, **69**, 1331-1340.

Behmann, T., M. Weissenmayer, and J. P. Burrows, 1995: Measurements of peroxy radicals in a coastal environment. Manuscript in preparation.

Borucki, W. J., and W. L. Chameides, 1984: Lightning: Estimates of the rates of energy dissipation and nitrogen fixation. Rev. Geophys. Space. Phys., **22**, 363-372.

Bradshaw, J. D., M. O. Rodgers, S. T. Sandholm, S. KeShang, and D. D. Davis, 1985: A two-photon laser-induced fluorescence field instrument for ground-based and airborne measurements of atmospheric NO. J. Geophys. Res., 90, 12,861-12,873.

Brinsfield, R. B., and K. W. Staver, 1991: The role of cover crops in reduction of cropland nonpoint source pollution. Report submitted to Department of Agriculture Soil Conservation Service, S.C.S. Agreement No. 25087.

Buhr, M. P., D. D. Parrish, R. B. Norton, F. C. Fehsenfeld, R. E. Sievers, and J. M. Roberts, 1990: Contribution of organic nitrates to the total reactive nitrogen budget at a rural eastern U. S. site. J. Geophys. Res., **95**, 9809-9816.

Cantrell, C. A., J. A. Lind, R. E. Shetter, J. G. Calvert, P. D. Goldan, W. Kuster, F. C. Fehsenfeld, S. A. Montzka, D. D. Parrish, E. J. Williams, M. P. Buhr, H.

Westberg, G. Allwine, and R. Martin, 1992: Peroxy radicals in the ROSE experiment: Measurements and theory. J. Geophys. Res., **97**, 20,671-20,686.

Carroll, M. A., M. McFarland, B. A. Ridley, and D. L. Albritton, 1985: Ground-based nitric oxide measurements at Wallops Island, Virginia. J. Geophys. Res., **90**, 12,853-12,860.

Carroll, M. A., and A. M. Thompson, 1994: NO_x in the non-urban troposphere. Manuscript in preparation.

Chameides, W., and J. C. G. Walker, 1973: A photochemical theory of tropospheric ozone. J. Geophys. Res., **78**, 8751-8760.

Chesapeake Bay Research and Monitoring (CBRM) Division, 1995: Acid deposition in Maryland: Summary of 1993 research and monitoring results and evaluation of status and trends. Maryland Dept. of Natural Resources, CBRM Division, Annapolis, MD.

Cicerone, R. J., 1989: Analysis of sources and sinks of atmospheric nitrous oxide (N_2O). J. Geophys. Res., **94**, 18,265-18,271.

Civerolo, K. L., and R. R. Dickerson, 1991: An ultrahigh sensitivity nitric oxide detector. Chemrawn VII Conference.

Clough, P. N., and B. A. Thrush, 1967: Mechanism of chemiluminescent reaction between nitric oxide and ozone. Trans. Faraday Soc., **63**, 915-925.

Crutzen, 1973: A discussion of the chemistry of some minor constituents in the stratosphere and troposphere. Pure Appl. Geophys., **106**, 1385-1399.

Crutzen, P. J., 1974: Photochemical reactions initiated by and influencing ozone in unpolluted tropospheric air. Tellus, **26**, 47-56.

Crutzen, P. J., L. E. Heidt, J. P. Krasnec, W. H. Pollack, and W. Seiler, 1979: Biomass burning as a source of atmospheric gases CO, H_2, N_2O, NO, CH_3Cl, and COS. Nature, **282**, 253-256.

Dabberdt, W. F., D. H. Lenschow, T. W. Horst, P. R. Zimmerman, S. P. Oncley, and A. C. Delany, 1993: Atmosphere-surface exchange measurements. Science, **260**, 1472-1481.

Davis, D. D., J. D. Bradshaw, M. O. Rodgers, S. T. Sandholm, and S. KeShang,

1987: Free tropospheric and boundary layer measurements of NO over the central and eastern North Pacific Ocean. J. Geophys. Res., **92**, 2049-2070.

Delany, A. C., R. R. Dickerson, F. L. Melchior, and A. F. Wartburg, 1982: Modification of a commercial NO_x detector for high sensitivity. Rev. Sci. Instrum., **53**, 1899-1902.

Delany, A. C., D. R. Fitzjarrald, D. H. Lenschow, R. Pearson, Jr., G. J. Wendel, and B. Woodruff, 1986: Direct measurements of nitrogen oxides and ozone fluxes over grassland. J. Atmos. Chem., **4**, 429-444.

deServes, C., and C. Johansson, 1995: A chemical model study of the wet season boundary layer. Report to the International Meteorological Institute in Stockholm, Sweden, Report No. CM-86.

Dickerson, R. R., and A. C. Delany, 1988: Modifications of a commercial gas filter correlation CO detector for enhanced sensitivity. J. Atmos. Oceanic Technol., **5**, 424-431.

Dickerson, R. R., A. C. Delany, and A. F. Wartburg, 1984: Further modification of a commercial NO_x detector for high sensitivity. Rev. Sci. Instrum., **55**, 1995-1998.

Dickerson, R. R., B. G. Doddridge, P. Kelley, and K. P. Rhoads, 1995: Large-scale pollution of the atmosphere over the remote Atlantic Ocean: Evidence from Bermuda. J. Geophys. Res., **100**, 8945-8952.

Dickerson, R. R., G. J. Huffman, W. T. Luke, L. J Nunnermacker, K. E. Pickering, A. C. D. Leslie, C. G. Lindsey, W. G. N. Slinn, T. J. Kelly, P. H. Daum, A. C. Delany, J. P. Greenberg, P. R. Zimmerman, J. F. Boatman, J. D. Ray, and D. H. Stedman, 1987: Thunderstorms: An important mechanism in the transport of air pollutants. Science, **235**, 460-465.

Dickerson, R. R., D. H. Stedman, and A. C. Delany, 1982: Direct measurements of ozone and nitrogen dioxide photolysis rates in the troposphere. J. Geophys. Res., **87**, 4933-4946.

Doddridge, B. G., R. R. Dickerson, J. Z. Holland, J. N. Cooper, R. G. Wardell, O. Poulida, and J. G. Watkins, 1991: Observations of tropospheric trace gases and meteorology in rural Virginia using an unattended monitoring system: Hurricane Hugo (1989), a case study. J. Geophys. Res., **96**, 9341-9360.

Doddridge, B. G., R. R. Dickerson, T. G. Spain, S. J. Oltmans, and P. C. Novelli, 1994: Carbon monoxide measurements at Mace Head, Ireland. In "Proceedings of the Quadrennial Ozone Symposium 1992," R. D. Hudson (ed.), NASA, Greenbelt, MD.

Doddridge, B. G., R. R. Dickerson, R. G. Wardell, K. L. Civerolo, and L. J. Nunnermacker, 1992: Trace gas concentrations and meteorology in rural Virginia, 2, reactive nitrogen compounds. J. Geophys. Res., **97**, 20,631-20,646.

Doebelin, E. O., 1990: Measurement Systems: Application and Design. McGraw-Hill, New York, 960 pp.

Draxler, R. R., 1992: Hybrid single-particle Lagrangian integrated trajectories (HY-SPLIT) version 3.0: User's guide and model description. National Oceanic and Atmospheric Administration, Dept. of Commerce, Technical Memorandum No. ARL-195.

Drummond, J. W., A. Volz, and D. H. Ehalt, 1985: An optimized chemiluminescence detector for tropospheric NO measurements. J. Atmos. Chem., **2**, 287-306.

Eastman, J. A., and D. H. Stedman, 1974: A fast response sensor for ozone eddy-correlation flux measurements. Anal. Chem., **11**, 1209-1211.

Environmental Protection Agency (EPA), 1992: Aeronometric Information Retrieval System. Internal report, National Air Data Branch, Research Triangle Park, NC.

EPA, 1995: National Air Pollution Emission Trends, 1900-1994. Internal report, Research Triangle Park, NC.

Fehsenfeld, F. C., R. R. Dickerson, G. Hubler, W. T. Luke, L. J. Nunnermacker., E. J. Williams, J. M. Roberts, J. G. Calvert, C. M. Curran, A. C. Delany, C. S. Eubank, D. W. Fahey, A. Fried, B. W. Gandrud, A. O. Langford, P. C. Murphy, R. B. Norton, K. E. Pickering, and B. A. Ridley, 1987: A ground-based intercomparison of NO, NO_x, and NO_y measurement techniques. J. Geophys. Res., **92**, 14,710-14,722.

Finlayson-Pitts, B. J., and J. N. Pitts, 1986: Atmospheric Chemistry: Fundamentals and Experimental Techniques. John Wiley and Sons, New York, 1098 pp.

Firestone, M. K., and E. A. Davidson, 1989: Microbiological basis of NO and N_2O production and consumption in soil. In "Exchange of Trace Gases Between Terrestrial Ecosystems and the Atmosphere," M. O. Andrae and D. S. Schimel (eds.), John Wiley, New York.

Fisher, D., J. Ceraso, T. Mathew, and M. Oppenheimer, 1988: Polluted coastal waters: The role of acid rain. Report to the Environmental Defense Fund, New York.

Fisher, D. C., and M. Oppenheimer, 1991: Atmospheric nitrogen deposition and the Chesapeake Bay estuary. Ambio, **20**, 102-108.

Fishman, J., and P. J. Crutzen, 1978: The origin of ozone in the troposphere. Nature, **274**, 855.

Folinsbee, L. J., W. E. McDonnell, and D. H. Horstman, 1988: Pulmonary function and symptom responses after 6.6-hour exposure to 0.12 ppm ozone with moderate exercise. J. Air Pollut. Control Assoc., **38**, 28-35.

Fontijn, A. A., A. J. Sabadell, and R. J. Ronco, 1970: Homogeneous chemiluminescent measurement of nitric oxide with ozone. Implications for con tinuous selective monitoring of gaseous air pollutants. Anal. Chem., **42**, 575-579.

Fried, A., J. R. Drummond, B. Henry, and J. Fox, 1991: A tunable diode laser spectrometer for high precision concentration and ratio measurements of long-lived atmospheric gases. In "Measurement of Atmospheric Gases," Society of Photo-Optical Instrumentation Engineers, Bellington, WA, pp. 145-156.

Galbally, I. E., and C. R. Roy, 1978: Loss of fixed nitrogen from soils by nitric oxide exhalation. Nature, **275**, 734-735.

Galloway, J. N., and G. E. Likens, 1981: Acid precipitation: The importance of nitric acid. Atmos. Environ., **15**, 1081-1085.

Gao, W., M. L. Wesely, and I. Y. Lee, 1991: A numerical study of the effects of air chemistry on fluxes of NO, NO_2, and O_3 near the surface. J. Geophys. Res., **96**, 18,761-18,769.

Haagen-Smit, A. J., 1952: Chemistry and physiology of Los Angeles smog. Ind. Eng. Chem., **44**, 1342-1346.

Harrison, R. M., S. Yamulki, K. W. T. Goulding, and C. P. Webster, 1995:

Effect of fertilizer application on NO and N_2O fluxes from agricultural fields. J. Geophys. Res., **100**, 25,923-25,931.

Heck, W. W., O. C. Taylor, R. Adams, G. Bingham, J. Miller, E. Preston, and L. Weinstein, 1982: Assessment of crop loss from ozone. J. Air Pollut. Control Assoc., **32**, 353-361.

Hicks, B. B., 1970: The measurement of atmospheric fluxes near the surface: A generalized approach. J. Appl. Meteor., **9**, 386-388.

Hicks, B. B., M. L. Wesely, R. L. Coulter, R. L. Hart, J. L. Durham, R. Speer, and D. H. Stedman, 1986: An experimental study of sulfur and NO_x fluxes over grassland. Boundary-Layer Meteorol., **34**, 103-121.

Hoell, J. M., G. L. Gregory, D. S. McDougal, A. L. Torres, D. D. Davis, J. Bradshaw, M. O. Rodgers, B. A. Ridley, and M. A. Carroll, 1987: Air borne intercomparison of nitric oxide measurement techniques. J. Geophys. Res., **92**, 1995-2008.

Huebert, B. J., W. T. Luke, A. C. Delany, and R. A. Brost, 1988: Measurements of concentrations and dry surface fluxes of atmospheric nitrates in the presence of ammonia. J. Geophys. Res., **93**, 7127-7136.

Huebert, B. J., and C. H. Robert, 1985: The dry deposition of nitric acid to grass. J. Geophys. Res., **90**, 2085-2090.

Hyson, P., J. R. Garratt, and R. J. Francey, 1977: Algebraic and electronic corrections of measured uw covariance in the lower atmosphere. J. Appl. Meteor., **16**, 43-47.

Johansson, C., and I. E. Galbally, 1984: Production of nitric oxide in loam under aerobic and anaerobic conditions. Appl. Env. Microbiol., **47**, 1284-1289.

Johansson, C., and L. Granat, 1984: Emission of nitric oxide from arable land. Tellus, **36B**, 25-37.

Kaimal, J. C., and J. J. Finnigan, 1994: Atmospheric Boundary Layer Flows. Oxford University Press, New York, 289 pp.

Kaimal, J. C., J. C. Wyngaard, Y. Izumi, and O. R. Cote, 1972: Spectral characteristics of surface layer turbulence. Quart. J. Roy. Meteor. Soc.,

33, 2152-2169.

Kley, D., and M. McFarland, 1980: Chemiluminescence detector for NO and NO_2. Atmos. Technol., **12**, 63-69.

Lawrence, M. G., W. L. Chameides, P. S. Kasibhatla, H. Levy, and W. Moxim, 1994: Lightning and atmospheric chemistry: The rate of NO production. In "Handbook of Atmospheric Electrodynamics," Vol. 1, CRC Press, Boca Raton, FL.

Lee, Y-N, X. Zhou, and K. Hallock, 1995: Atmospheric carbonyl compounds at a rural southeastern United States site. J. Geophys. Res., **100**, 25,933-25,944.

Lenschow, D. H., and A. C. Delany, 1987: An analytic formulation for NO and NO_2 flux profiles in the atmospheric surface layer. J. Atmos. Chem., **5**, 301-309.

Levy, H., 1971: Natural atmosphere: Large radical and formaldehyde concentrations predicted. Science, **173**, 141-143.

Levy, H., J. D. Mahlman, and W. J. Moxim, 1980: A stratospheric source of reactive nitrogen in the unpolluted troposphere. Geophys. Res. Lett., **7**, 854.

Lin, B.-H., M. Padgitt, L. Bull, H. Delvo, D. Shank, and H. Taylor, 1995: Pesticide and fertilizer use and trends in U. S. agriculture. U. S. Dept. of Agriculture, Report No. AER-717.

Lipschultz, F., O. C. Zafiriou, S. C. Wofsy, M. B. McElroy, F. W. Valois, and S. W. Watson, 1981: Production of NO and N_2O by soil nitrifying bacteria: A source of atmospheric nitrogen oxides. Nature, **294**, 641-643.

Logan, J. A., 1983: Nitrogen oxides in the troposphere: Global and regional budgets, J. Geophys. Res., **88**, 10,785-10,807.

Madronich, S., 1987: Intercomparison of NO_2 photodissociation and U.V. radiometer measurements. Atmos. Environ., **21**, 569-578.

Maryland Department of the Environment (MDE), 1993: 1990 base year inventory for precursors of ozone for the state of Maryland. Air and Radiation Management Administration.

McFarland, M., D. Kley, J. W. Drummond, A. L. Schmeltekopf, and R. H.

Winkler, 1979: Nitric oxide measurements in the equatorial Pacific region. Geophys. Res. Lett., **6**, 605-608.

McMillen, R. T., 1987: An eddy correlation technique with extended applicability to non-simple terrain. Boundary-Layer Meteorol., **43**, 231-245.

Moy, L. A., R. R. Dickerson, and W. F. Ryan, 1994: How meteorological conditions affect tropospheric trace gas concentrations in rural Virginia. Atmos. Environ., **28**, 2789-2800.

National Atmospheric Deposition Program (NADP), 1990: Annual data: Precipitation chemistry in the United States, 1989. National Resource Ecology Laboratory, Colorado State University, Fort Collins, CO, 482 pp.

Nunnermacker, L. J., 1990: Calibration and detection techniques for trace nitrogen compounds in the atmosphere. Ph.D. Dissertation, University of Maryland, College Park, MD, 248 pp.

Officer, C. B, R. B. Biggs, J. L. Taft, L. E. Cronin, M. A. Tyler, and W. R. Boynton, 1984: Chesapeake Bay anoxia: Origin, development, and significance. Science, **223**, 22-27.

Oncley, S. P., A. C. Delany, T. W. Horst, and P. P Tans, 1993: Verification of flux measurement using relaxed eddy accumulation. Atmos. Environ., **27A**, 2417-2426.

Parrish, D. D., M. P. Buhr, M. Trainer, R. B. Norton, J. P. Shimshock, F. C. Fehsenfeld, K. G. Anlauf, J. W. Bottenheim, Y. Z. Tang, H. A. Wiebe, J. M. Roberts, R. L. Tanner, L. Newman, V. C. Bowersox, K. J. Olszyma, E. M. Bailey, M. O. Rodgers, T. Wang, H. Buresheim, U. K. Roychowdhury, and K. L. Demerjian, 1993: The total reactive oxidized nitrogen level and the partitioning between the individual species at six rural sites in eastern North America. J. Geophys. Res., **98**, 2927-2940.

Parrish, D. D., M. Trainer, M. P. Buhr, B. A. Watkins, and F. C. Fehsenfeld, 1991: Carbon monoxide concentrations and their relation to concentrations of total reactive oxidized nitrogen at two rural U. S. sites. J. Geophys. Res., **96**, 9309-9320.

Parrish, D. D., E. J. Williams, D. H. Fahey, S. C. Liu, and F. C. Fehsenfeld, 1987: Measurement of nitrogen oxide fluxes from soils: Intercomparison of enclosure and gradient measurement techniques. J. Geophys. Res., **92**, 2165-2171.

Phillips, R. E., and S. H. Phillips, 1984: No-Tillage Agriculture: Principles and Practices. Van Nostrand Reinhold, New York, 306 pp.

Pickering, K. E., A. M. Thompson, R. R. Dickerson, W. T. Luke, D. P. McNamara, J. P. Greenberg, and P. R. Zimmerman, 1990: Model calculations of tropospheric ozone production potential following observed convective events. J. Geophys. Res., **95**, 14,049-14,062.

Poulida, O., 1993: Observations and photochemistry of reactive trace gases in the atmosphere. Ph.D. Dissertation, University of Maryland, College Park, MD, 295 pp.

Poulida, O., K. L. Civerolo, and R. R. Dickerson, 1994: Observations and tropospheric photochemistry in central North Carolina. J. Geophys. Res., **99**, 10,553-10,563.

Poulida, O., R. R. Dickerson, B. G. Doddridge, J. Z. Holland, R. G. Wardell, and J. G. Watkins, 1991: Trace gas concentrations and meteorology in rural Virginia, 1, ozone and carbon monoxide. J. Geophys. Res., **96**, 22,461-22,475.

Priestley, C. H. B., 1959: Turbulent Transfer in the Lower Atmosphere. University of Chicago Press, Chicago, IL, 130 pp.

Reid, J., D. T. Cassidy, and R. T. Menzies, 1982: Linewidth measurements of tunable diode lasers using heterodyne and etalon techniques. Appl. Opt., **21**, 3961-3968.

Rhoads, K. P., P. P. Kelley, T. Carsey, M. Farmer, S. J. Oltmans, and D. Savoie, 1996: The composition of the troposphere over the Indian Ocean during the winter monsoon. Eos Trans. Amer. Geophys. Union, **77**, S52.

Ridley, B. A., and F. E. Grahek, 1990: A small, low flow, high sensitivity reaction vessel for NO chemiluminescence detectors. J. Atmos. Oceanic. Technol., **7**, 307-311.

Ridley, B. A., S. Madronich, R. B. Chatfield, J. G. Walega, and R. E. Shetter, 1992: Measurements and model simulations of the photostationary state during the Mauna Loa Observatory Photochemistry Experiment: Implications for radical concentrations and ozone production and loss rates. J. Geophys. Res., **97**, 10,375-10,388.

Rondon, A., C. Johansson, and E. Sanhueza, 1993: Emission of nitric oxide

from soils and termite nests in a Trachypogon savanna of the Orinoco basin. J. Atmos. Chem., **17**, 293-306.

Ryan, W. F., B. G. Doddridge, and R. R. Dickerson, 1996: Observations of O_3 and its precursors during the severe O_3 event of July 12-15, 1995 in the Baltimore-Washington metropolitan areas. Draft of a manuscript submitted to the Air and Waste Management Association.

Schiff, H. I., D. R. Hastie, G. I. Mackay, T. Iguchi, and B. A. Ridley, 1983: Tunable diode laser systems for measuring trace gases in tropospheric air. Environ. Sci. Technol., **17**, 352A-364A.

Singh, H. B., and P. L. Hanst, 1981: Peroxyacetyl nitrate (PAN) in the unpolluted atmosphere: An important reservoir for nitrogen oxides. Geophys. Res. Lett., **8**, 941-944.

Slemr, F., and W. Seiler, 1984: Field measurements of NO and NO_2 emissions from fertilized and unfertilized soils. J. Atmos. Chem., **2**, 1-24.

Slemr, F., and W. Seiler, 1991: Field study of environmental variables controlling the NO emissions from soil and the NO compensation point. J. Geophys. Res., **96**, 13,017-13,031.

Smith, S., J. D. Schreiber, and R. F. Cullum, 1995: Upland soybean production: Surface and shallow groundwater quality as affected by tillage and herbicide use. Trans. Amer. Soc. Agr. Eng., **38**, 1061-1068.

Spivakovsky, C. M., R. Yevich, J. A. Logan, S. C. Wofsy, and M. B. McElroy, 1990: Tropospheric OH in a three-dimensional chemical tracer model: An assessment based on observations of CH_3CCl_3. J. Geophys. Res., **95**, 18,441-18,471.

Staver, K. W., and R. B. Brinsfield, 1990: Patterns of soil nitrate availability in corn production systems: Implications for reducing groundwater contamination. J. Soil and Water Cons., **45**, 318-323.

Stedman, D. H., and J. O. Jackson, 1975: The photostationary state in photochemical smog. Int. J. Chem. Kinetics, Symposium I, 493-501.

Stedman, D. H., and R. E. Shetter, 1983: The global budget of atmospheric nitrogen species. In "Trace Atmospheric Constituents: Properties, Transformations, and Fates," S. E. Schwartz (ed.), John Wiley, New York.

Steffenson, D. M., and D. H. Stedman, 1974: Optimization of the operating parameters of chemiluminescent nitric oxide detectors. Anal. Chem., **46**, 1704-1709.

Taft, J. L., W. R. Taylor, E. O. Hartwig, and R. Loftus, 1980: Seasonal oxygen depletion in Chesapeake Bay. Estuaries, **3**, 242-247.

Tennekes, H., and J. L. Lumley, 1972: A First Course in Turbulence. MIT Press, Cambridge, MA, 300 pp.

Torres, A. L., 1985: Nitric oxide measurements at a nonurban eastern United States site: Wallops instrument results from July 1983 GTE/CITE mission. J. Geophys. Res., **90**, 12,875-12,880.

Torres, A. L., and A. M. Thompson, 1993: Nitric oxide in the equatorial Pacific boundary layer: SAGA 3 Measurements. J. Geophys. Res., **98**, 16,949-16,954.

United States Department of Commerce, 1994: Statistical abstract of the United States. Economics and Statistics Administration, Bureau of the Census.

Wesely, M., 1970: Eddy correlation measurements in the atmospheric surface layer over agricultural crops. Ph.D. Dissertation, University of Wisconsin, Madison, WI, 102 pp.

Wesely, M. L., 1983: Turbulent transport of ozone to surfaces common in the eastern half of the United States. In "Trace Atmospheric Constituents: Properties, Transformations, and Fates," S. E. Schwartz (ed.), John Wiley, New York.

Wesely, M. L., J. A. Eastman, D. R. Cook, and B. B. Hicks, 1978: Daytime variations of ozone eddy fluxes to maize. Boundary-Layer Meteorol., **15**, 361-373.

Wesely, M. L., J. A. Eastman, D. H. Stedman, and E. D. Yalvac, 1982: An eddy-correlation measurement of NO_2 flux to vegetation and comparison to O_3 flux. Atmos. Environ., **16**, 815-820.

Wesely, M. L., D. L. Sisterson, R. L. Hart, D. L. Drapcho, and I. Y. Lee, 1989: Observations of nitric oxide fluxes over grass. J. Atmos. Chem., **9**, 447-463.

Williams, E. J., and E. A. Davidson, 1993: An intercomparison of two chamber methods for the determination of emission of nitric oxide from soil. Atmos. Environ., **27A**, 2107-2113.

Williams, E. J., and F. C. Fehsenfeld, 1991: Measurement of soil nitrogen oxide emissions at three North American ecosystems. J. Geophys. Res., **96**, 1033-1042.

Williams, E. J., A. Guenther, and F. C. Fehsenfeld, 1992: An inventory of nitric oxide emissions from soils in the United States. J. Geophys. Res., **97**, 7511-7519.

Williams, E. J., D. D. Parrish, M. P. Buhr, F. C. Fehsenfeld, and R. Fall, 1988: Measurement of soil NO_x emissions in Central Pennsylvania. J. Geophys. Res., **93**, 9539-9546.